

UNCLASSIFIED  
Security Classification

AD 748644

DOCUMENT CONTROL DATA - R & D

(Security classification of title, body of abstract and indexing annotation must be entered when the overall report is classified)

1. ORIGINATING ACTIVITY (Corporate author) Battelle Columbus Laboratories 505 King Avenue Columbus, Ohio 43201		2a. REPORT SECURITY CLASSIFICATION Unclassified
		2b. GROUP Not applicable
3. REPORT TITLE  Fracture and Fatigue-Crack-Propagation Characteristics of $\frac{1}{2}$ -Inch Mill-Annealed Ti-6Al-4V Titanium Alloy Plate		
4. DESCRIPTIVE NOTES (Type of report and, inclusive dates) Final Report for Period January 5, 1970 to June 30, 1971		
5. AUTHOR(S) (First name, middle initial, last name) Charles E. Feddersen and Walter S. Hyler		
6. REPORT DATE November 1, 1971	7a. TOTAL NO. OF PAGES 74	7b. NO. OF REFS 8
8a. CONTRACT OR GRANT NO. N00156-70-C-1336	9a. ORIGINATOR'S REPORT NUMBER(S) G-9706 ✓	
b. PROJECT NO.		
c.	9b. OTHER REPORT NO(S) (Any other numbers that may be assigned this report)	
d.		
10. DISTRIBUTION STATEMENT  This document has been approved for public release, distribution is unlimited.		
11. SUPPLEMENTARY NOTES	12. SPONSORING MILITARY ACTIVITY Department of the Navy Naval Air Development Center Aero Structures Department Warminster, Pennsylvania 18974	
13. ABSTRACT  The fracture and fatigue-crack-propagation behavior of central through-the-thickness cracks has been evaluated in $\frac{1}{2}$ -inch-thick mill-annealed titanium alloy plate. The influence of crack aspect ratio on the fracture or residual strength of three panel widths has been determined. The fatigue-crack-propagation rates for various maximum stresses, stress ratios, and panel widths have been evaluated. It was observed that elastic fractures in the presence of central through-cracks do not occur in panels of this material less than 18 inches wide. Uniform and regular fatigue-crack-propagation behavior is noted in this material when analyzed on the basis of a stress-intensity factor range, $\Delta K$ . A fatigue-crack-propagation threshold is evident below 3 or 4 ksi-in. $^{1/2}$ . Power law modeling of rate data, crack life prediction, and interpretive discussions were also considered.		

**UNCLASSIFIED**

Security Classification

14. KEY WORDS	LINK A		LINK B		LINK C	
	ROLE	WT	ROLE	WT	ROLE	WT
Fatigue Fatigue-crack propagation Fracture Fracture toughness Residual strength Titanium alloy Ti-6Al-4V plate						

DD FORM 1 NOV 65 1470

S/N 0101-507-6921

(K)

II

Security Classification

A-314C9

AD 748644

FINAL REPORT

on

FRACTURE AND FATIGUE-CRACK-PROPAGATION  
CHARACTERISTICS OF 1/4-INCH MILL-ANNEALED  
Ti-6Al-4V TITANIUM ALLOY PLATE

November 1, 1971

by

Charles E. Feddersen and Walter S. Hyler

Prepared for the  
Aero Structures Department  
Naval Air Development Center  
Warminster, Pennsylvania 18974

This document has been approved  
for public release,  
distribution is unlimited.

Report No. G-9706

BATTELLE  
Columbus Laboratories  
505 King Avenue  
Columbus, Ohio 43201

III

## FOREWORD

This research program has been conducted by the Engineering Systems Department of Battelle's Columbus Laboratories, Columbus, Ohio, under Contract No. N00156-70-C-1336. This contract was initiated under Work Unit No. 3104 of basic AIRTASK No. A320320N/202A/2R02303001. The program was administered by the Aero Structures Department, Naval Air Development Center, Warminster, Pennsylvania, with Mr. Paul Kozel providing technical liaison. This report summarizes work performed during the period from January 5, 1970, through June 30, 1971.

The experimental portions of this research program were accomplished at Battelle-Columbus by James F. Wood and Henry J. Malik of the Structural Engineering Laboratories of Battelle's Columbus Laboratories. The cinematography associated with the fracture studies was developed and conducted by Theodore L. Porfilio. The metallographic appraisals contained in this report were contributed by Richard A. Wood.

The support of the Naval Air Development Center and the cooperation of the liaison engineer are gratefully acknowledged.

TABLE OF CONTENTS

	<u>Page</u>
SUMMARY . . . . .	1
INTRODUCTION . . . . .	1
PROGRAM DETAILS . . . . .	4
Materials . . . . .	4
Chemistry . . . . .	4
Mechanical Properties . . . . .	4
Metallography . . . . .	6
Test Specimens . . . . .	9
Specimen Design . . . . .	9
Specimen Preparation . . . . .	9
Test Matrix . . . . .	9
Experimental Procedures . . . . .	12
Test Setup . . . . .	12
Fatigue-Crack-Propagation Procedures . . . . .	12
Fracture or Residual Strength Tests . . . . .	14
EXPERIMENTAL RESULTS . . . . .	17
Fracture and Residual Strength . . . . .	17
Control Tests . . . . .	17
Test Results . . . . .	17
Graphical Displays . . . . .	19
Crack Surface Characteristics . . . . .	24
Fatigue-Crack Propagation . . . . .	26
Crack-Growth Curves . . . . .	26
Crack Surface Observations . . . . .	32
Terminal Crack Behavior . . . . .	34
Stress-Lifetime Summary . . . . .	40
Frequency Effects . . . . .	40
DATA ANALYSES . . . . .	42
Crack-Propagation Rates . . . . .	42
Power Law Modeling . . . . .	50
Crack Growth Prediction . . . . .	53
DISCUSSION AND INTERPRETATION . . . . .	58
Fatigue-Crack-Propagation Behavior . . . . .	58
Terminal Crack Behavior . . . . .	58
Observations on Curve-Fitting Fatigue-Crack-Propagation Data . . . . .	59
Comparison of Phase I and Phase II Programs . . . . .	61
CONCLUSIONS AND RECOMMENDATIONS . . . . .	63
REFERENCES . . . . .	64

TABLE OF CONTENTS (continued)

	<u>Page</u>
APPENDIX A	
BASIC FATIGUE-CRACK-PROPAGATION DATA . . . . .	A-1
APPENDIX B	
ESTIMATION OF FATIGUE-CRACK LENGTH AT FINAL LOADING CYCLE . . . . .	B-1

LIST OF TABLES

	<u>Page</u>
TABLE 1. MECHANICAL PROPERTIES OF 1/4-INCH Ti-6Al-4V MILL-ANNEALED PLATE, LONGITUDINAL GRAIN DIRECTION, RMI INGOT 295338 . . . . .	5
TABLE 2. PHASE II TEST MATRIX . . . . .	10
TABLE 3. FRACTURE AND RESIDUAL STRENGTH DATA FOR 1/4-INCH-THICK Ti-6Al-4V TITANIUM ALLOY PLATE . . . . .	20
TABLE 4. RESULTS OF FATIGUE-CRACK-PROPAGATION RATE ANALYSES USING FORMAN-KEARNEY-ENGLE MODEL . . . . .	54
TABLE 5. COMPARISON OF ACTUAL AND PREDICTED PANEL LIFETIMES . . . . .	57
TABLE A-1. CYCLE LIMITS AND CRACK LENGTH MEASUREMENTS FOR 9.6-INCH-WIDE PANELS AT LOW STRESS LEVELS . . . . .	A-2
TABLE A-2. CYCLE LIMITS AND CRACK LENGTH MEASUREMENTS FOR 9.6-INCH-WIDE PANELS AT HIGH STRESS LEVELS . . . . .	A-3
TABLE A-3. CYCLE LIMITS AND CRACK LENGTH MEASUREMENTS FOR 16-INCH-WIDE PANELS . . . . .	A-4
TABLE A-4. CYCLE LIMITS AND CRACK LENGTH MEASUREMENTS FOR 32-INCH-WIDE PANELS . . . . .	A-5
TABLE B-1. CORRELATION OF ESTIMATED AND MEASURED FINAL CRACK LENGTHS . . . . .	B-5

LIST OF FIGURES

	<u>Page</u>
FIGURE 1. VARIATION OF AVERAGE CRITICAL STRESS INTENSITY FACTOR WITH PANEL THICKNESS FOR MILL ANNEALED Ti-6Al-4V TITANIUM ALLOY SHEET AND PLATE AS DETERMINED FROM CENTER CRACKED TENSION SPECIMENS . . . . .	3
FIGURE 2. TYPICAL MICROSTRUCTURE OF THICKNESS SECTION . . . . .	7
FIGURE 3. MICROSTRUCTURE OF NONBANDED REGION . . . . .	8
FIGURE 4. MICROSTRUCTURE OF BANDED REGION . . . . .	8
FIGURE 5. SPECIMEN CONFIGURATION . . . . .	11
FIGURE 6. EXPERIMENTAL TEST SETUP SHOWN PRIOR TO FRACTURE TEST . . . . .	13
FIGURE 7. TYPICAL VIEWING FIELD OF MOVIE RECORD . . . . .	16
FIGURE 8. TYPICAL STRESS-CRACK SIZE HISTORY . . . . .	18
FIGURE 9. DATA DISPLAYS FOR ONSET OF STABLE TEAR AND FRACTURE CAPABILITY . . . . .	21
FIGURE 10. RESIDUAL STRENGTH DATA DISPLAYS . . . . .	22
FIGURE 11. SURFACES OF 9.6-INCH-WIDE FRACTURE SPECIMENS . . . . .	25
FIGURE 12. FATIGUE CRACK GROWTH IN 9.6-INCH-WIDE PANELS AT LOW STRESS LEVELS . . . . .	27
FIGURE 13. FATIGUE CRACK GROWTH IN 9.6-INCH-WIDE PANELS AT HIGH STRESS LEVELS . . . . .	28
FIGURE 14. FATIGUE CRACK GROWTH IN 16-INCH-WIDE PANELS AT MODERATE STRESS LEVELS . . . . .	29
FIGURE 15. FATIGUE CRACK GROWTH IN 16-INCH-WIDE PANELS AT A HIGH STRESS LEVEL . . . . .	30
FIGURE 16. FATIGUE CRACK GROWTH IN 32-INCH-WIDE PANELS AT R = 0.1 . . . . .	31
FIGURE 17. SURFACES OF 9.6-INCH-WIDE FATIGUE-CRACK-PROPAGATION SPECIMENS TESTED AT R = 0.4 . . . . .	33
FIGURE 18. TERMINAL CRACK BEHAVIOR IN 9.6-INCH-WIDE PANELS . . . . .	35
FIGURE 19. TERMINAL CRACK BEHAVIOR IN 16-INCH-WIDE PANELS . . . . .	36
FIGURE 20. TERMINAL CRACK BEHAVIOR IN 32-INCH-WIDE PANELS . . . . .	37
FIGURE 21. CYCLIC LIFETIMES OF PANEL FROM 1-INCH CRACK LENGTH . . . . .	41
FIGURE 22. FATIGUE-CRACK-PROPAGATION RATES AT R = 0.1 IN 9.6-INCH-WIDE PANELS . . . . .	44
FIGURE 23. FATIGUE-CRACK-PROPAGATION RATES AT R = 0.1 IN 16-INCH-WIDE PANELS . . . . .	45

LIST OF FIGURES (continued)

	<u>Page</u>
FIGURE 24. FATIGUE-CRACK-PROPAGATION RATES AT $R = 0.1$ IN 32-INCH-WIDE PANELS . . . . .	46
FIGURE 25. FATIGUE-CRACK-PROPAGATION RATES AT $R = 0.4$ IN 9.6-INCH-WIDE PANELS . . . . .	48
FIGURE 26. FATIGUE-CRACK-PROPAGATION RATES AT $R = 0.4$ IN 16-INCH-WIDE PANELS . . . . .	49
FIGURE 27. FATIGUE-CRACK-PROPAGATION RATES AT $R = 0.7$ IN 9.6-INCH-WIDE PANELS . . . . .	51
FIGURE 28. FATIGUE-CRACK-PROPAGATION RATES AT $R = 0.7$ IN 16-INCH-WIDE PANELS . . . . .	52
FIGURE 29. COMPARISON OF RATE DATA AND FORMAN-KEARNEY-ENGLE RATE MODEL . . . . .	55
FIGURE 30. FATIGUE-CRACK-PROPAGATION RATE MODELS . . . . .	60
FIGURE B-1. IDEALIZED CRACK GROWTH CURVE WITH THREE TERMINAL DATA POINTS . . . . .	B-2
FIGURE B-2. FINITE DIFFERENCE EXTRAPOLATION OF TERMINAL CRACK GROWTH MEASUREMENTS . . . . .	B-3

IX

### LIST OF SYMBOLS

- C = coefficient of power law for fatigue-crack propagation, microinches/cycle
- E = elastic modulus, ksi
- K = stress intensity factor, ksi-in.<sup>1/2</sup>
- K<sub>app</sub> = apparent stress intensity factors, ksi-in.<sup>1/2</sup>
- K<sub>c</sub> = critical stress intensity factor at fracture instability, ksi-in.<sup>1/2</sup>
- K<sub>o</sub> = stress intensity factor at threshold of slow tear, ksi-in.<sup>1/2</sup>
- N = cycle count, cycles
- R = stress ratio, nondimensional
- S = gross stress, ksi
- $\dot{S}$  = stress rate,  $dS/dt$ , ksi/min.
- W = panel width, inches
- c = half crack length, inches
- d = notation for differential
- e = subscript denoting "estimated"
- f = subscript denoting "final"
- l = subscript denoting "last"
- m = subscript denoting "measured"
- max = subscript denoting "maximum"
- min = subscript denoting "minimum"
- n = exponent of power law for fatigue-crack propagation, nondimensional; or subscript denoting "net section".
- $\Delta$  = notation for increment; in particular,  $\Delta K$  is increment of stress-intensity factor, or stress-intensity factor range, defined as  $\Delta K = (1-R)K$ .

FRACTURE AND FATIGUE-CRACK-PROPAGATION  
CHARACTERISTICS OF 1/4-INCH MILL-ANNEALED  
Ti-6Al-4V TITANIUM ALLOY PLATE

by

Charles E. Feddersen and Walter S. Hyler

SUMMARY

The fracture and fatigue-crack-propagation behavior of central through-the-thickness cracks has been evaluated for one thickness of mill-annealed titanium alloy plate. The influence of crack aspect ratio on the fracture or residual strength of three panel widths has been determined. The fatigue-crack-propagation rates for various maximum stresses, stress ratios, and panel widths have also been evaluated. It has been observed that elastic fractures in the presence of central through-cracks do not occur in panels of this material less than 18 inches wide. Uniform and regular fatigue-crack-propagation behavior is noted in this material on the basis of a stress-intensity factor range,  $\Delta K$ , analysis. A fatigue-crack-propagation threshold is evident below 3 or 4 ksi-in.<sup>1/2</sup>. Power law modeling of rate data, crack life prediction, and interpretive discussions are also considered.

INTRODUCTION

Characterization of the fracture and fatigue-crack-propagation behavior of structural materials is essential for determining the potential service life of a structure. For high-performance aircraft, such characterization of materials is necessary to define the required structural inspection intervals during normal flight service, as well as to assess the vulnerability of the structure to other forms of damage. One typical mode of structural damage in aircraft occurs as through-the-thickness cracks in tension skin (wing) panels. These cracks may nucleate at fastener holes, design discontinuities, or other service-induced defects, and may propagate until catastrophic fracture instability is triggered.

To investigate this crack behavior phenomenon more thoroughly, the Naval Air Development Center recently sponsored an experimental research program<sup>(1)\*</sup> at Battelle's Columbus Laboratories on the fracture and fatigue-crack propagation characteristics of 7075-T7351 aluminum alloy sheet and plate. As an outgrowth of that program (hereinafter referred to as Phase I), and with an increasing interest in titanium materials, this second-phase program (hereinafter referred to as Phase II) was initiated to study fracture and fatigue-crack-propagation behavior in mill annealed Ti-6Al-4V titanium alloy.

The principal objectives of this program were to characterize the fracture, residual strength, and fatigue-crack-propagation behavior of mill-annealed Ti-6Al-4V titanium alloy plate, building upon the general developments and observations of crack behavior derived from Phase I. This program was planned to cover a broader range of test variables with more detailed experimental measurements. However, the significant cost factors associated with purchasing and machining titanium materials necessitated a program of lesser specimen quantities. To maintain a broad test matrix, only one plate thickness, 1/4 inch, was considered. This particular thickness was selected because it appeared from the limited, available fracture toughness data to be near the apex of the toughness versus thickness (i.e.,  $K$  versus  $t$ ) curve, as illustrated in Figure 1. Furthermore, this thickness was intermediate to thicknesses being evaluated on related Navy programs.

In the following report, the program details are outlined first. The general experimental results for both fracture and fatigue-crack propagation are described in broad form. Specific data analyses, particularly on the fatigue-crack propagation, then follow. The report closes with interpretive discussion, conclusions, and recommendations.

---

\*Superscripts in parentheses denote references cited at the end of the report.

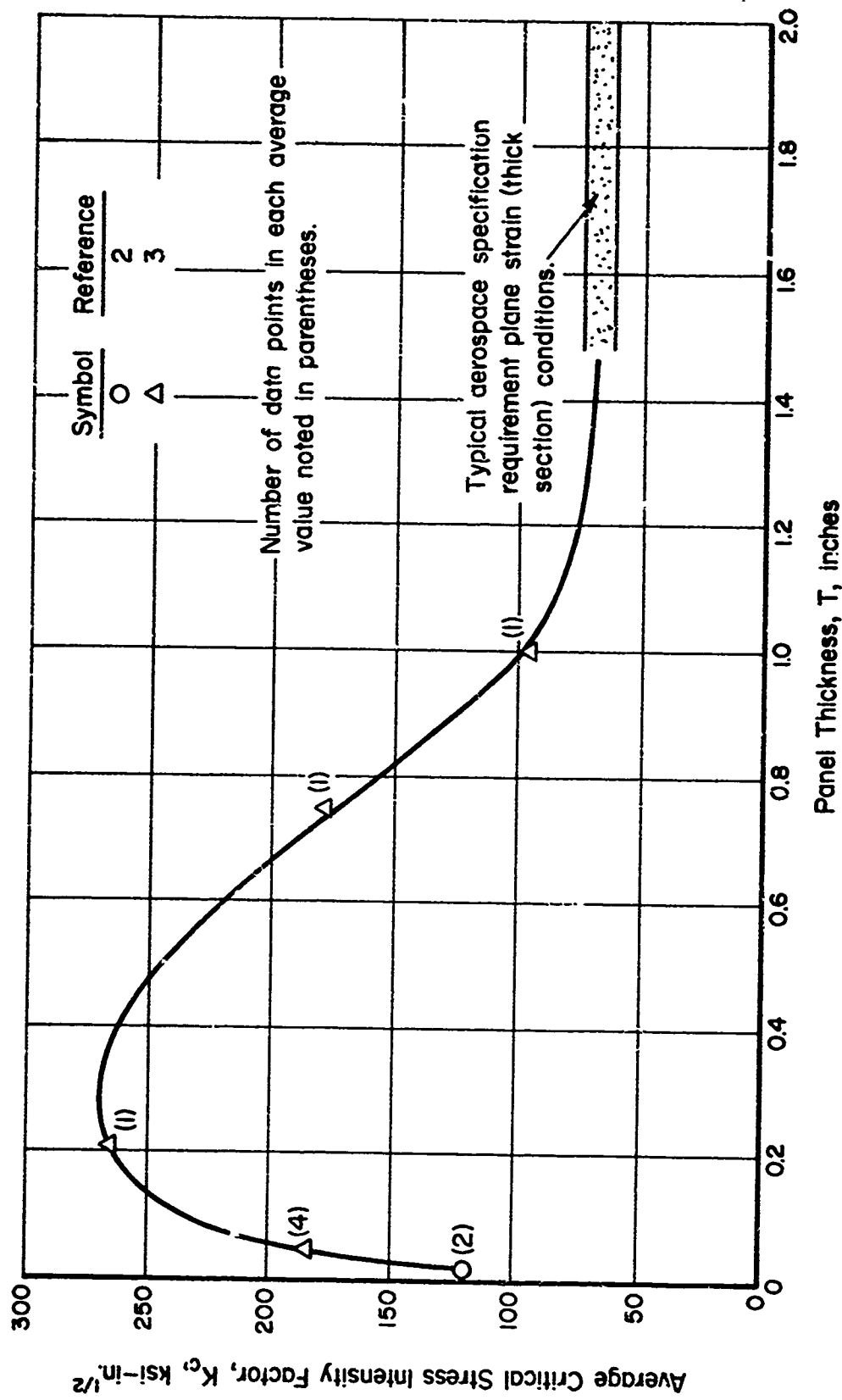


FIGURE 1. VARIATION OF AVERAGE CRITICAL STRESS INTENSITY FACTOR WITH PANEL THICKNESS FOR MILL ANNEALED Ti-6Al-4V TITANIUM ALLOY SHEET AND PLATE AS DETERMINED FROM CENTER CRACKED TENSION SPECIMENS.

## PROGRAM DETAILS

### Materials

Mill-annealed Ti-6Al-4V titanium alloy plate was selected for this experimental program because of its increasing application in Naval aircraft. The 1/4-inch thickness was selected as most representative of structural applications in wide flat panels. Furthermore, this thickness is intermediate to the thin gage sheet and very thick (1-inch thick and greater) plate data available, and thereby fills a void in experimental information.

The material for this program was purchased from Reactive Metals, Inc. (RMI), Niles, Ohio, from one heat of material to meet Specification MIL-T-904C, Type III, Composition C. The plates were sheared into specimen blanks by RMI and then shipped to Battelle-Columbus for final specimen machining and testing. The material received represented three lots from one heat of titanium alloy.

### Chemistry

The average chemistry certified by RMI for Ingot 295338 is:

C	N	Percent	Fe	Al	V	O	PPM (in Final Product)
0.02	0.010	0.18	6.4	4.2	0.127		81

### Mechanical Properties

The static tensile properties of each lot of material were sampled by Battelle and are summarized in Table 1. Also shown for comparison are the property ranges for these lots of materials, as reported by RMI. Within this tabulation, it can be noted that the strength results derived at Battelle are below those obtained by RMI; for elongation, the opposite trend is noted. Since both sources agree closely within themselves, the differences are attributed to differing testing rates.

TABLE 1. MECHANICAL PROPERTIES OF  $\frac{1}{2}$ -INCH Ti-6Al-4V MILL-ANNEALED PLATE, LONGITUDINAL GRAIN DIRECTION, RMI INGOT 295338

Lot No.	Specimen No.	Tensile Strength, TUS, ksi	0.2% Offset Tensile Yield Strength, TYS, ksi	Elongation in 2-inch Gage Length, e, %	Reduction in Area, RA, %
1	1	136.0	128.0	15.5	33.1
	2	138.0	129.0	18.5*	28.5*
	3	137.0	129.0	15.0	34.3
	Average	137.0	128.7	15.3	33.7
RMI Range		137.3/143.3	135.5/135.9	11.0/12.0	--
2	4	136.5	129.8	13.5	30.4
	5	136.8	131.6	15.0	37.5
	6	136.6	129.2	14.0	30.2
	Average	136.6	130.2	14.2	32.7
RMI Range		142.4/143.2	135.5/136.0	12.0/12.0	--
3	7	136.3	130.5	16.5	38.9
	8	136.5	131.6	14.5	38.6
	9	136.6	130.4	16.0	35.8
	Average	136.5	130.8	15.7	37.8
RMI Range		143.0/143.4	134.2/135.2	12.0/13.0	--

\*This specimen exhibited double necking. For average elongation and reduction in area values, only Specimens 1 and 3 are considered.

For purposes of subsequent data analyses, a grand average of tensile ultimate strength (TUS) values and tensile yield strength (TYS) values derived by Battelle-Columbus are used for reference properties. These values are TUS = 137 ksi and TYS = 130 ksi.

#### Metallography

Cross-section plate samples from widely separated locations were cut from each of the three lots of the single heat of Ti-6Al-4V alloy. Plate cross-sections were mounted for metallographic examination of the rolling direction (longitudinal). Standard metallographic techniques were used in grinding and polishing samples. Krolls' etchant (HF, HNO<sub>3</sub>) was used to reveal microstructure.

The most prominent microstructural feature observed at low magnification (35 to 100X) was banding. Banding is a feature commonly found in alpha-beta alloy plate. Both locations from each of the three lots of plate showed banding although the banding in samples from Lot 1 was more prominent than banding found in Lots 2 and 3. Figure 2 is a typical section across the thickness of samples from Lot 1. Figures 3 and 4 are photomicrographs at 250X of the typical microstructures of nonbanded and banded regions, respectively, from the same section shown in Figure 2.

Examination of the microstructure in the banded regions reveals that these areas are characterized by very elongated alpha grains, and by occasional differences in the alpha-to-beta ratio from that found in nonbanded areas. Although in some locations the bands appear to be beta phase rich, and in others alpha phase rich, most banded areas have nearly the same alpha-to-beta ratio as nonbanded areas. Rarely is the alpha-to-beta ratio of the banded area greatly different from that in the nonbanded areas. Thus, the most prominent feature of bands is the very elongated alpha grains.

The photomicrograph of Figure 3 shows structure that is typical of nonbanded areas from all three lots of plate examined. Typically, there is a mixture of equiaxed and elongated alpha grains interposed with the beta matrix and its transformation products. The small grain size is immediately apparent. The microstructure is typical of nonequilibrium-annealed Ti-6Al-4V mill product.

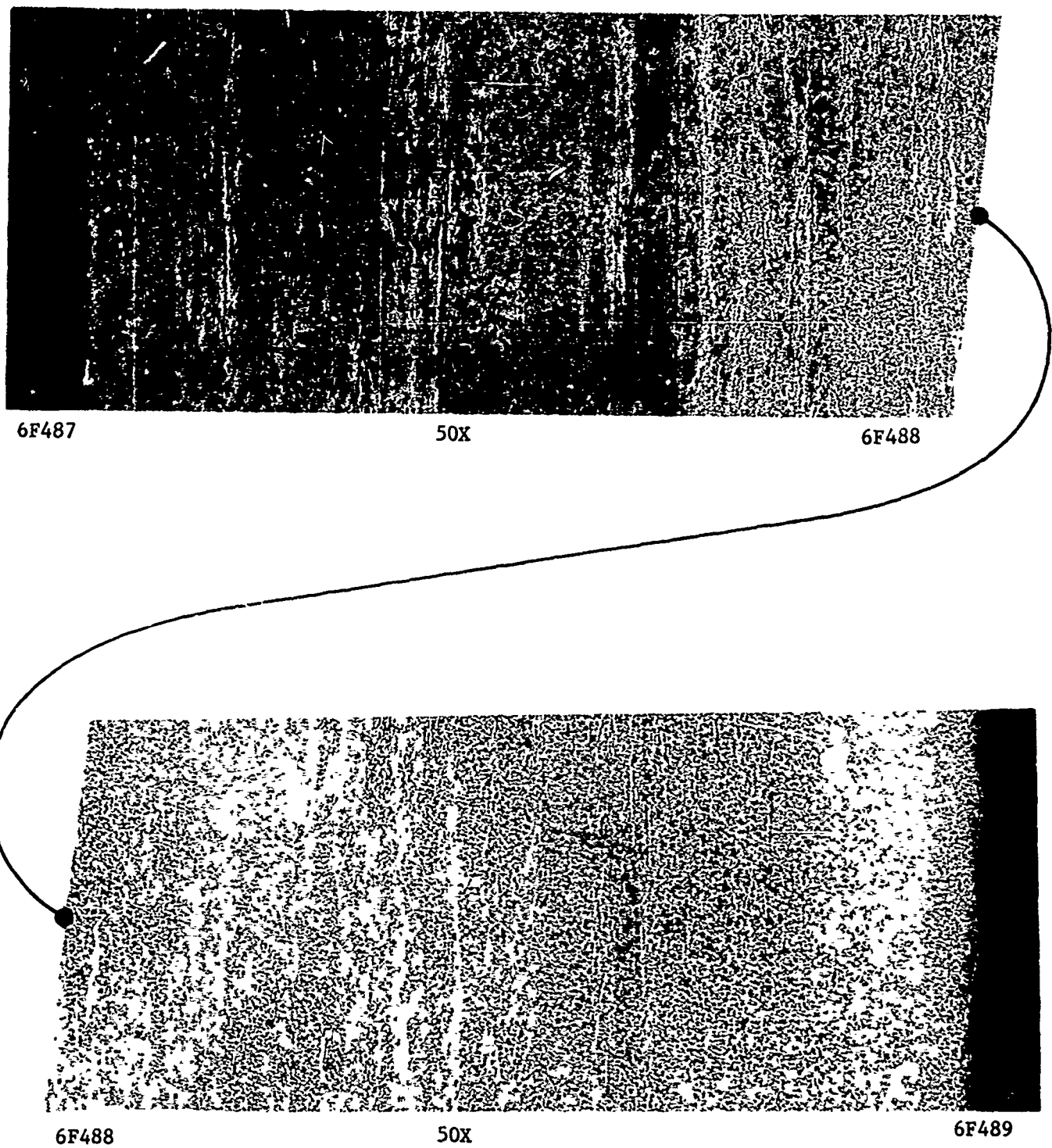
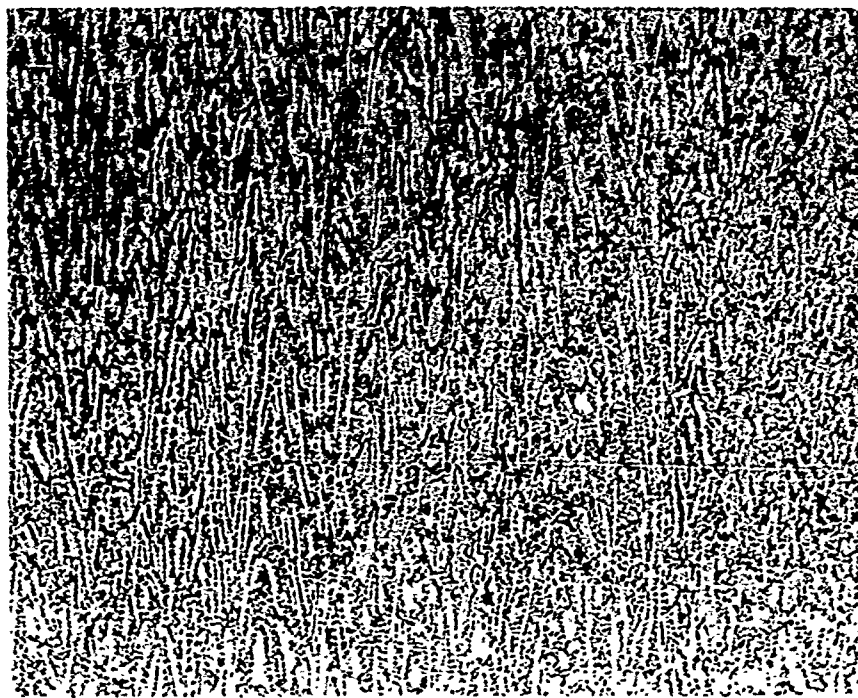


FIGURE 2. TYPICAL MICROSTRUCTURE OF THICKNESS SECTION



250X

6F491

FIGURE 3. MICROSTRUCTURE OF NONBANDED REGION



250X

6F490

FIGURE 4. MICROSTRUCTURE OF BANDED REGION

### Test Specimens

#### Specimen Design

The general configuration of the test specimens is illustrated in Figure 5. Although the initial control test specimens had a reduced section to avoid grip failure, results of these tests indicated that a reduced section was not required for crack lengths greater than about 15 percent of the width, i.e.,

$$2c/W \geq 0.15 .$$

Since the test matrix was within this regime, all subsequent test specimens were used in the rectangular planform.

#### Specimen Preparation

The specimen materials were received as sheared rectangular blanks from RMI. The appropriate hole patterns for gripping were drilled into the ends of the blanks in the Battelle-Columbus machine shop. A central, diamond-shaped starter notch (detail shown in Figure 5) was put in the specimen by the electrical discharge machine (EDM) process. The finished specimens were then transferred to the Structural Engineering Laboratory for testing.

#### Test Matrix

The test matrix for this experimental program is presented in Table 2. It includes two control tests which were used to determine the subsequent panel sizes for testing, 13 residual strength or fracture tests, and 24 fatigue-crack-propagation tests. The test matrix was designed to cover a broad range of panel sizes, crack aspect ratios (for residual strength), and maximum cyclic stresses and stress ratios (for fatigue-crack propagation).

Two noticeable voids exist in the fatigue-crack-propagation portion of the matrix. At the low stress levels (5 ksi) in wide panels, cyclic lives in excess of  $10^7$  cycles were projected and were considered impractical timewise

TABLE 2. PHASE II TEST MATRIX

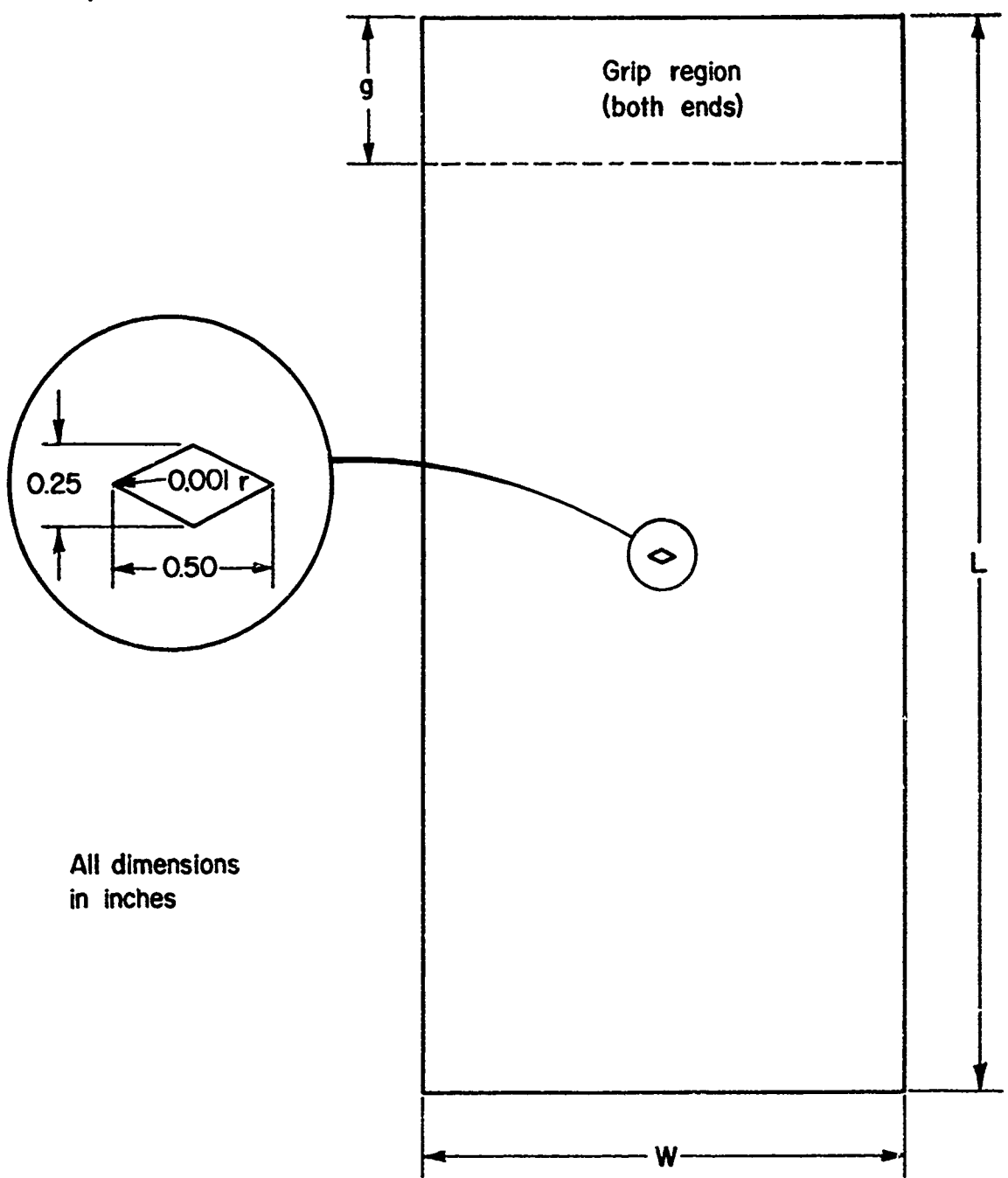
Specimen Width, W, in.	Center-Through Crack Fracture Test (Residual Strength)						Fatigue Crack Propagation Tests			
							Maximum Stress $S_{max}$ , ksi			
	Crack Aspect Ratio, 2c/W			Stress Ratio, R			5 <sup>a</sup>	10	30	50
18 (Initial Control Tests Only)	0.2	0.25	0.4	0.5	0.6	0.8				
9	9CC03 <sup>e</sup> 9CC17	--	9CC02	--	9CC01	9CC15	0.1 0.4 0.7	9CC13 9CC14 9CC16 <sup>d</sup>	9CC12 9CC07 9CC11	9CC04 9CC05 9CC06
16	--	16CC03	--	16CC06	--	16CC13	0.1 0.4 0.7	16CC04 <sup>b</sup> -- --	16CC10 16CC05 <sup>c</sup> 16CC12	16CC02 16CC11 16CC01
32	32CC03	32CC01	32CC07	--	32CC08	--	0.1 --	32CC06	32CC05	32CC04

a - This stress level is intended for FCP threshold studies.

b - Limited test data, specimen destroyed by equipment malfunction.

c -  $S_{max} = 15$  ksi, R as indicated.d - No continuous propagation. Test stopped after  $32 \times 10^6$  cycles.

e - Specimen overloaded machine. Second test substituted because of extensive plastic deformation.



$\frac{W}{}$	$\frac{L}{}$	$\frac{g}{}$
9.6	32	6 or 9*
16	48	6 or 12*
18	60	12
32	72	12

\* Depending on test system utilized

FIGURE 5. SPECIMEN CONFIGURATION

for this program. At the opposite extreme in the narrow panels, at high cyclic stresses and low stress ratio, the projected cyclic life was considered too short to be of practical value.

#### Experimental Procedures

##### Test Setup

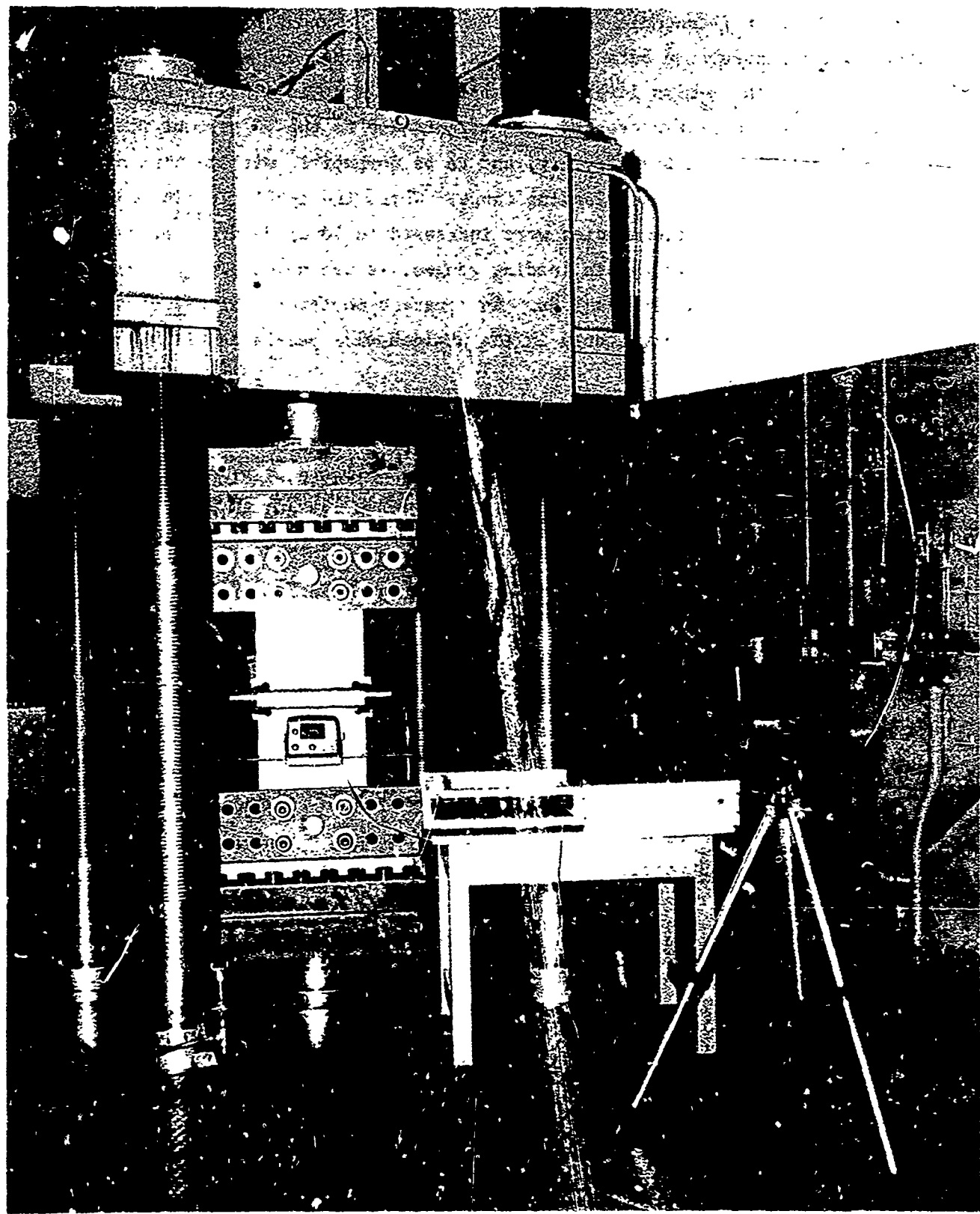
Similar experimental setups were used both for the fracture or residual strength tests and for the fatigue-crack-propagation studies. All tests were conducted in the Structural Engineering Laboratory of Battelle-Columbus on servocontrolled electrohydraulic testing systems of either 50, 130, or 500-kip dynamic capacity, as required by specimen size and loadings.

A typical test setup is illustrated in Figure 6. Shown is a 16-inch-wide test specimen, with buckling guides attached, ready for a rising-load fracture test. Between the guides, extending beyond the specimen, is a measurement scale. At the right is the recording camera, set up to follow the slow tear behavior associated with the residual strength test (discussed in Reference (1)). In front of the specimen, below the buckling guides, is a digital voltmeter to provide a load record in the field of the film. On the table in the central foreground is an X-Y recorder and transducer readout to monitor the load compliance of the specimen. A clip-type compliance gage (illustrated in Reference (1)) is inserted in the notch at the back of the panel.

This type of experimental setup also was used for the 9.6 and 32-inch-wide panels. During the fatigue tests, the load-recording voltmeter and movie equipment were not used. All fatigue crack propagation and fracture or residual strength tests were conducted in a laboratory with a controlled temperature and humidity system. The temperature was maintained at  $68^{\circ}\text{F} \pm 2^{\circ}\text{F}$ ; the humidity at 50 percent RH  $\pm$  5 percent.

##### Fatigue-Crack-Propagation Procedures

The test specimen was mounted in a testing machine of appropriate capacity. After buckling guides were attached and cycle counters were zeroed, a load-controlled, constant-amplitude fatigue-crack-propagation test was initiated at the maximum cyclic stress and stress ratio indicated in Table 2.



1927

FIGURE 6. EXPERIMENTAL TEST SETUP SHOWN PRIOR TO FRACTURE TEST

The test frequencies ranged from 1 to 25 Hz and are noted with the basic fatigue crack propagation data of Appendix A. A nominal cyclic frequency of 5 Hz was selected as the median level to accomplish the test in a reasonable period of time, to avoid synergistic crack growth effects due to the 50 percent relative humidity level of the laboratory air, and to be compatible with testing system response over the anticipated loading range. Where the cyclic loading range was relatively low, cyclic frequencies were increased to 10 or 25 Hz. For the larger panels at relatively high cyclic loading ranges, it was necessary to reduce the cyclic frequencies to as low as 1 Hz. An apparent environmental effect at this low frequency level was noted only in the 32-inch-wide panels as will be discussed later.

All cracks were initiated from the 1/2-inch EDM starter flaw. For short crack length measurements, the specimen surface was monitored with an optical comparator. At longer crack lengths, direct crack length readings from the attached scale were possible. During the test, measured crack lengths and associated cycle counts were tabulated in a laboratory record book. A graphical plot of crack length versus cycles was also maintained during the test as a visual guide to the progress of crack growth. The tests were run to failure, with frequency of measurements increasing toward termination of the test. An attempt was made to "catch" the last cycle crack length. However, because of the cyclic frequency and rapid growth rates near the end of the test, this was usually unsuccessful. In about half of the tests, the final crack length could be determined from striation markings after failure.

#### Fracture or Residual Strength Tests

The fracture test panels were initially precracked in accordance with the fatigue-crack propagation procedures discussed above. In order to maintain a flat fatigue crack and not plastically strain the uncracked section, the maximum stresses were adjusted to keep the applied stress-intensity factor below  $30 \text{ ksi} \cdot \text{in.}^{1/2}$ . This usually involved stepping down the stresses as the cracking proceeded. The crack was extended to the aspect ratio indicated in Table 2 and load cycling was stopped.

In preparation for the rising load fracture test, a digital voltmeter was mounted in the camera field in front of the specimen and a clip-type compliance

gage was mounted in the notch at the back of the panel. The panel was then loaded to fracture at a constant stress rate in the range

$$40 < S < 80 \text{ ksi/min} ,$$

which corresponds nominally to the gross strain rate of standard tensile testing. A film record of the test was made to determine the crack length and associated loadings leading to fracture instability.

The film field which was monitored is shown in Figure 7. The camera used was a 35-mm cine-pulsed photo recorder designed to operate with extreme accuracy and high reliability. The lens has a focal length of 100-mm and a maximum aperture of F/2. For detailed studies of small cracks, the lens has focusing capabilities from 1:1 to infinity and is corrected for both chromatic and spherical aberration. To realize the capabilities of this system, a film with ultra-high resolving power (630 lines per millimeter) and extremely fine grain was selected. A film speed of 10 frames per second and an exposure time of 1/60 second were used to detect fracture instability. The specimen lighting, provided by 3200 K photofloods, was measured by incident light metering techniques.



FIGURE 7. TYPICAL VIEWING FIELD OF MOVIE RECORD

EXPERIMENTAL RESULTSFracture and Residual Strength

In order to characterize the crack sensitivity of 1/4-inch-thick Ti-6Al-4V titanium alloy plate, a total of 15 fracture or residual strength tests were conducted. The panel widths ranged from 9.6 inches to 32 inches with crack aspect ratios from 0.2 to 0.8. The allocation of specimens has been indicated in Table 2.

Control Tests

Since few data were available on through-the-thickness cracks in this particular product form and thickness, two control tests were conducted to obtain estimates of the material toughness and of the panel width required for elastic instability. An 18-inch-wide panel was selected as a midrange panel size of practical interest. Results of the control tests indicated that this width is marginal for elastic fracture instability. To provide a large panel width which would fracture elastically and yet include fractional widths for a broad test matrix with reasonable material utilization, it was decided to select 32, 16, and 8-inch-wide panels. In the last instance, the available material allowed the use of a 9.6-inch-wide panel.

With this particular selection of panel sizes, it was recognized that two different failure modes would be encountered in the residual strength tests. The large panels would be expected to fail elastically while the smaller panels (smaller than control test size) would probably fail on a net-section-yielding criterion. Although such a mix of failure modes does not characterize either mode completely, this combination of panel sizes covers the practical range of structural interest. It is also a useful parametric combination of widths for the fatigue-crack-propagation portion of this study.

Test Results

As has been previously described by these authors in References (1) and (4), the non-plane-strain fracture of center through-cracked tension

panels under a slowly rising load is preceded by a measurable amount of slow crack growth or stable tearing. For convenient quick reference this behavior is schematically reviewed in Figure 8. Under a slowly rising load an initial

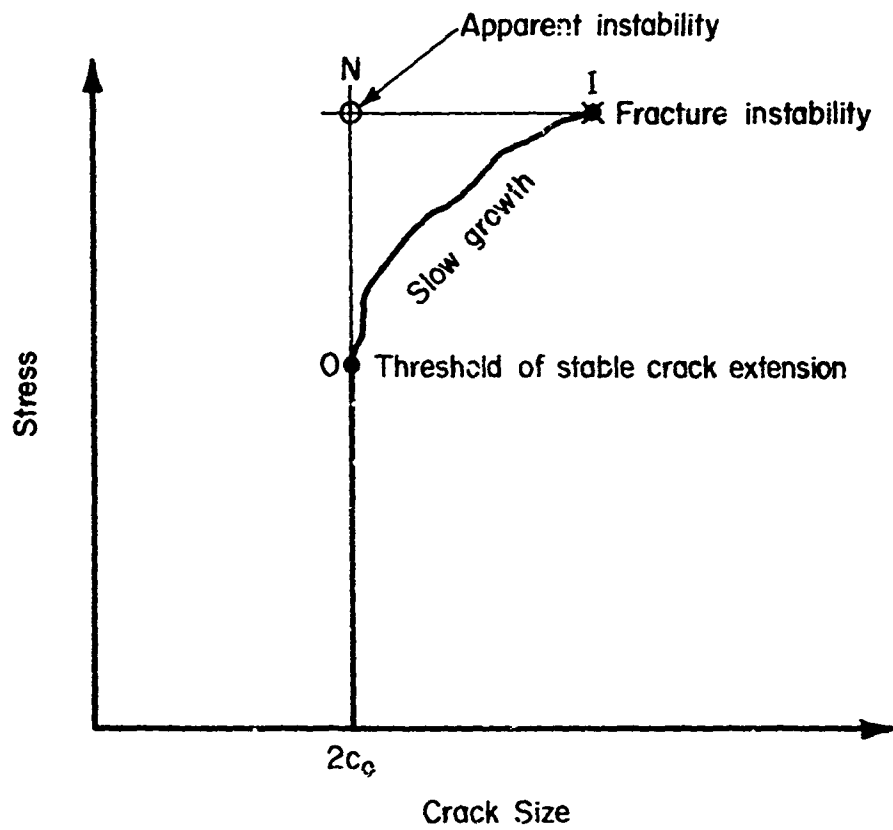


FIGURE 8. TYPICAL STRESS-CRACK SIZE HISTORY

crack length,  $2c_0$ , remains static until the applied stress reaches some characteristic threshold value. At this point, the crack appears to advance in a stable fashion with increasing load until crack instability is reached, wherein the crack rapidly accelerates to completely sever the panel. Two bench marks--threshold of cracking and fracture instability, respectively identified as Points 0 and 1--tend to bound this slow growth behavior. A third point--apparent instability, identified as Point N--is a coarse measure of this overall crack behavior.

The use of Point N (for Notch concept) stems from the practical consideration that the only flaw details which are positively known are the initial conditions of the pre-existing flaw, and the anticipated maximum load. Some design practitioners maintain that residual strength information beyond the notch-concept appraisal of crack behavior is an unnecessary and misleading refinement. However, from a research perspective, delineation of slow growth behavior can provide additional insight to the basic cracking process. In the following presentations, experimental results are presented and interpreted from both perspectives.

The basic data derived from the fracture and residual strength tests are presented in Table 3. First listed is the specimen identification number. This is followed by two columns denoting the measured specimen thickness and width. The last four columns list the measured crack and stress data derived from the test. The initial crack length,  $2c_0$ , was the fatigue crack length measured on the crack surface after fracture. The only obtainable measure of the onset of slow crack growth prior to fracture was the 5 percent secant offset stress as determined from the load record. No "pop-in" behavior was detected. The critical crack length and fracture-load measurements were determined from the film records previously described.

#### Graphical Displays

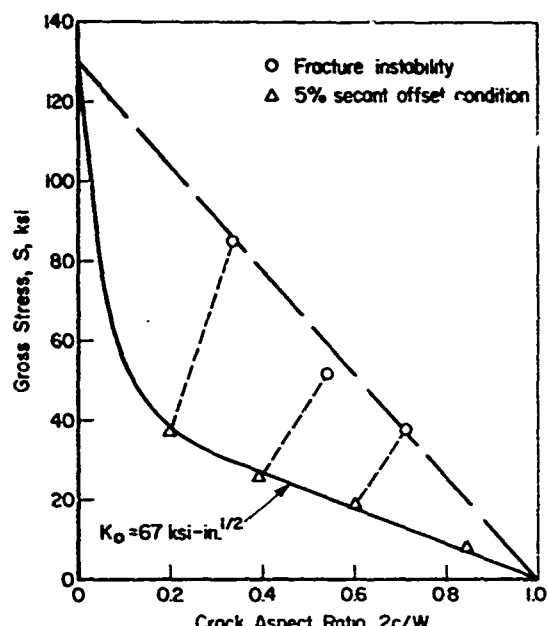
The experimental results listed in Table 3 are also presented graphically in Figures 9 and 10. The former figure presents the basic experimentally-derived crack behavior data; the latter figure displays the residual strength (or notch concept) interpretation thereof. The format of gross stress versus crack aspect ratio (i.e., crack size normalized for panel width) is used for both figures.

In addition to the data points which appear as discrete symbols, several lines are shown in these figures. The dashed lines denote the condition of net section yielding on the uncracked ligament over the full range of crack aspect ratios. These dashed lines extend from the point of material tensile yield strength on the gross stress axis (i.e., at zero crack-aspect ratio) to the unit point on the crack-aspect ratio axis (i.e., at zero gross stress).

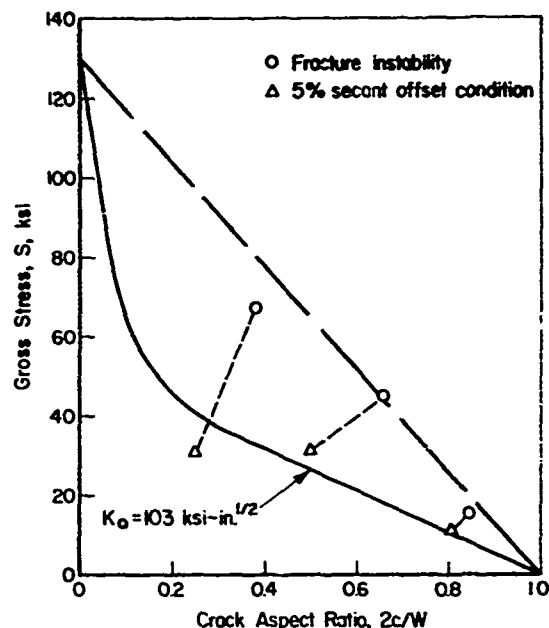
The solid lines on these figures represent the calculated average linear tangents model<sup>(1,4)</sup> of fracture behavior for each data set which is

TABLE 3. FRACTURE AND RESIDUAL STRENGTH DATA FOR 1/4-  
INCH-THICK Ti-6Al-4V TITANIUM ALLOY PLATE

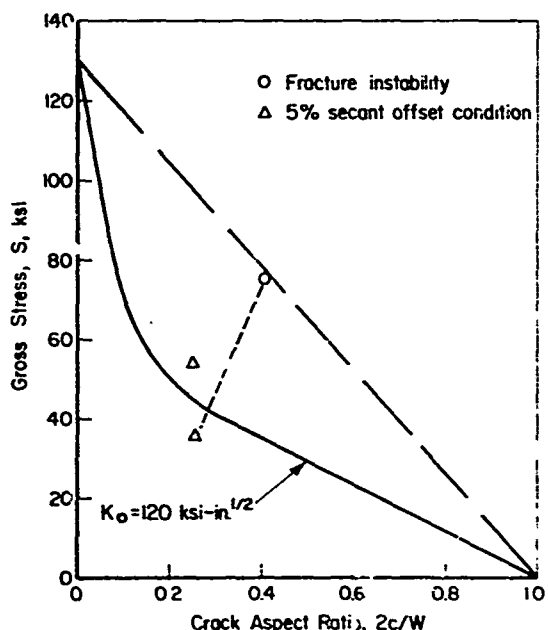
Specimen Number	Thickness, T, in.	Width, W, in.	Initial Crack, 2c <sub>0</sub> , in.	5% Secant Offset Stress, S <sub>o</sub> , ksi	Final Crack Length, 2c, in.	Maximum Stress, S <sub>max</sub> , ksi
9CC017	0.293	9.625	1.92	36.50	3.25	85.10
9CC003	0.286	9.625	1.92	36.70	--	--
9CC002	0.280	9.625	3.80	25.60	5.22	51.70
9CC01	0.286	9.625	5.78	18.70	6.86	37.80
9CC15	0.285	9.625	8.14	7.85	--	11.30
16CC03	0.275	16.116	3.99	31.10	6.10	67.50
16CC06	0.260	16.115	8.02	31.30	10.58	45.10
16CC13	0.285	16.110	12.93	11.30	13.55	15.40
18CC01	0.265	18.000	4.64	35.60	7.38	75.40
18CC02	0.265	18.000	4.54	53.90	--	75.30
32CC03	0.262	32.160	6.02	39.20	10.60	75.20
32CC01	0.288	32.160	8.07	40.20	--	55.40
32CC02	0.275	32.132	8.01	30.60	--	58.90
32CC08	0.270	32.150	12.72	33.40	17.00	47.00
32CC07	0.273	32.140	19.20	14.20	21.60	26.20



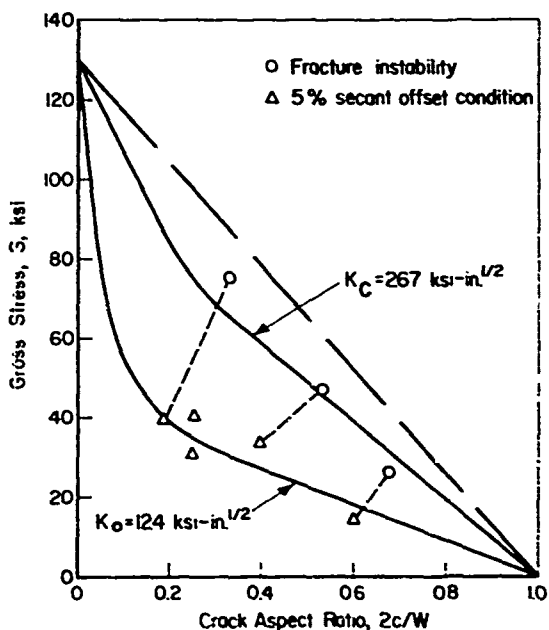
(a) 9.6-inch-wide panel



(b) 16-inch-wide panel

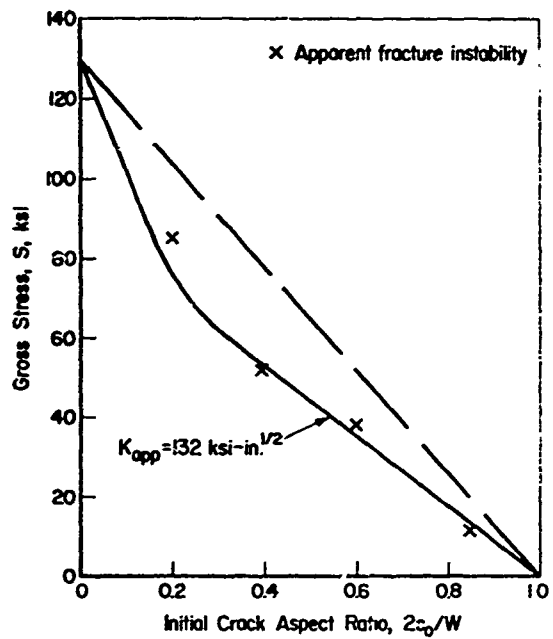


(c) 18-inch-wide panel

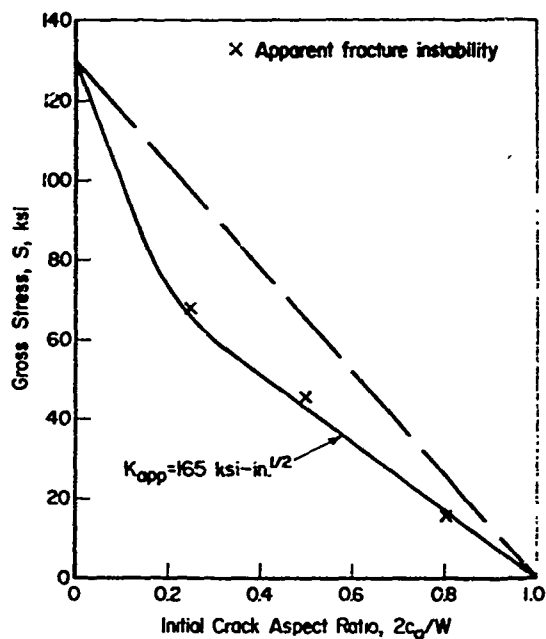


(d) 32-inch-wide panel

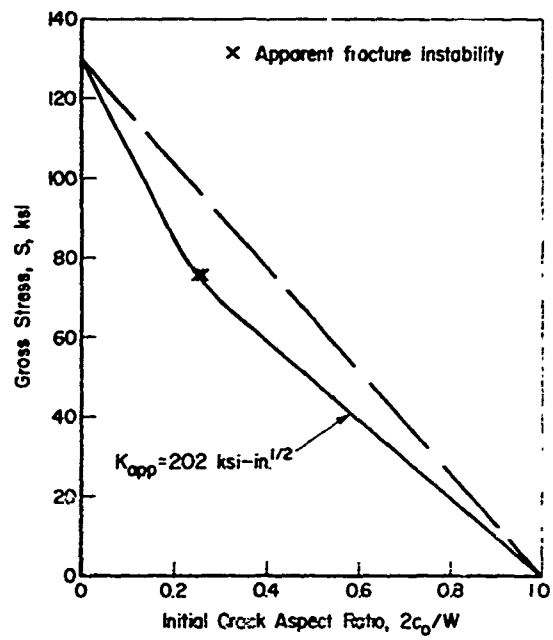
FIGURE 9. DATA DISPLAYS FOR ONSET OF STABLE TEAR AND FRACTURE INSTABILITY



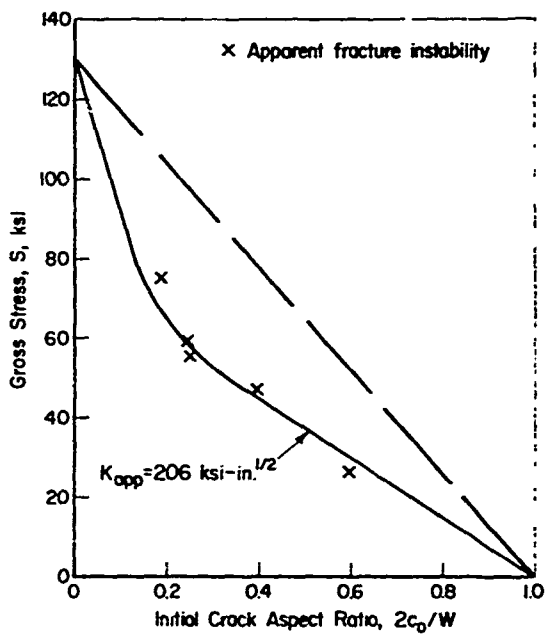
(a) 9.6-inch-wide panel



(b) 16-inch-wide panel



(c) 18-inch-wide panel



(d) 32-inch-wide panel

FIGURE 10. RESIDUAL STRENGTH DATA DISPLAYS

distinctly within the elastic regime (i.e., below the dashed line, net section yielding condition). To determine an average value for the linear tangents model, a characteristic value of the stress-intensity factor parameter,  $K$ , is determined for each data point of the data set in accordance with the procedures of Reference (4). These individual  $K$  values are then summed and averaged for the entire set. The resultant average  $K$  value is used to determine the unique continuous curve representative of that data set.

In each portion of Figure 9, two sets of data points are shown. The fracture instability points represent the instantaneous stress-crack size conditions at instability as determined from film records. The 5 percent secant-offset data points represent those data associated with onset of nonlinearity (i.e., manifestation of both slow crack extension and limited plasticity) on the load record.

For the 9.6, 16, and 18-inch-wide panel data, displayed in Figures 9(a), 9(b), and 9(c), respectively, net section yielding appears to be an approximate criterion for fracture instability. Hence, no linear-tangents curve is determined for these three data sets. However, as illustrated in Figure 9(d), the corresponding data for the largest panel width (32 inches) are well below the net section yielding condition as defined by the dashed line. Thus, the fracture criterion is considered to be elastic instability and the linear-tangent model is applied. Analysis by this technique indicates that a  $K_c$  value of  $267 \text{ ksi-in.}^{1/2}$  is representative of this material. The minimum panel width which can be calculated from the size limit of Expression (13) in Reference (4) is

$$W_{\min} = 4.3 \left( \frac{K}{TYS} \right)^2 = 4.3 \left( \frac{267}{130} \right)^2 = 18.1 \text{ inches.}$$

This implies that the control tests were only marginally valid as would be expected from the net-section stress analysis.

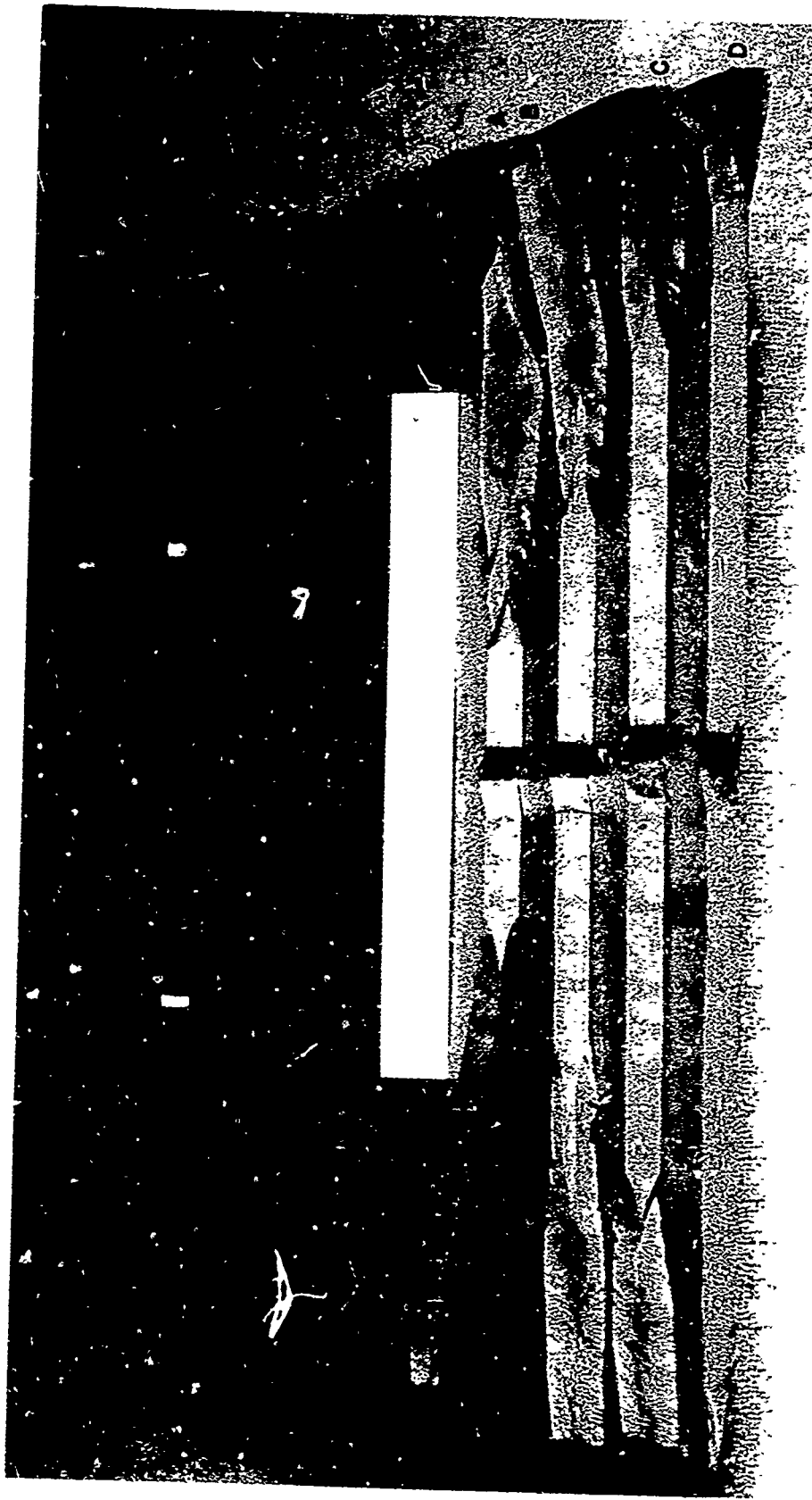
Each portion of Figure 9 also contains a linear-tangent curve fit to the data associated with the onset of nonlinearity, or the threshold of slow stable tear as determined by the 5 percent secant-offset criterion. It can be noted that the average  $K_o$  values for each panel width are different, but appear to stabilize for widths greater than 18 inches. This implies that there is an influence of width on the onset of slow stable tear. It is also interesting to note that if the right-hand linear tangent on each curve is projected or extended to the ordinate axis, the intercepts fall in the range of 40 to 60 ksi. This is

equivalent to the net section stress which exists on the uncracked ligament and corresponds to a range of one-third to one-half of the tensile yield strength. This behavior correlates closely to the observations on threshold of cracking in the aluminum alloy of Phase I. Thus, it appears that the onset of threshold of cracking in the rising load test may be associated with a critical net section stress or strain level, while final fracture remains an energy instability.

The residual strength (or notch concept) interpretation of fracture data is illustrated in Figure 10. The data are displayed on a format of initial crack aspect ratio and maximum gross stress at fracture. Since the extent of slow crack growth or stable tear is not evident on this type of plot, the significance of the net section stress cutoff is not emphasized. As the panel width increases the calculated average  $K_{app}$  values appear to increase asymptotically to a value of about  $205 \text{ ksi-in.}^{1/2}$ . This asymptotic behavior is the only indication of a limiting elastic instability condition.

#### Crack Surface Characteristics

The fracture surfaces of the 1/4-inch titanium specimen exhibited full shear on all test specimens. A representative set of fractured specimens is displayed in Figure 11. The sequence of crack aspect ratios is shown. The central flat smooth surface is the result of the fatigue precrack. At the end of the precrack, a short transition region (one to two thicknesses in length) from flat to full shear fracture is noted.



<u>Specimen</u>	<u>Specimen No.</u>	<u>2c/W</u>	<u>Specimen</u>	<u>Specimen No.</u>	<u>2c/W</u>
A	9CC17	0.2	C	9CC01	0.6
B	9CC02	0.4	D	9CC15	0.8

FIGURE 11. SURFACES OF 9.6-INCH-WIDE FRACTURE SPECIMENS

Fatigue-Crack Propagation

In this portion of the research program, the effects of panel width, maximum cyclic stress, stress ratio, and frequency on fatigue crack propagation in 1/4-inch-thick mill-annealed Ti-6Al-4V titanium alloy plate were evaluated. A total of 24 specimens as indicated in Table 2 were allocated specifically to this study. The basic crack length-cycle count data are recorded in Appendix A. These data have been analyzed and interpreted in terms of general crack growth characteristics, terminal crack growth behavior, and panel lifetimes. These results are summarized in this section of the report. Additional analyses are provided in the Data Analysis Section.

Crack-Growth Curves

The basic experimental data derived on this program and recorded in Appendix A are summarized graphically in crack-growth curves of Figures 12 through 16. In these figures crack length is plotted versus cycle count for each panel width to permit a visual comparison of the relative effects of maximum cyclic stress and stress ratio within each panel size. Although all fatigue cracks were initiated from similar starter notches, precracking for the low stress tests was accomplished by a procedure of stepping down from higher stresses in order to avoid prolonged initiation times. For a common basis of comparison, the crack growth curves have been referenced to growth from either 3/4-inch (0.75) crack length or a 1-inch crack length.

In these figures, continuous lines have been plotted over the range of data recorded. As will be discussed in the next section, terminal points could not always be identified positively. Where such points are estimated, they are indicated by a + symbol. Where positive measurements could be made by means of striations, this symbol is enclosed in a circle. Voids between terminal points and data curves indicate the rapid growth taking place during the final cyclic interval.

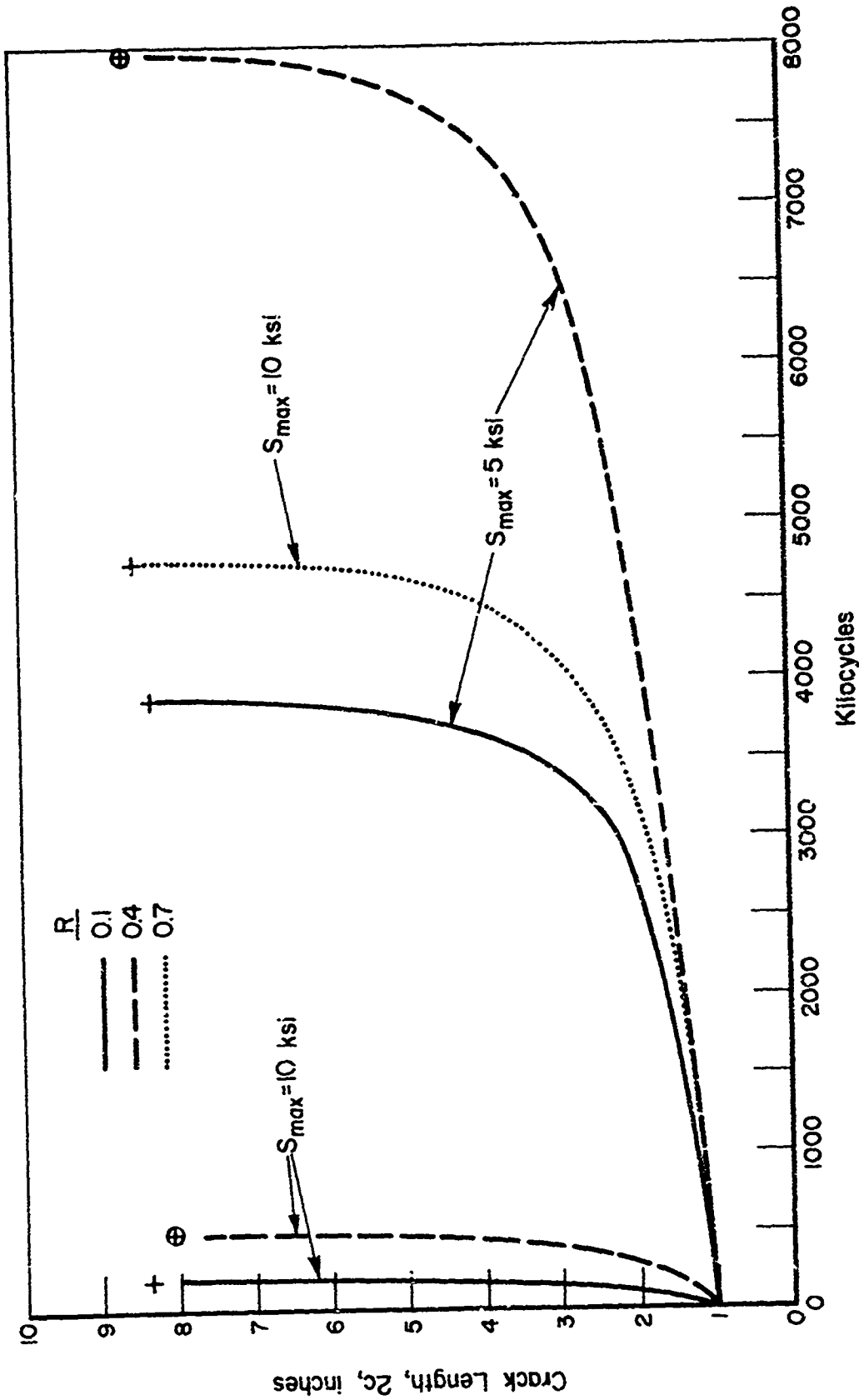


FIGURE 12. FATIGUE CRACK GROWTH IN 9.6-INCH WIDE PANELS AT LOW STRESS LEVELS

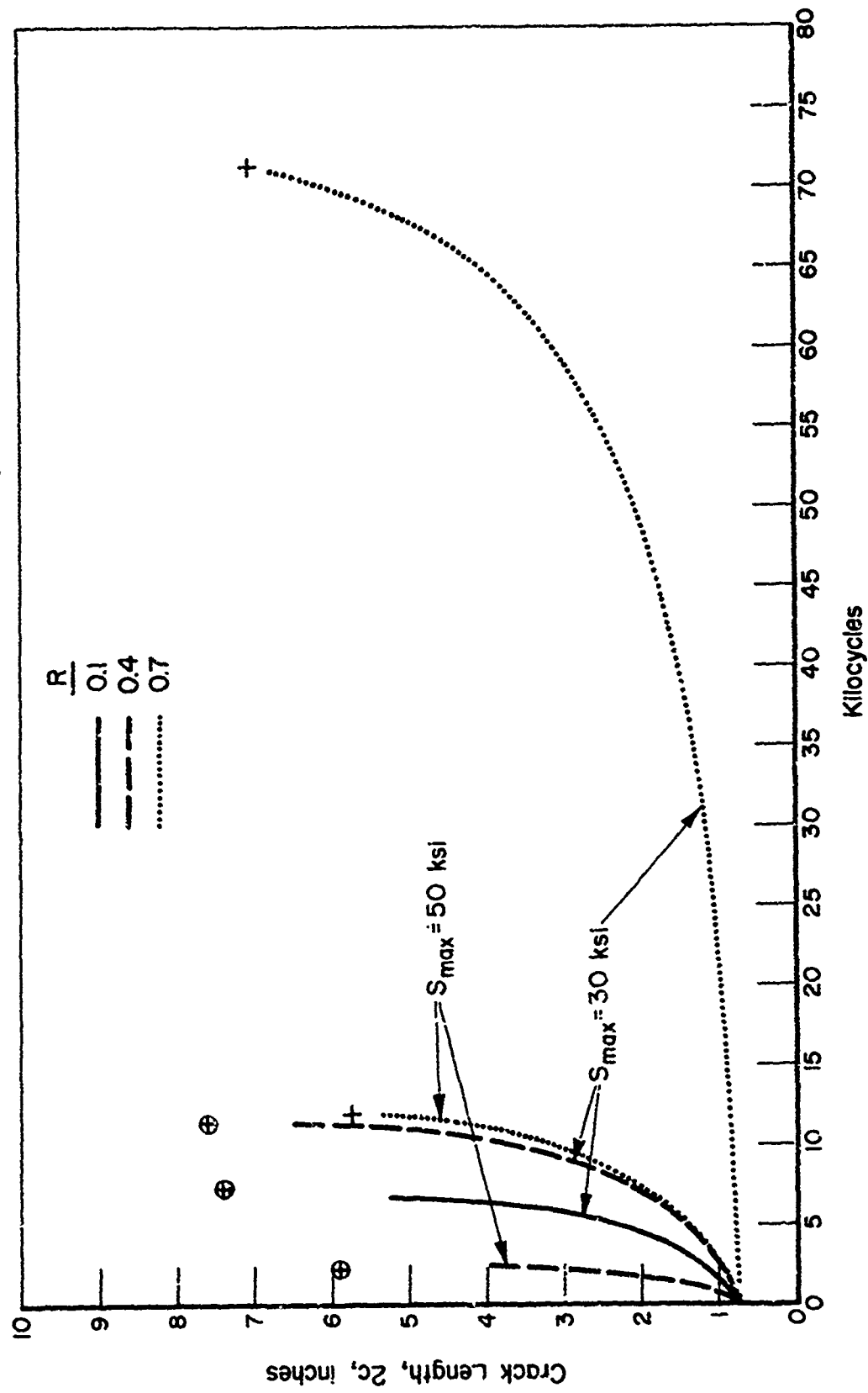


FIGURE 13. FATIGUE CRACK GROWTH IN 9.6-INCH WIDE PANELS AT HIGH STRESS LEVELS

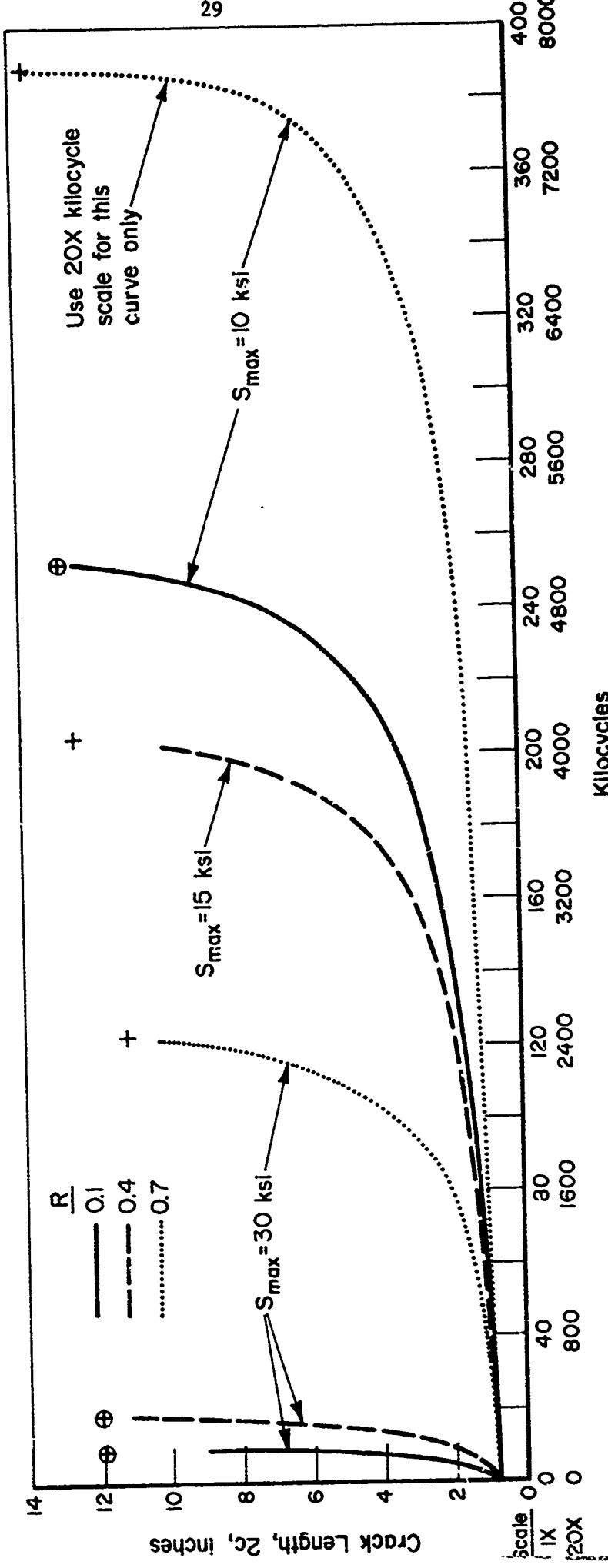


FIGURE 14. FATIGUE CRACK GROWTH IN 16-INCH WIDE PANELS AT MODERATE STRESS LEVELS

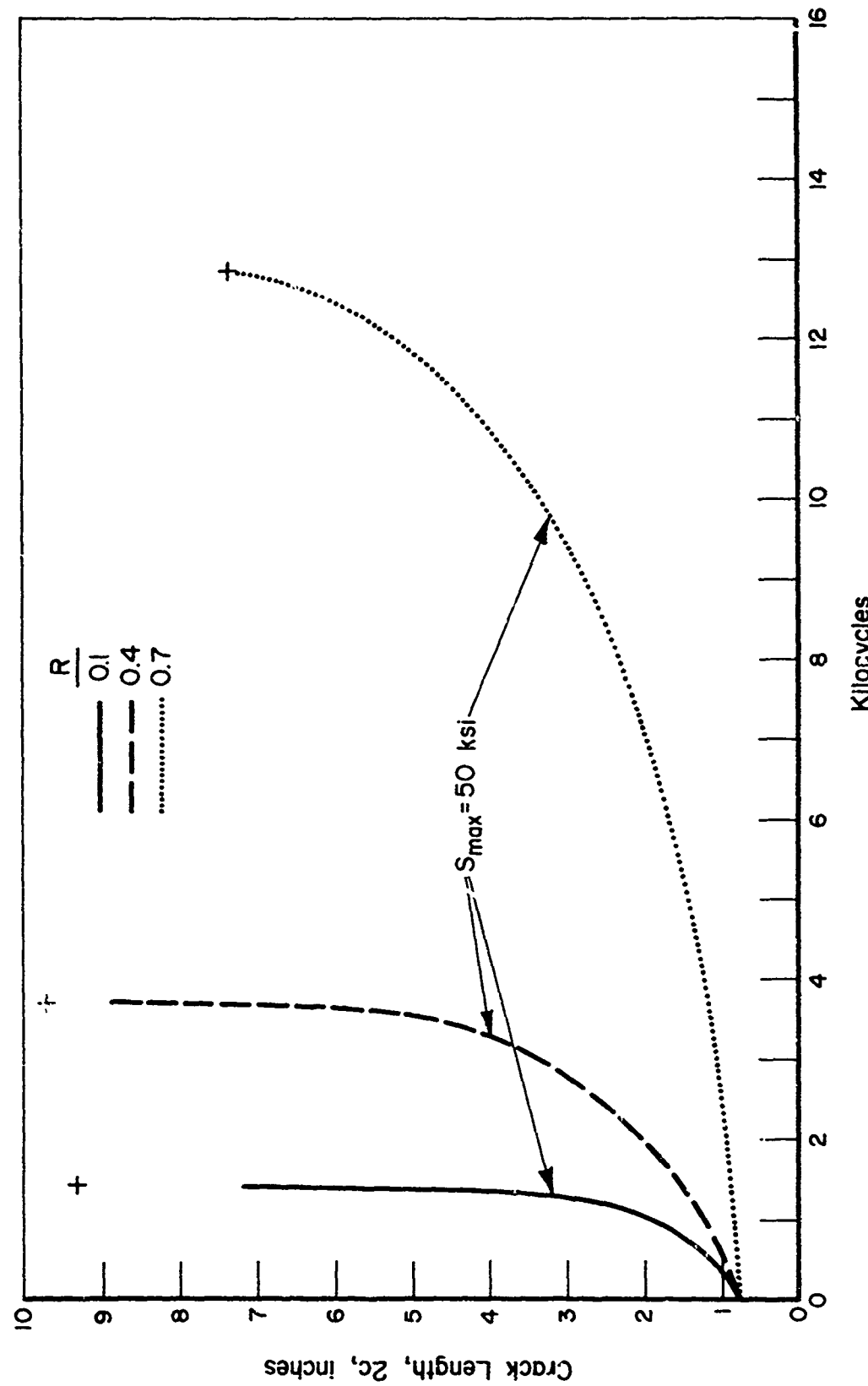


FIGURE 15. FATIGUE CRACK GROWTH IN 16-INCH WIDE PANELS AT A HIGH STRESS LEVEL

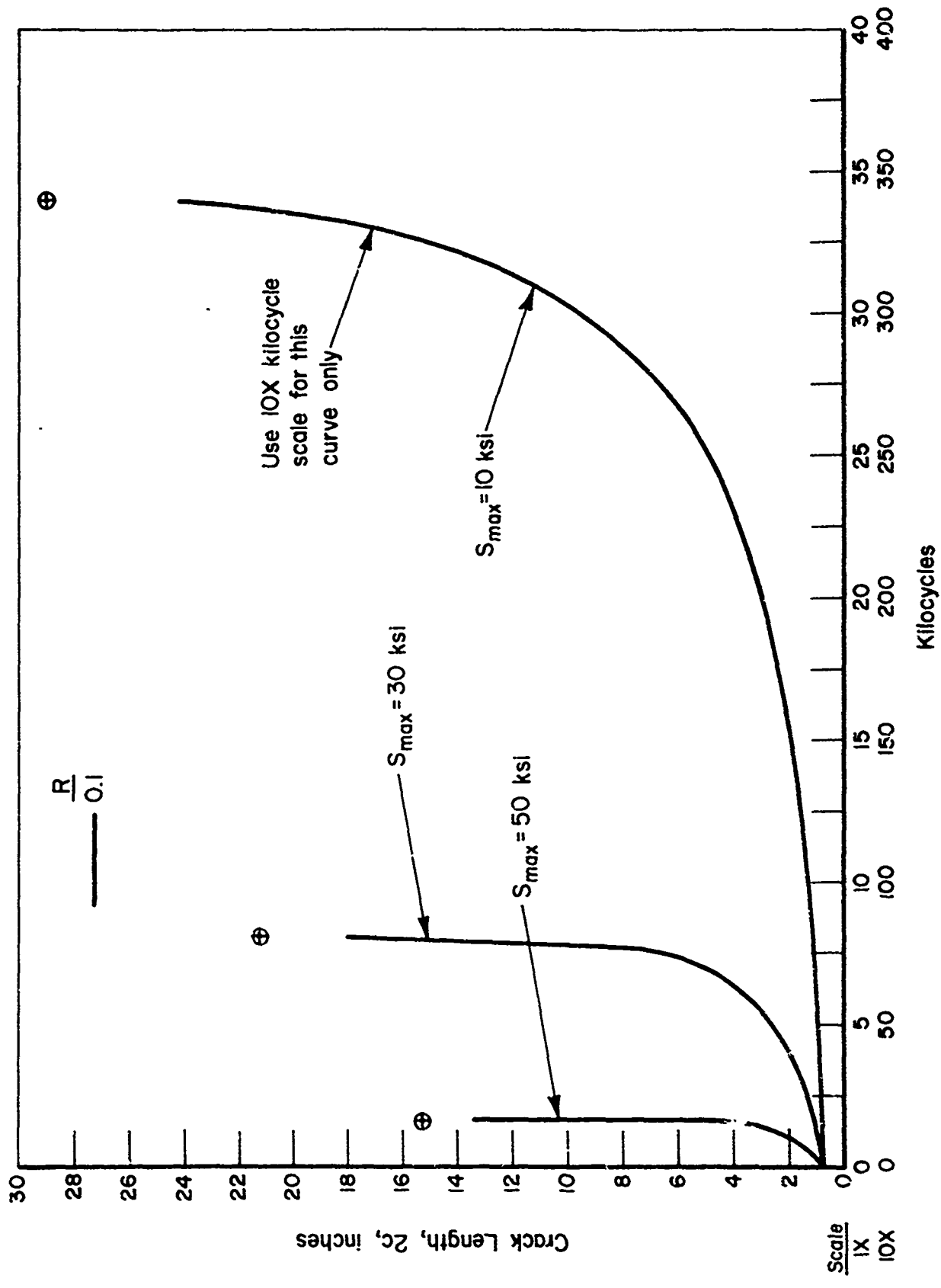


FIGURE 16. FATIGUE CRACK GROWTH IN 32-INCH WIDE PANELS AT  $R = 0.1$

The crack growth curves obtained in 9.6-inch-wide panels are shown in two figures (Figures 12 and 13), because of the grossly different ranges of cyclic lives associated with the low (5 and 10-ksi) maximum cyclic stresses and the high (30 and 50-ksi) maximum cyclic stresses. In Figure 12, crack growth is referenced to a 1-inch crack length for the low maximum cyclic stresses. As would be expected, cyclic life is shortened by increased maximum stress and lengthened by increased stress ratio. In Figure 13, crack growth data from a 3/4-inch crack length at the high maximum cyclic stresses are displayed. The behavior is very regular. It should be noted that the cyclic scale span is one-hundredth that of the previous figure.

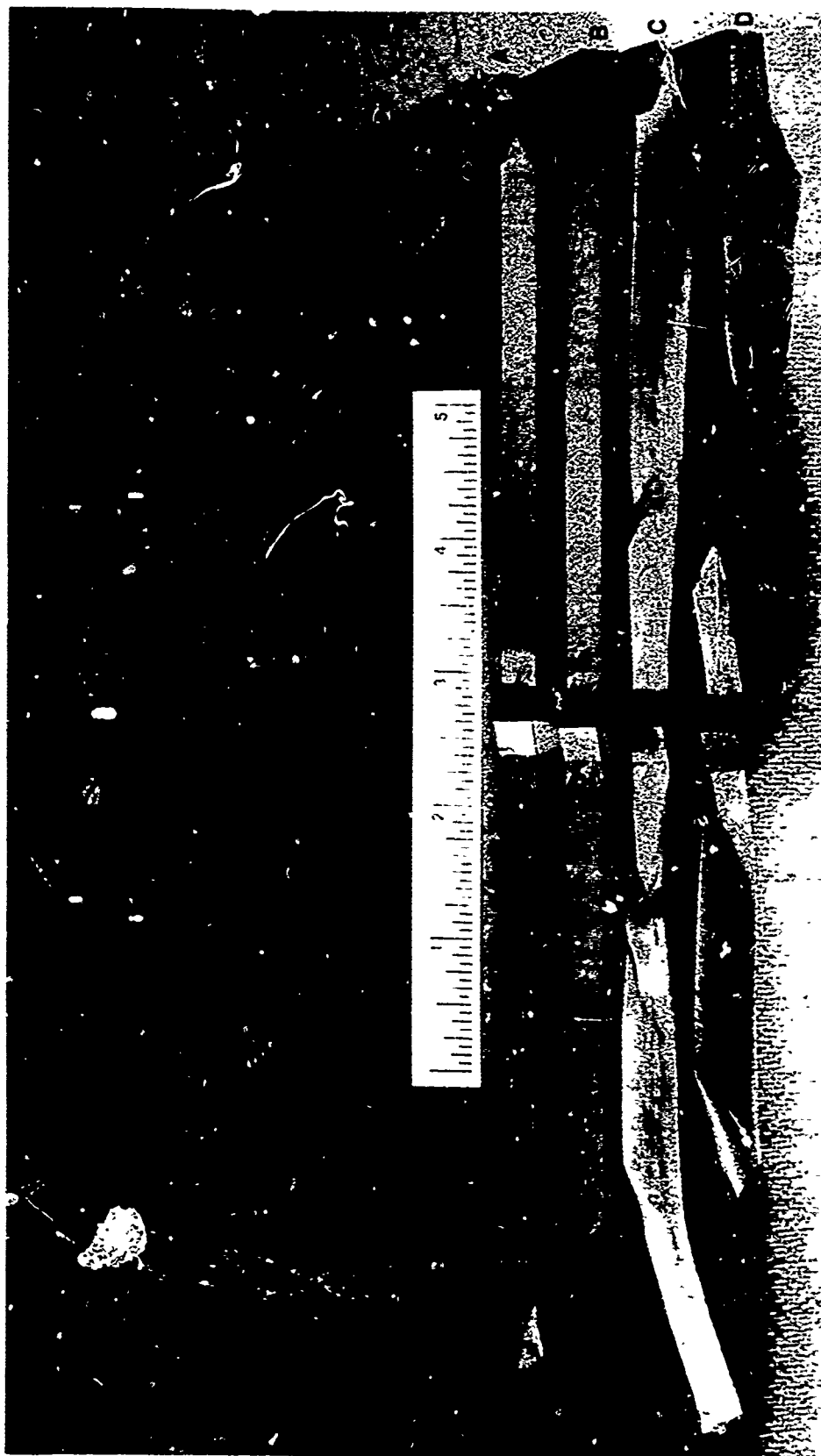
The crack growth curves obtained from 16-inch-wide panels are illustrated in Figures 14 and 15 for different maximum cyclic stresses. The broad range of cycle counts for this test series necessitated the use of two figures. Note that in Figure 14 behavior of one specimen was scaled down 20-fold to incorporate it within this reference grid.

For the 32-inch-wide panels, the crack growth curves for the single stress ratio, 0.10, at all three maximum stresses, are shown in Figure 16. Regular behavior, consistent with the other panel widths, is observed.

#### Crack Surface Observations

The topography of the fatigue crack surfaces is influenced both by the maximum cyclic stress and by the stress ratio. The maximum cyclic stress appears to control the general angularity or shear behavior of the surface. As maximum cyclic stresses increase, greater variations in angularity across both the thickness and width are evident. Local surface texture appears to be influenced primarily by the stress ratio. An increase both in surface roughness and in clarity of the terminal striations is noted with decreasing stress ratio.

The general variations in crack surface topography are illustrated in Figure 17 for four different maximum cyclic stress levels on 9.6-inch-wide specimens tested at a stress ratio,  $R = 0.4$ . The overall surface topography becomes more rugged with increasing maximum cyclic stress. The surface texture and striation markings evident here are also evident at  $R = 0.1$ , but they vanish into a more satin finish at  $R = 0.7$ .



<u>Specimen</u>	<u>Specimen No.</u>	<u>S<sub>max</sub></u>	<u>Specimen</u>	<u>Specimen No.</u>	<u>S<sub>max</sub></u>
A	9CC14	5 ksi	C	9CC05	30 ksi
B	9CC07	10 ksi	D	9CC10	50 ksi

FIGURE 17. SURFACES OF 9.6-INCH-WIDE FATIGUE-CRACK PROPAGATION SPECIMENS TESTED AT  $R = 0.4$

### Terminal Crack Behavior

In order to establish a useful failure criterion or end condition for fatigue-crack propagation, it is necessary to be able to identify the material characteristics which influence terminal crack instability. The data generated on this experimental program have been evaluated to gain further insight to this condition.

As the fatigue cracks advance toward instability, surface measurements were made with increasing frequency in an attempt to pinpoint the crack length immediately prior to final instability. In general, this was unsuccessful due to the rapid advance of the crack at this stage. However, in many cases, it was possible to detect and measure the last striation after fracture as a marker of the final crack length. Furthermore, from fundamental characteristics of the crack growth curve, it is possible to extrapolate a reasonably close, yet conservative, estimate of the final crack length from the three last measurements. This procedure, its results, and a comparison with final striation measurements (where available) are presented in Appendix B.

To assess the terminal conditions of fatigue-crack propagation, the applied stress-intensity factor for each maximum cyclic stress level is displayed as a function of the advancing crack length in Figures 18 through 20 for the three panel widths. In these figures, it is expected that the applied stress-intensity factor increases with increasing crack length in a continuous manner until one of two failure conditions is reached. Either the average net section stresses will exceed the tensile yield or ultimate strength and failure will occur by overload, or elastic instability will be triggered when the applied stress-intensity factor exceeds the critical fracture toughness,  $K_c$ . The former case would be expected for the narrow (9.6 and 16-inch) panels, while the latter mode would be expected for the wide (32-inch) panels.

The stress-intensity factor formulation used is

$$K = S \sqrt{\pi c} \sec \frac{\pi c}{W}. \quad (1)$$

On these curves, the terminal points are illustrated by symbols which identify the stress ratio and indicate whether the point is an actual final striation measurement or an estimated value, preference being given to the former, where available. Limiting lines denoting conditions of net section yielding, net

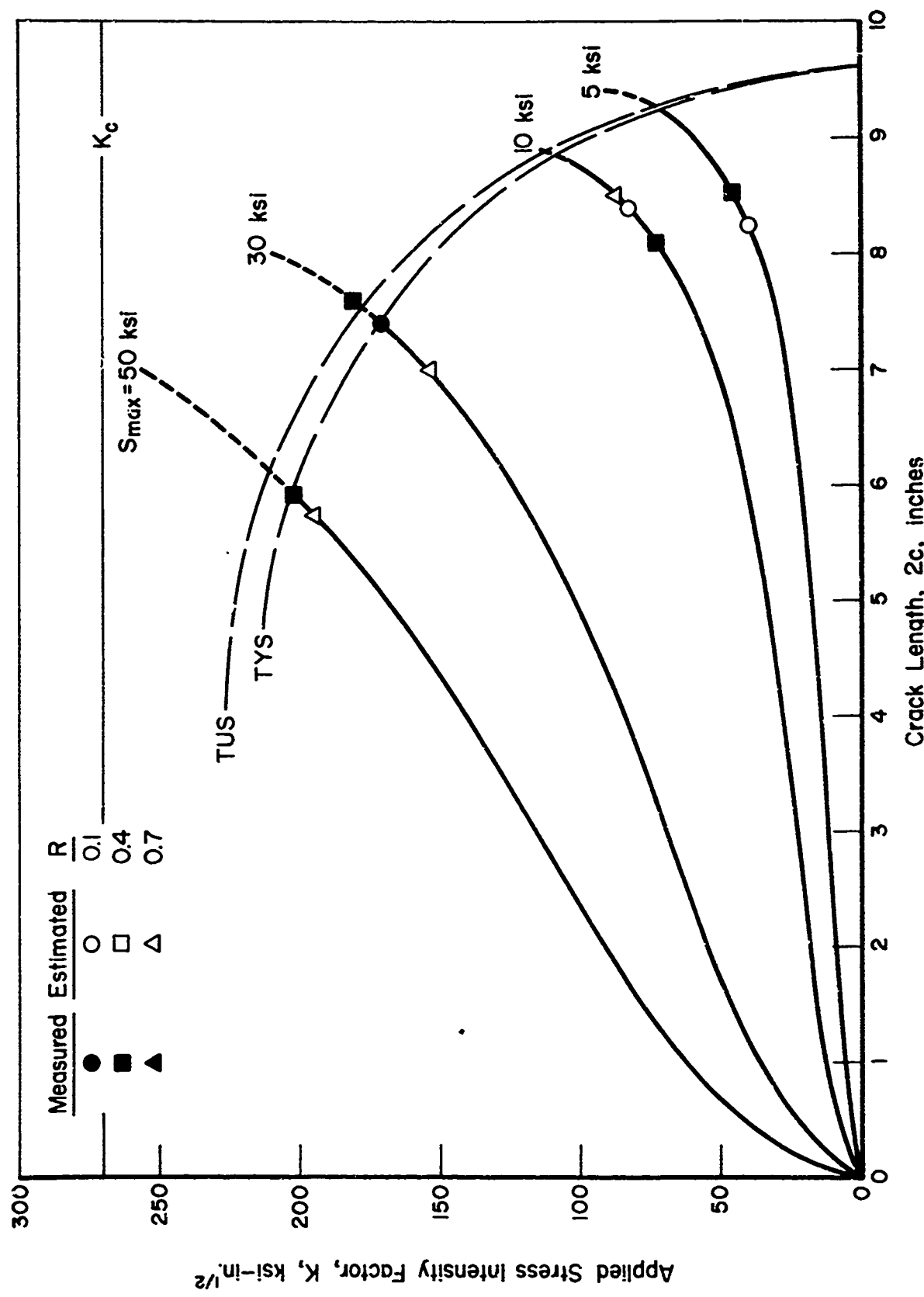


FIGURE 18. TERMINAL CRACK BEHAVIOR IN 9.6-INCH WIDE PANELS

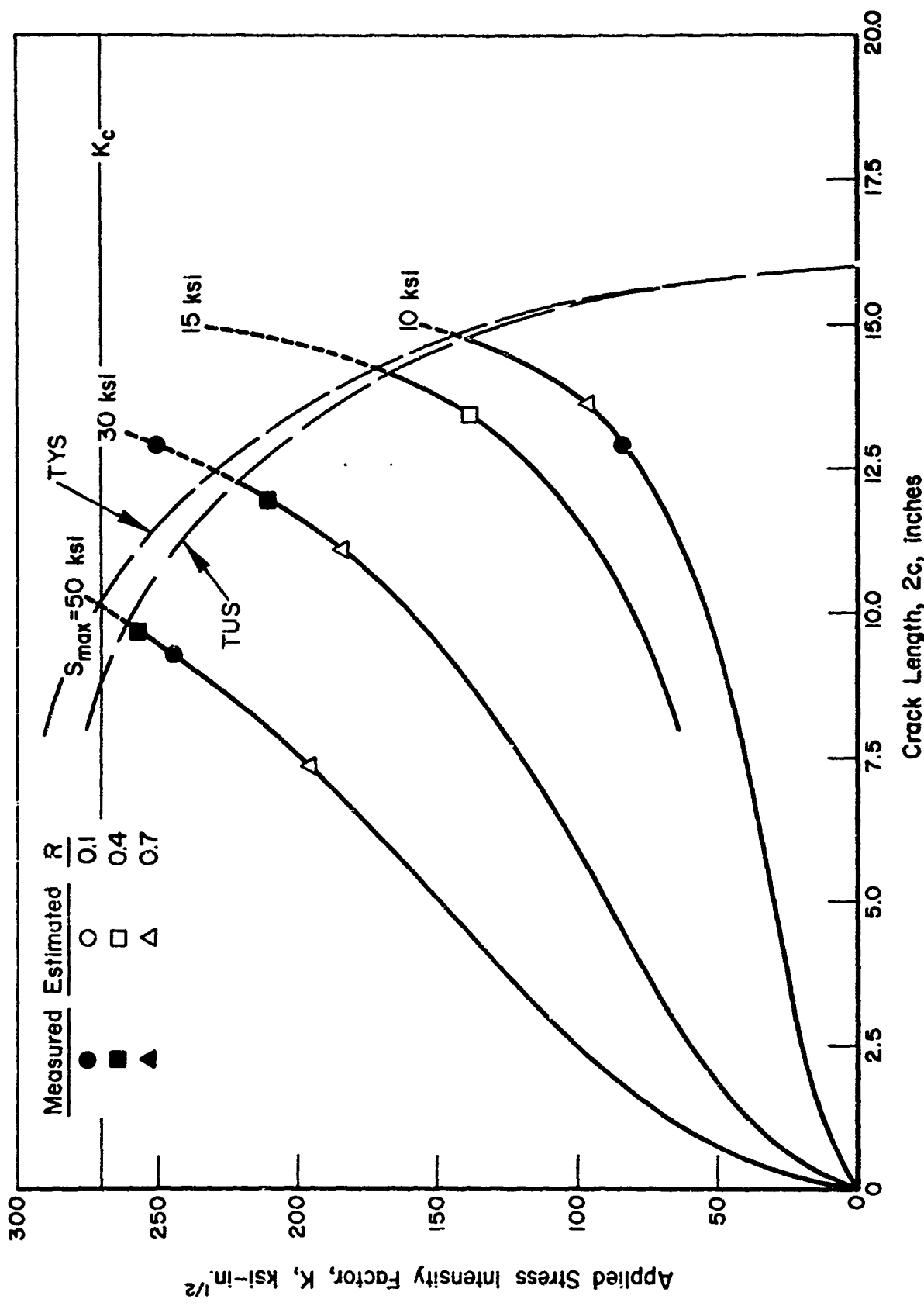


FIGURE 19. TERMINAL CRACK BEHAVIOR IN 16-INCH WIDE PANELS

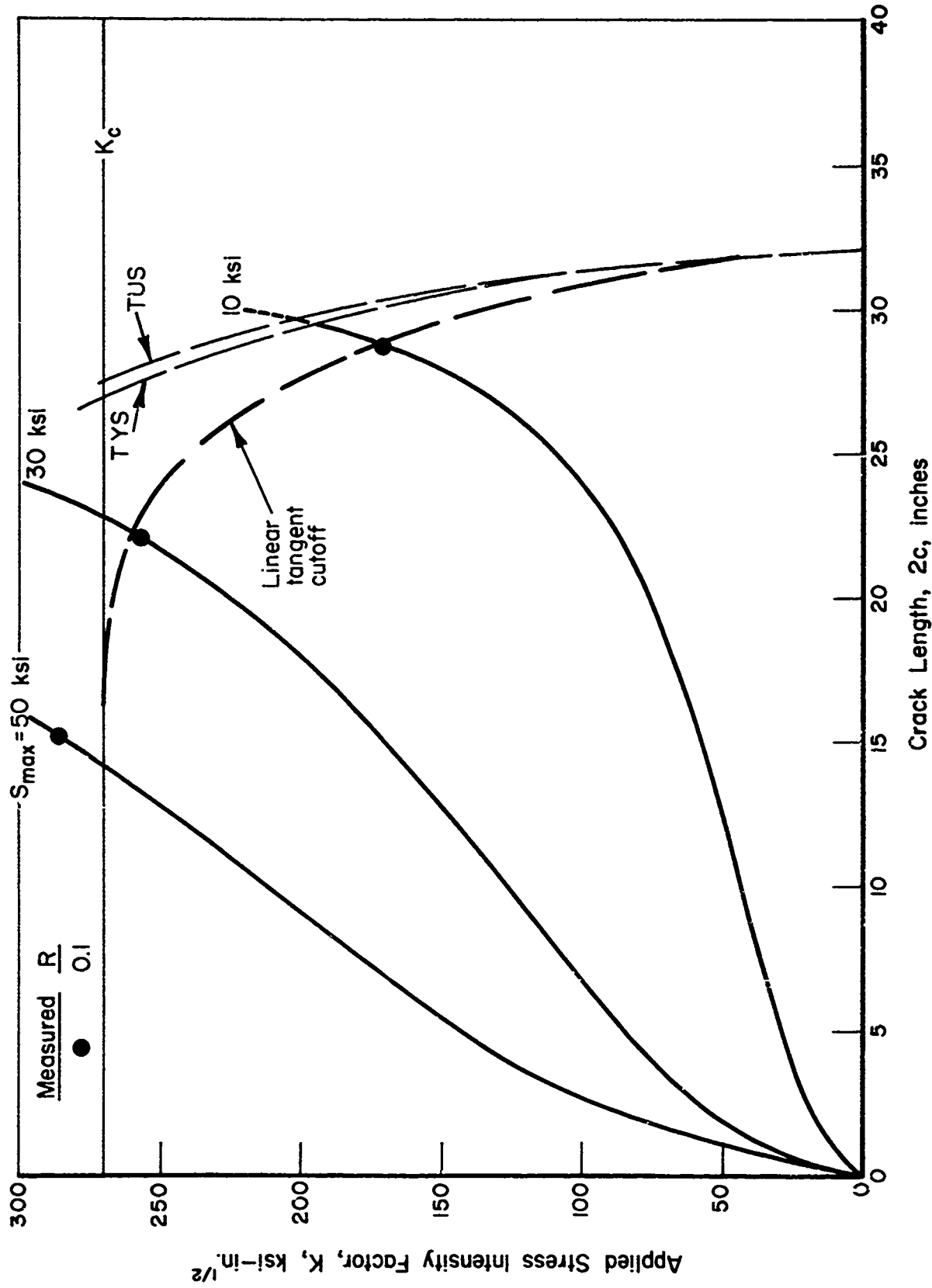


FIGURE 20. TERMINAL CRACK BEHAVIOR IN 32-INCH-WIDE PANELS

section ultimate strength, and critical fracture toughness,  $K_c$ , are superimposed as natural limits on terminal instability. The net section stress lines are introduced by substituting the net section stress defined by

$$S_n = S/(1 - 2c/W) , \quad (2)$$

into Expression (1) to obtain

$$K = S_n (1 - 2c/W) \sqrt{\pi c \sec \pi c/W} . \quad (3)$$

Then by equating  $S_n$  to either TYS or TUS, the loci of points described by

$$K_{tys} = TYS(1 - 2c/W) \sqrt{\pi c \sec \pi c/W} , \quad (4)$$

and

$$K_{tus} = TUS(1 - 2c/W) \sqrt{\pi c \sec \pi c/W} \quad (5)$$

can be established as reference limits.

The behavior of fatigue crack growth in 9.6-inch-wide panels is illustrated in Figure 18. At the higher maximum cyclic stress levels, it is apparent that net section yielding is a reasonable criteria for these narrow panels which are not subject to an elastic-type fracture. At the lower maximum cyclic stress levels, however, the actual terminal conditions are not close to either a net-section yielding condition or an elastic fracture condition.

The terminal behavior of fatigue-crack growth in 16-inch-wide panels is illustrated in Figure 19. The correlation between the measured or estimated terminal points and the hypothesized failure conditions appears to be similar to that for the 9.6-inch-wide panels. The higher maximum cyclic stress level tests (measured values) appear also to be limited by a net-section-yield criterion, while the low cyclic stress level tests fall short of either failure condition.

The terminal fatigue-crack-propagation behavior in 32-inch-wide panels is shown in Figure 20. The crack lengths for all three data points are the measured values and were easily discernible on the fracture surfaces. Since this panel width was large enough to exhibit elastic fracture instability, the linear tangents cutoff line has also been incorporated in Figure 20 and appears to be a valid fracture criterion for these data.

It is important to note that generally in these fatigue crack propagation studies failures were noted below the classical conditions of elastic fracture instability. In the case of the 9.6- and 16-inch wide panels, the geometrical limitations of panel size imposed critical net section stress constraints before elastic fracture condition could be achieved. That is, these panel widths were less than the minimum for which elastic fracture instability would be expected. However, as was the primary purpose of this portion of the program, these panel sizes were studied to evaluate the validity of elastic stress intensity factor concepts for describing the fatigue crack growth process in panels which may be subsized relative to terminal fracture conditions.

In the case of the 32-inch wide panels where terminal elastic fracture instability would be expected, such did occur in accord with the linear tangents model and well below the  $K_c$  criterion. Although these data are limited in quantity, they are consistent in their trend. They appear to indicate that there is a complex interaction between elastic instability and net section yielding, and that strict adherence to a  $K_c$  criterion may be an unconservative prediction of failure conditions at large crack lengths.

### Stress-Lifetime Summary

An immediate grasp of the general fatigue-crack-propagation response of this material product form can be gained from Figure 21. Specimen lifetimes extending from a reference 1-inch crack length are indicated for the various maximum cyclic stresses and panel widths. It is obvious that for given maximum cyclic stresses, lifetimes decrease with increasing stress-intensity factor range (i.e., decreasing stress ratio). It is also interesting to note that panel lifetimes do not increase significantly with panel width. This, of course, is due to the fact that once a crack is established and propagating in a panel, its growth increases geometrically. Mere doubling or quadrupling of the width does little to stem this rapid progress.

### Frequency Effects

The test matrix of this program did not permit an extensive evaluation of frequency effects. However, the data are consistent in revealing that no distinct frequency effects are apparent in the 5 to 25 Hz range of cycling. As cycling approaches 1 Hz one distinct example of frequency effect can be noted among the 32-inch-wide panel data. This will be illustrated in the Data Analyses section. The summary result is that at 1 to 2 Hz, effective cyclic growth rates may be increased about 50 percent in a laboratory atmosphere of  $50 \pm 10$  percent relative humidity. Although this is very limited evidence, it is an effect that should be evaluated further, preferably in a more concentrated (but yet representative) aqueous or vapor environment.

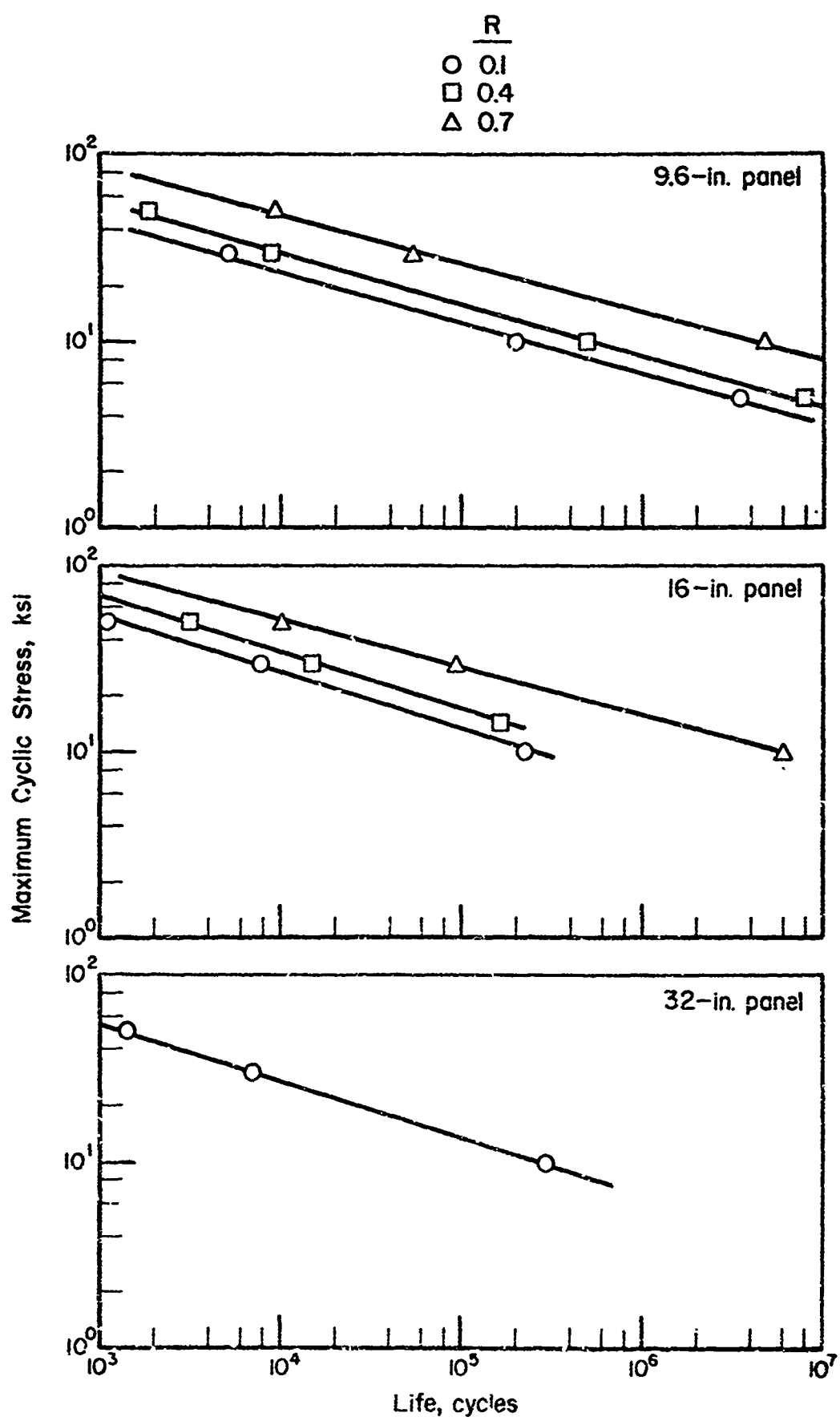


FIGURE 21. CYCLIC LIFETIMES OF PANEL FROM 1-INCH CRACK LENGTH

## DATA ANALYSES

Further analyses of the experimental data derived on this program are presented in this portion of the report. Since the fracture and residual strength results were discussed when presented earlier, the following evaluations are limited to the fatigue-crack-propagation data. These data have been analyzed to characterize material behavior and to assess the design value of the particular modeling technique. In the following subsections are presented rate analyses, power law modeling, and panel life prediction.

### Crack-Propagation Rates

The most important aspect of the fatigue-crack-propagation (FCP) studies is the evaluation of the rate process and the manner in which it is influenced by cyclic stress range, stress ratio, panel width, and frequency. It is this information which is used in the design function to predict the required inspection intervals and safe structural life for airframe structures.

In this program, fatigue-crack-propagation (FCP) rates have been analyzed in terms of the stress-intensity factor range,  $\Delta K$ . The results of the 24 FCP tests, as well as the supporting data derived from the precracking of fracture test panels indicate that the stress-intensity factor range is the dominant variable. Stress ratio has a significant, but secondary, influence over and above that reflected with the  $\Delta K$  variable. With one exception, it appears that the crack-propagation rates are independent of frequency and panel width (other than that reflected in the finite width correction included in  $\Delta K$ ) over the range considered. The one exception is the rate data for the wide (32-inch) panels cycled at 1 and 2 Hz at relatively high values of  $\Delta K$ . The accelerated rates observed at this frequency are associated with the synergistic effect of laboratory air humidity. In general, maximum stress itself does not appear to be influential except as it is contained in the stress ratio mentioned above.

As the maximum stress-intensity factor approaches the critical fracture toughness,  $K_c$ , of the material, a definite acceleration in fatigue crack growth rates is noted. However, this is not apparent as a distinct factor until  $K_{max}$  is approximately 90 ksi-in.<sup>1/2</sup> or greater as evidenced in Figures 23, 24, and 25.

In the following subsections, the fatigue-crack-propagation rates are graphically related to the stress-intensity factor range for each stress

ratio and panel width. Then, in the following section, these data are analyzed in accordance with a power law model of rate behavior.

Stress Ratio, R = 0.1. The rate of fatigue-crack propagation at a stress ratio of 0.1 for the three panel widths (9.5, 16, and 32 inches) are displayed in Figures 22, 23, and 24, respectively. Each figure contains at least three different maximum cyclic stress levels as indicated by the different symbols. The general overlap and continuity of the data trends indicate that there is no significant effect of maximum cyclic stress, other than that implicit to the stress ratio.

Over most of the test range, i.e.,

$$10 \text{ ksi-in.}^{1/2} < \Delta K < 90 \text{ ksi-in.}^{1/2},$$

the rate logarithm appears to be linear with respect to the  $\Delta K$  logarithm in these three figures. Over this range, the rate behavior for all three panel widths agrees quite closely.

At the lower end of the data band, i.e., where

$$\Delta K < 10 \text{ ksi-in.}^{1/2},$$

there is a noticeable decay in FCP rates, and considerably more scatter among the data. The rate decay is attributed to threshold effects; the scatter is believed to be intrinsic to the measurement inaccuracies at short crack lengths and low stress levels.

At the high end of the data band, i.e., where

$$\Delta K > 90 \text{ ksi-in.}^{1/2},$$

there is distinct evidence of rate acceleration as the applied  $K_{max}$  approaches a critical  $K_c$  value. In the 32-inch-wide panels, this departure from linearity is noted at  $\Delta K$  levels of about  $80 \text{ ksi-in.}^{1/2}$ .

The largest inconsistency noted in these figures occurs in the 32-inch-wide panel data of Figure 24. There is a missignment of the rate data development at 10 ksi with that developed at the two higher stresses. This is

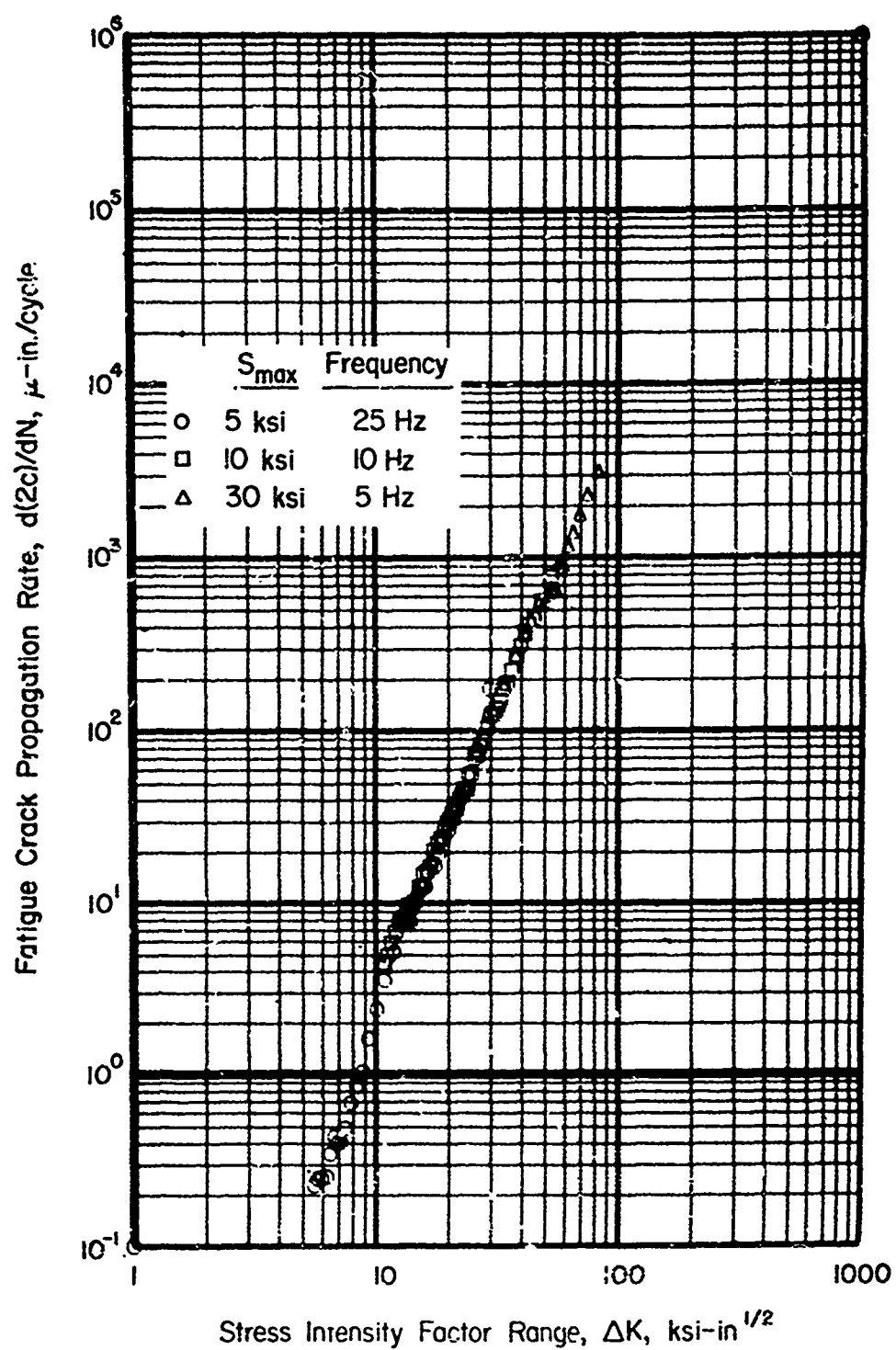


FIGURE 22. FATIGUE-CRACK-PROPAGATION RATES AT  $R = 0.1$   
IN 9.6-INCH-WIDE PANELS

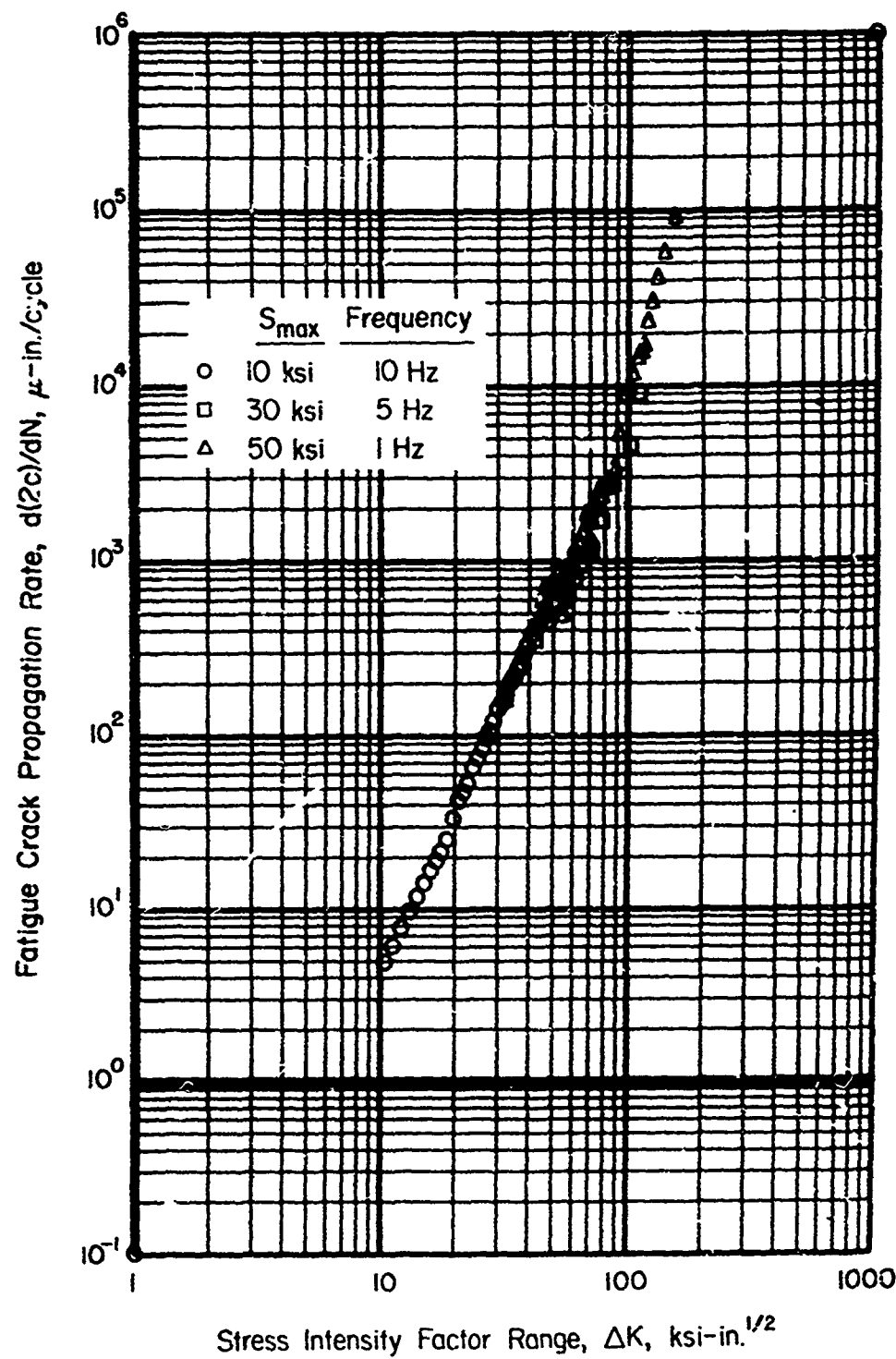


FIGURE 23. FATIGUE-CRACK-PROPAGATION RATES AT  $R = 0.1$   
IN 16-INCH-WIDE PANELS

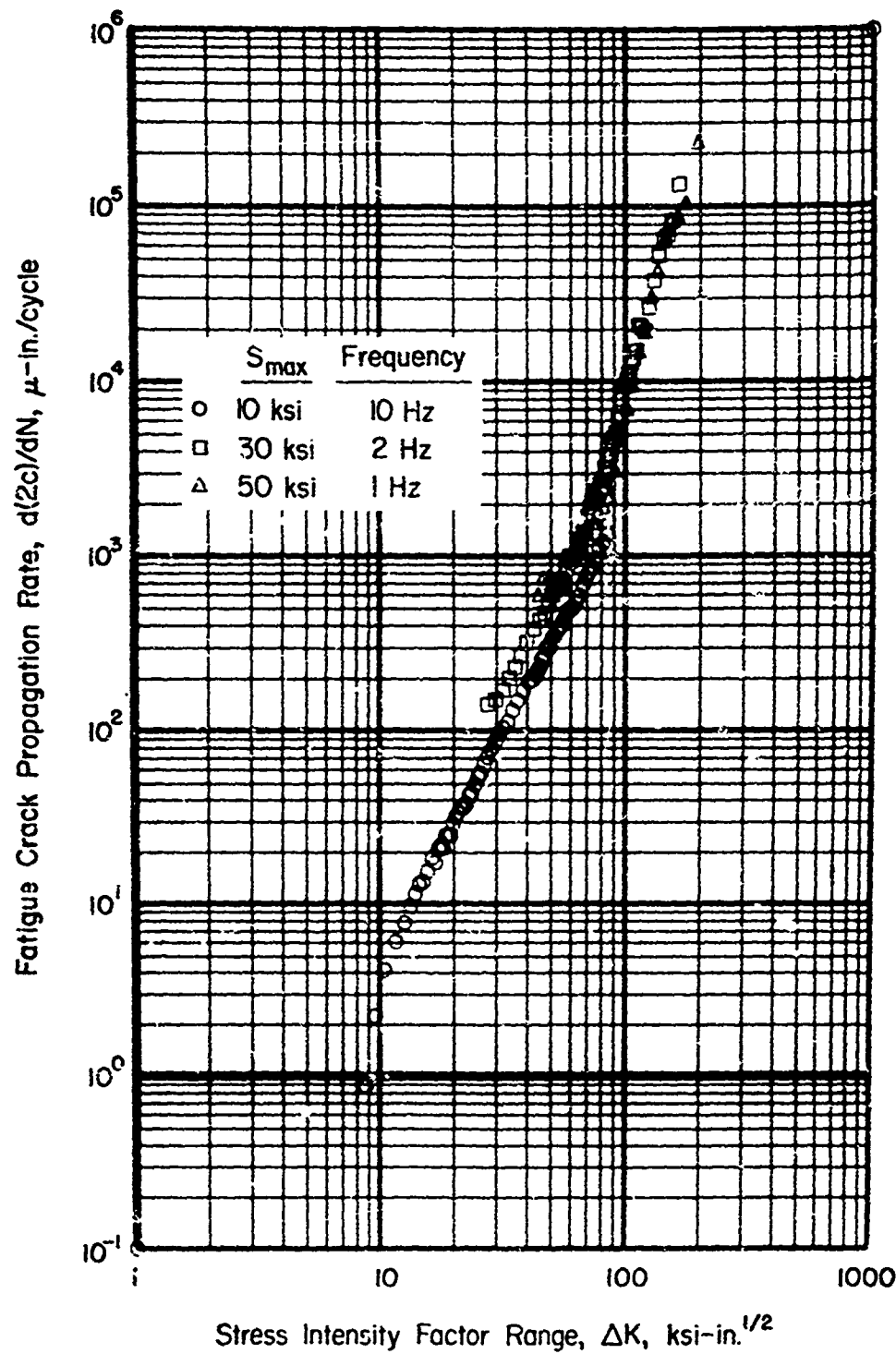


FIGURE 24. FATIGUE-CRACK-PROPAGATION RATES AT  $R = 0.1$   
IN 32-INCH-WIDE PANELS

considered to be a manifestation of frequency effects as mentioned earlier. The 10-ksi rate data were generated at 10 Hz, while the higher stress data were generated at 2 and 1 Hz, respectively.

Stress Ratio, R = 0.4. The influence of an increased stress ratio is illustrated in Figures 25 and 26 for 9.6 and 16-inch panel widths, respectively. Both of these figures exhibit more scatter along the data trend than did the previous figures; however, they still correlate closely with each other. Over the central  $\Delta K$  range of 10 to 90 ksi-in.<sup>1/2</sup>, rate behavior is approximately linear on the log-log coordinates.

In Figure 25, the rate behavior at four different maximum cyclic stress levels is shown. The overlap and continuity among the data indicate no particular effects of maximum cyclic stress and support those same observations from the  $R = 0.1$  tests. An increase in the scatter and some decay in the rate data can be seen for this stress ratio at  $\Delta K$  values of 4 and 5 ksi-in.<sup>1/2</sup>. In Figure 26, some terminal deviations from linearity in the general rate behavior are noted above a  $\Delta K$  value of 80 ksi-in.<sup>1/2</sup>.

The most significant effect that can be attributed to stress ratio is a slight increase in the crack-propagation rates. If one selects a reference  $\Delta K$  value of 30 ksi-in.<sup>1/2</sup>, Figures 25 and 26 for  $R = 0.4$  indicate a typical growth rate value of

$$d(2c)/dN \approx 2 \times 10^{-4} \text{ in./cycle} .$$

For the lower stress ratio,  $R = 0.1$  of previous Figures 22 through 24, a value of

$$d(2c)/dN \approx 1.5 \times 10^{-4} \text{ in./cycle}$$

is noted at 30 ksi-in.<sup>1/2</sup>.

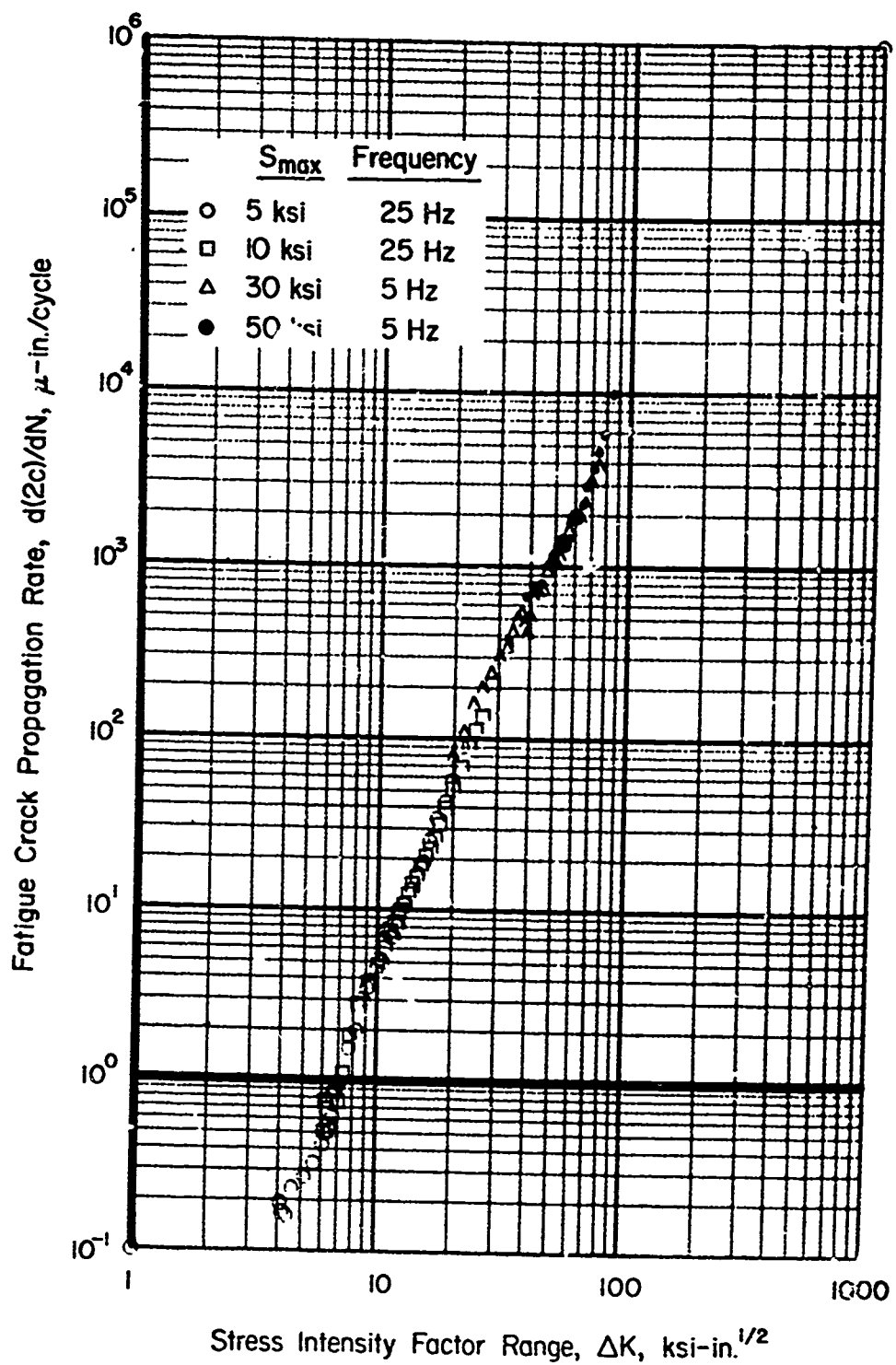


FIGURE 25. FATIGUE-CRACK-PROPAGATION RATES AT  $R = 0.4$   
IN 9.6-INCH-WIDE PANELS

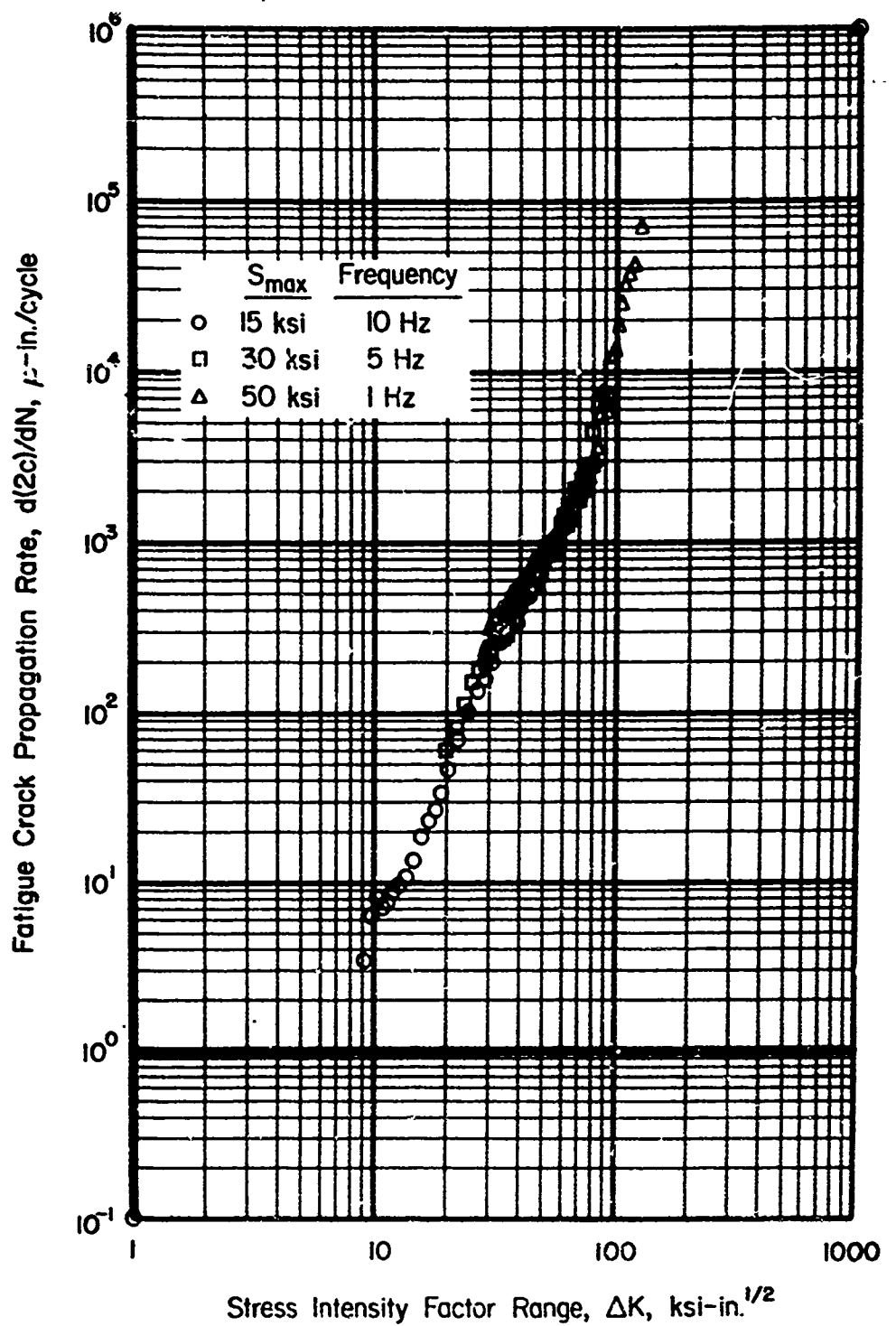


FIGURE 26. FATIGUE-CRACK-PROPAGATION RATES AT  $R = 0.4$   
IN 16-INCH-WIDE PANELS

Stress Ratio, R = 0.7. Regular and consistent fatigue-crack-propagation rate behavior continues to be observed at this stress ratio which is the highest in the program. Figures 27 and 28 illustrate the  $d(2c)/dN$  data for 9.6 and 16-inch-wide panels, respectively. (Note the coordinate scale change in these figures.) A significant acceleration in the propagation rates is noted for this stress ratio in comparison with the previous. At a  $\Delta K$  value of 30 ksi-in.<sup>1/2</sup>,

$$d(2c)/dN = 3.5 \times 10^{-4} \text{ in./cycle} ,$$

or almost doubling the rate for the corresponding  $\Delta K$  level at a stress ratio of 0.4.

In both figures, linearity is observed over most of the testing range. In Figure 28, a threshold  $\Delta K$  level is apparent at  $\Delta K$  values of 3 to 4 ksi-in.<sup>1/2</sup>. At the higher propagation rates, i.e., where

$$\Delta K > 20 \text{ ksi-in.}^{1/2} ,$$

a slight inflection in the general rate trend is noted for this stress ratio on both figures. Although a specific mechanism for this behavior cannot be cited, it does not appear to be more severe than the minor scatter evident in the preceding results when considered on equivalent coordinate scales.

#### Power Law Modeling

Representation of fatigue-crack-propagation rate behavior by various analytical models has been considered previously in Phase I. In that work it was concluded that the Forman-Kearney-Engle<sup>(5)</sup> relation was the most versatile means of modeling experimental data at the present time. This same approach has been utilized in this program.

The basic fatigue-crack-propagation data of Appendix A have been fit by the rate model

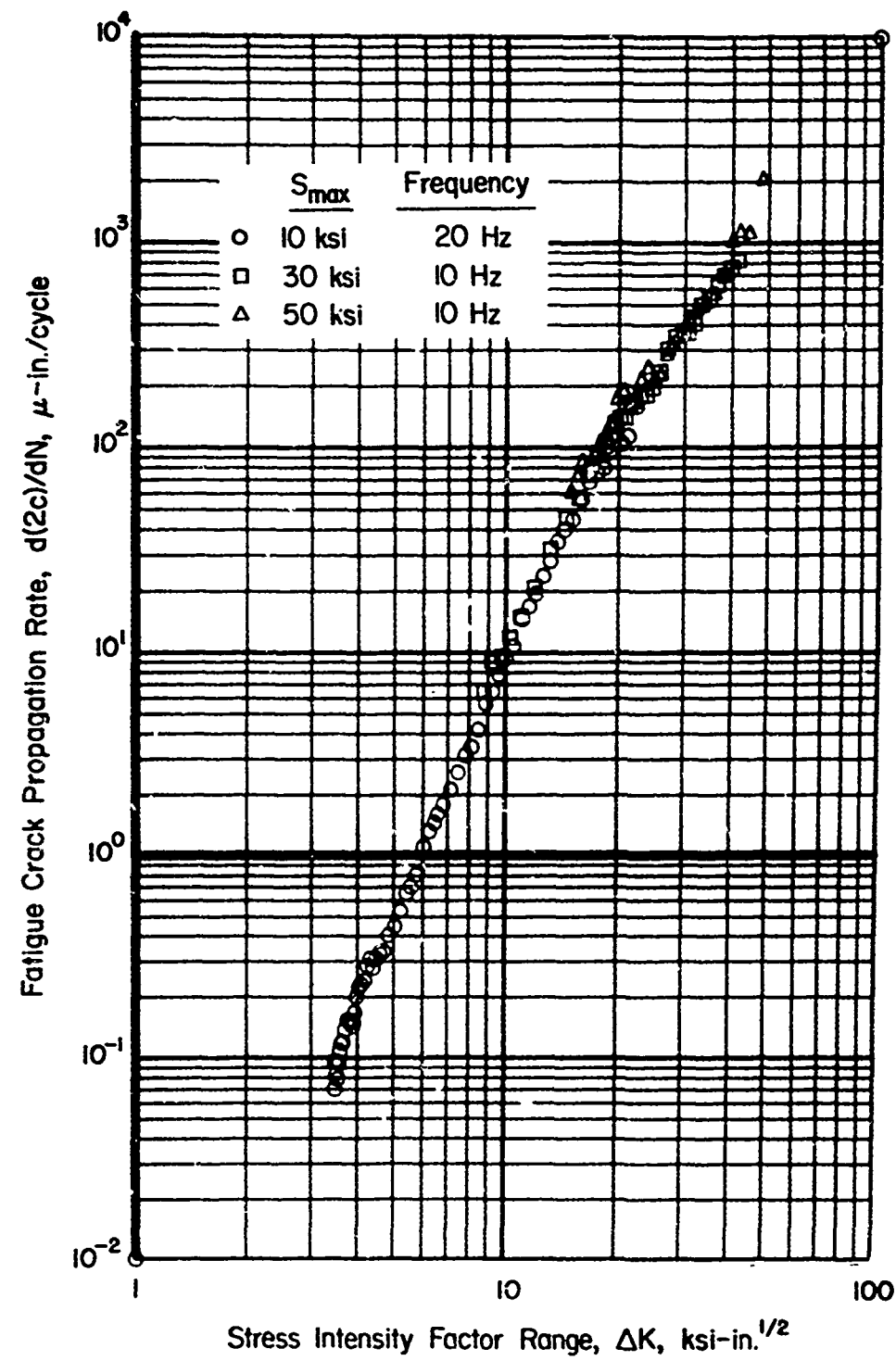


FIGURE 27. FATIGUE-CRACK-PROPAGATION RATES AT  $R = 0.7$   
IN 9.6-INCH-WIDE PANELS

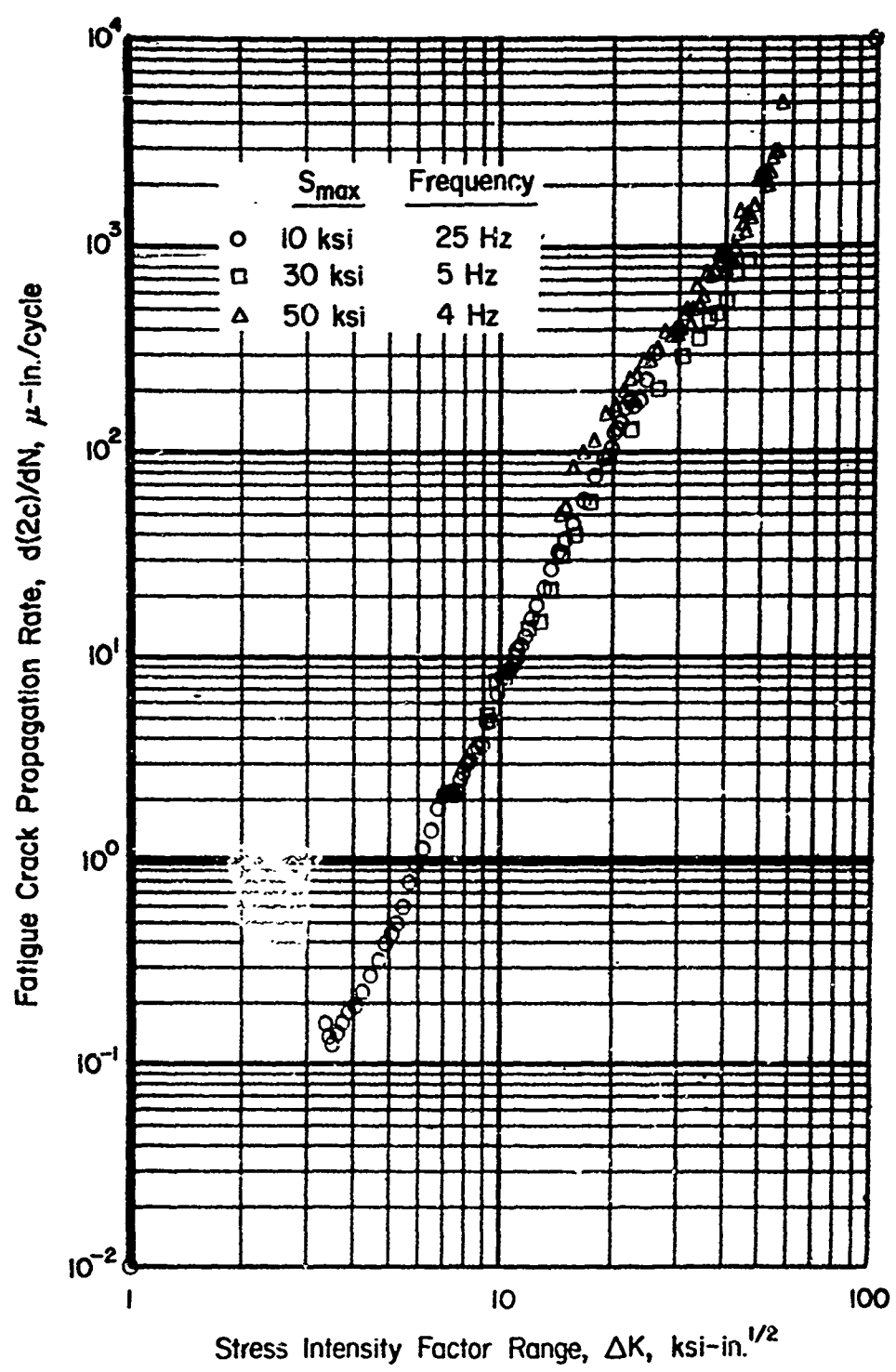


FIGURE 28. FATIGUE-CRACK-PROPAGATION RATES AT  $R = 0.7$   
IN 16-INCH-WIDE PANELS

$$\frac{d(2c)}{dN} = \frac{C(\Delta K)^n}{(1-R)K_c - \Delta K} \quad (6)$$

in a least squares regression. The coefficient, C, and exponent, n, which result from this analysis, characterize the material performance in accord with this and only this rate model.

Table 4 summarizes the results of this analysis for each individual data set, groupings of data sets by panel width and stress ratio, and a composite of all data sets. The average C and n values associated with the successive groupings of data in this analysis are a cumulative regression computation of Equation (6) including all individual data points in that group. An alternate scheme, as used in Reference 1, is simply to average the net results of the individual specimens. In this instance, the former technique was selected because there was a considerable variation in total number of data readings per specimen. Hence, a more representative average would be expected by weighing in all data points.

It can be noted that there are significant numerical variations in C and n values among the individual data sets. However, this is a consequence of the modeling technique, and should not be interpreted as implying grossly different rate behavior over the range of applicability. As will be discussed in the Observations on Curve Fitting Fatigue Crack Propagation Data section, there is a regularity in the variations of C and n such that the rates are indeed consistent.

As the data sets are combined into larger and larger groupings (moving to the right-hand side of Table 4), the C and n values represent larger data samplings over a wider range of parameters. These values converge to an aggregate average of

$$C = 0.267 \mu\text{-in./cycle}$$

and

$$n = 3.30$$

for 22 specimens.

The agreement of the aggregate average C and n values with the basic data is illustrated in Figure 29. A shaded band of all experimental data for each stress ratio is shown along with the best-fit rate curve based on the aggregate average C and n values.

TABLE 4. RESULTS OF FATIGUE CRACK PROPAGATION RATE ANALYSES USING FORMAN-KEARNEY-ENGLE MODEL

Specimen No.	Panel Width W inches	Stress Ratio R	Max Stress Smax ksi	Individual Data Sets		Common Width And Stress Ratio C n	Stress Ratio C n	Composite of All Data Sets C n
				C	n			
9CC13	9.6	0.1	5	.0564	3.89			
9CC12			10	.5600	3.13			
9CC04			30	.680	2.73			
16CC10	16	0.1	10	.936	3.02			
16CC02			30	.30	2.63			
16CC07			50	.0766	3.61			
32CC06	32	0.1	10	2.46	2.59			
32CC05			30	.198	3.39			
32CC04			50	.140	3.44			
9CC14			5	.0833	3.87			
9CC07	9.6	0.4	10	.112	3.72			
9CC05			30	10.5	2.39			
9CC10			50	4.92	2.61			
16CC05			15	.756	3.02			
16CC11	16	0.4	30	7.09	2.42			
16CC09			50	2.81	2.69			
9CC11			10	.0560	3.99			
9CC06	9.6	0.7	30	1.91	2.71			
9CC09			50	14.7	2.13			
16CC12			10	.0788	3.78			
16CC01	16	0.7	30	1.11	2.73			
16CC16			50	14.4	2.14			

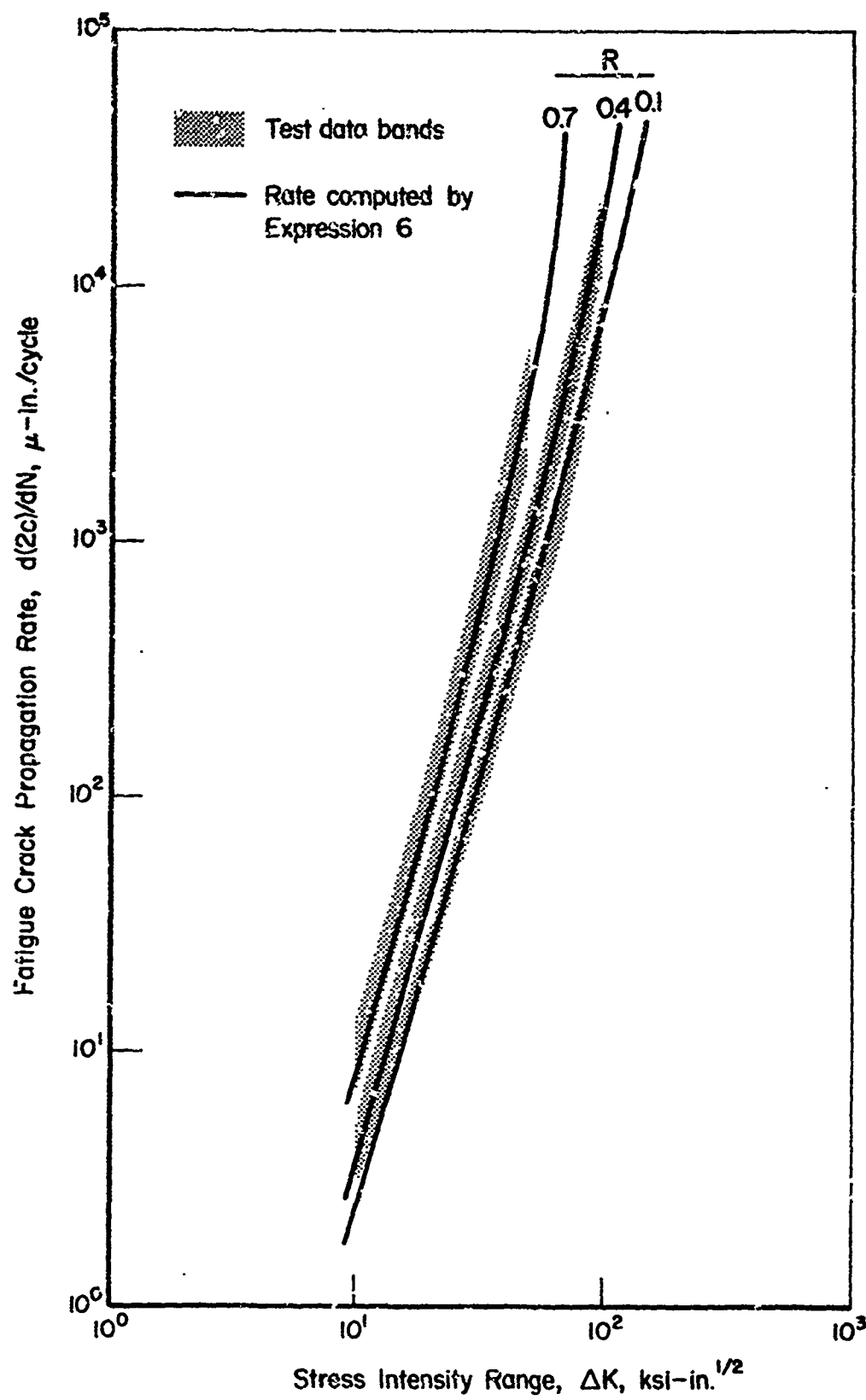


FIGURE 29. COMPARISON OF RATE DATA AND FORMAN-KEARNEY-ENGLE RATE MODEL

Crack Growth Prediction

The adequacy of a fatigue-crack-propagation model is best reflected in the reliability and accuracy with which it can be used in predicting crack growth. In the Phase I program studying an aluminum alloy, the life prediction program LIFE procedure was proposed as a simple, yet functional, procedure for integrating crack growth behavior. More recently, a generalized crack growth analysis program, CRACKS<sup>(6)</sup>, has been developed and made available. Although this analytical procedure was developed to accommodate variable amplitude loading with the more complex, attendant effects of retardation, it is still a useful integration procedure for straightforward constant-amplitude loading.

In this research study, program CRACKS has been utilized to predict the crack growth behavior of the test panels on the basis of the composite results. Using the values,

$$C = 0.267, n = 3.33, K_C = 267 \text{ ksi-in.}^{1/2},$$

from Table 4, a crack growth prediction for each test panel has been made. The results are summarized in Table 5.

In general, the predicted lives compare favorably with the actual lives. With three exceptions, the predictions deviate less than 40 percent from the actual values. This is believed to be quite good for the rates and cyclic counts involved. The three exceptions (i.e., deviations over 40 percent) all occur in the 9.6-inch-wide panels for the stress ratios least well fit by the average rate parameters. In these three cases, the prediction was conservative (i.e., overestimated) and is considered to be the result of the average rate curve being distinctly less than the scatterband illustrated in Figure 29.

TABLE 5. COMPARISON OF ACTUAL AND PREDICTED PANEL LIFETIMES

Specimen Number	Panel Width W inches	Max. Stress $S_{max}$ inches	Stress Ratio R	Panel Life From 1-inch Crack		Percent Deviation
				Actual kilocycles	Predicted kilocycles	
9CC13		5		3910.	2840.	-27.
9CC12	9.6	10	0.1	199.	275.	+38.
9CC04		30		5.4	6.2	+15.
16CC10		10		230.	320.	+39
16CC09	15	30	0.1	7.8	7.1	- 9.0
16CC07		50		1.0	1.0	0
32CC06		10		295.	355.	+20.
32CC05	32	30	0.1	6.9	7.7	+11.6
32CC04		50		1.4	1.1	-21.
9CC14		5		7965.	7260.	- 8.8
9CC07	9.6	10	0.4	488.	705.	+45.0
9CC05		30		8.8	15.9	+81.
9CC10		50		1.9	2.4	+26.
16CC05		15		167.	204.	+22.
16CC11	16	30	0.4	14.4	18.0	+25.
16CC09		50		3.1	2.7	-12.9
9CC11		10		4764.	3480.	-27.
9CC06	9.6	30	0.7	54.	78.0	+42.
9CC09		50		9.4	11.8	+26.
16CC12		10		6007.	4000.	-33.
16CC01	16	30	0.7	91.7	88.0	- 4.0
16CC16		50		10.1	13.0	+22.

DISCUSSION AND INTERPRETATION

The important, general observations, both experimental and analytical, which may be gleaned from these results of this program are briefly presented in the following subsections.

Fatigue-Crack-Propagation Behavior

Perhaps the most significant feature of the experimental work accomplished is the apparent consistency, uniformity, and linearity (on the log-log coordinate system) of the fatigue-crack-propagation rate data. The consistency and uniformity of the data imply that low scatter, high reliability, and reproducibility can be achieved when adequate and accurate measurements are made. The linearity of the data imply that the Paris model of crack propagation is indeed a useful model, and for this material is applicable to  $\Delta K$  levels up to nearly one-half of the  $K_c$  value.

The use of the Forman-Kearney-Engle model of fatigue-crack propagation does provide a useful refinement of the rate model as conditions of fracture instability are approached.

Terminal Crack Behavior

As the moderate to high stress level fatigue-crack-propagation tests approached fracture instability, there was an interaction evident between fatigue-crack propagation and the slow stable tear process usually noted in the residual strength or fracture tests. To the observer, it frequently appeared that if the cyclic load were sustained for a longer time increment at its maximum value (i.e., if the frequency were effectively reduced), fracture instability would occur at a crack length shorter than was actually noted. It seemed as though the rapid frequency of load application and load release did not permit the advancing crack sufficient time to accelerate into an unstable growth mode. Further study of frequency effects on terminal crack growth behavior would provide more insight into the crack instability process.

Observations on Curve-Fitting  
Fatigue-Crack-Propagation Data

Of the fatigue-crack-propagation rate analyses currently in vogue, that of Forman, Kearney, and Engle, and its parent developed by Paris<sup>(7,8)</sup> appear to be the most popular. Each of these models contains two parameters,  $C$  and  $n$ , which align the models in the coordinate system. The parameter  $C$  positions the curve on the ordinate axis, while the parameter  $n$  orients the direction (or slope of the line) as illustrated in Figure 30. In the Forman-Kearney-Engle model, an additional parameter, the toughness  $K_c$ , is introduced to accommodate terminal crack growth behavior. This provides a slight curvature to the straight line model (on log-log coordinates) originally proposed by Paris, and serves to provide a better data fit as the crack propagation approaches terminal instability. Although the absolute numerical values of  $C$  and  $n$  for each model are usually different, the essence of  $C$  and  $n$  is the same.

As illustrated in Figure 30, the parameter  $C$  is a numerical quantity remote to the actual experimental data. Slight variations in the experimental data (i.e., translations and rotations of the shaded data band), may be reflected as large changes in the numerical value of both  $C$  and  $n$ . For example, as the stress ratio is increased, propagation rates usually increase also. This may be manifested as both a translation and rotation of the data bands such that the "best-fit" curves flex through a wide range of  $C$  and  $n$  values. This has been seen already in the foregoing analysis. The large variance in  $C$  and  $n$  values does not imply grossly different rate behavior, it only reflects the coupling present within the model.

Because of this behavior, one cannot gain a comfortable intuition about the relative or comparative fatigue-crack-propagation behavior from the  $C$  and  $n$  quantities alone. It takes a much deeper investigation. Although it is beyond the scope of this task to develop a new model (and such an effort would probably add more confusion to this subject), it is appropriate to note that a greater physical significance could be attached to the current models if the parameters were "anchored" or identifiable with some distinctive feature within the data field rather than something remote to the data field. That is, for example, the physical reality of  $C_p$  at  $\Delta K = 1 \text{ ksi-in.}^{1/2}$  is of minimal value if propagation thresholds exist at stress-intensity factor ranges from 3

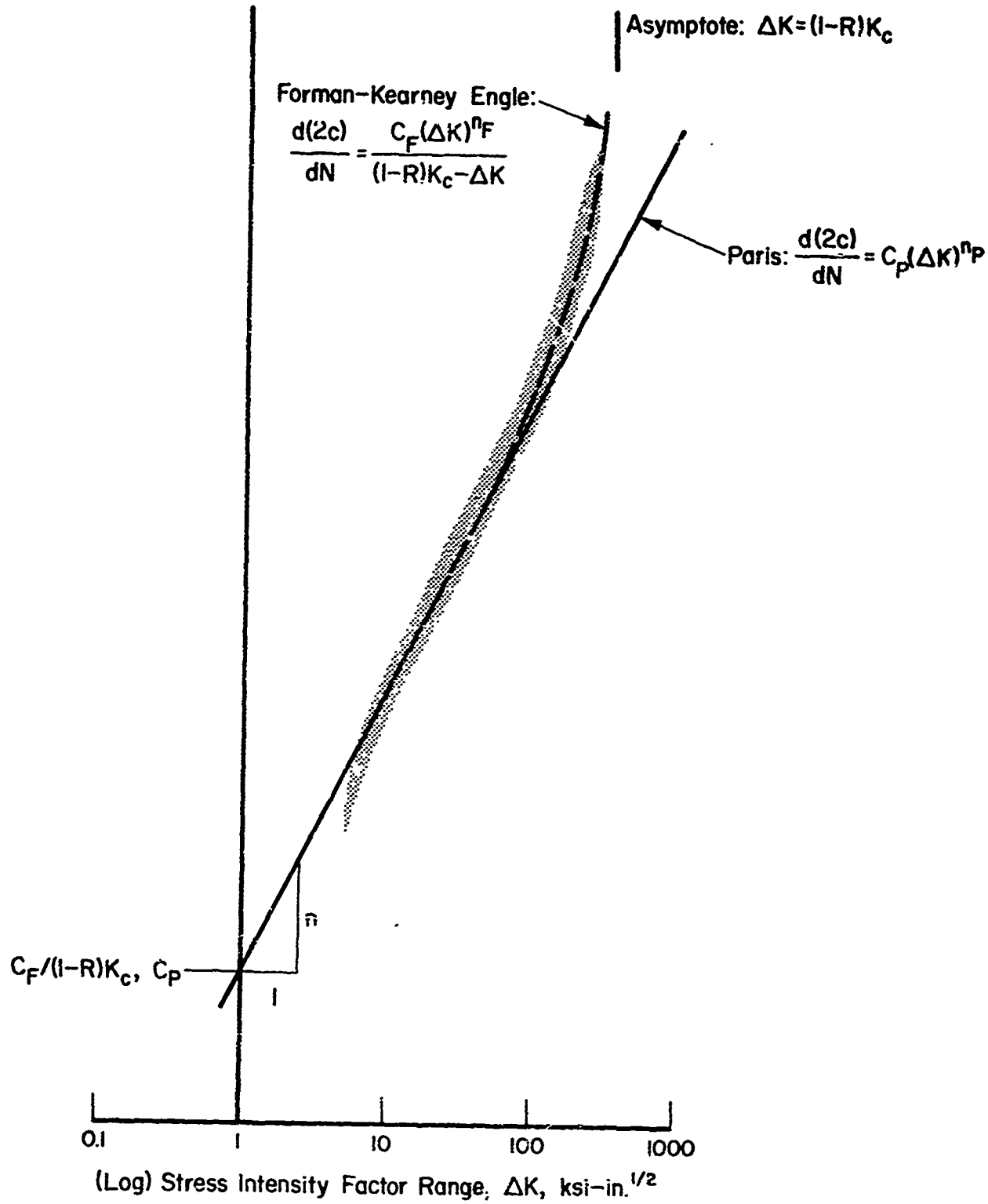
(Log) Fatigue Crack Propagation Rate,  $d(2c)/dN$ ,  $\mu\text{-in./cycle}$ 

FIGURE 30. FATIGUE-CRACK-PROPAGATION RATE MODELS

to 8 ksi-in.<sup>1/2</sup>. A more representative parameter may be something associated with a  $\Delta K$  value in the range of 20 to 50 ksi-in.<sup>1/2</sup>.

Another facet to be recognized is the impending importance of accommodating threshold behavior. It is evident that the current models are quite conservative in this regard. In this program, it was evident that the comparative predictions of the very long-life tests were always underestimated (see Table 5). This is due to the conservative (i.e., unrealistically high) FCP rates assigned to the low stress intensity factor levels.

#### Comparison of Phase I and Phase II Programs

To maintain the proper perspective on the experimental work which has been accomplished, it is appropriate to note some of the similarities and differences in Phases I and II, and their implications. The programs are similar in their goals of evaluating fracture and fatigue-crack-propagation characteristics of center-cracked tension panels of various widths. They differ in the basic materials considered (aluminum versus titanium) and the number of thicknesses evaluated (four versus one). Because of this latter point, stress state or thickness effects were not evaluated in Phase II.

In general, the Ti-6Al-4V titanium alloy appears tougher and more crack resistant than the 7075-T7351 aluminum alloy in equivalent product form (i.e., 1/4-inch rolled plate) on both a relative and absolute scale. A semi-quantitative appraisal is indicated in the following tabulation:

Property	1/4-inch Plate	
	Aluminum*	Titanium
7075-T7351	Ti-6Al-4V	
Yield Strength, TYS, ksi	60	130
Density, $\rho$ , lb/in. <sup>3</sup>	0.10	0.16
Specific Strength, TYS/ $\rho$ , in.	$6 \times 10^5$	$8.1 \times 10^5$
Relative Specific Strength	1.0	1.35
Toughness, $K_c$ , ksi-in. <sup>1/2</sup>	100	267
Relative Toughness, $K_c/TYS$ , in. <sup>1/2</sup>	1.7	2.0
Reference $\Delta K^{**}$ , ksi-in. <sup>1/2</sup>	20	27
FCP Rate at R = 0.1, $d(2c)/dN$ , $\mu\text{-in.}/\text{cycle}$	100	70
Relative FCP Rate	1.0	0.7

\*Reference (1).

\*\*Assuming high-performance systems operate in proportion to their specific strengths, see below also.

The relative toughness of the titanium is about 18 percent greater than that of the aluminum. The relative fatigue-crack propagation rate in titanium is about 30 percent less than that in the aluminum. It is important to note that comparisons of fatigue-crack-propagation data cannot be based directly on a single common  $\Delta K$  value. Since stress-intensity factor range,  $\Delta K$ , represents a flight service range, reference values must reflect the structural efficiency levels. As footnoted, the above tabulation assumes that the  $\Delta K$  range for each material will be proportional to its specific strength. The reference baseline of  $20 \text{ ksi-in.}^{1/2}$  is an arbitrary selection to represent typical flight conditions.

CONCLUSIONS AND RECOMMENDATIONS

The crack behavior of mill-annealed Ti-6Al-4V titanium alloy in 1/4-inch thickness appears to be consistent and predictable. The material is quite tough with no elastic fracture instabilities noted in panels less than 18 inches wide. However, slow stable tear (or stable crack extension) in the rising load test is noted at net section stresses above 40 ksi. The fatigue-crack-propagation ratios,  $d(2c)/dN$ , are very consistent when evaluated on a  $\Delta K$  basis. However, there is an additional distinct effect of stress ratio, R, over and above that reflected in  $\Delta K$ .

A threshold stress-intensity factor range is evident and varies with stress ratio. The lowest  $\Delta K$  level at which propagation was noted was about 3.5 ksi-in.<sup>1/2</sup>.

It is evident that the crack propagation models currently used need to be modified for threshold effects and for improved accumulation of stress ratio, R. This is a definite necessity in order to obtain a more reliable predictive tool for design purposes.

This experimental program has characterized this particular thickness of the subject titanium alloy quite well. A parallel, but more selective, program at other thickness is recommended.

A very critical issue, now that consistent FCP rates have been demonstrated, is a study on environmental effects wherein significantly lower frequencies are applied for much longer time periods.

REFERENCES

- (1) Feddersen, C. E., and Hyler, W. S., "Fracture and Fatigue-Crack Propagation Characteristics of 7075-T7351 Aluminum Alloy Sheet and Plate", Final Report from Battelle's Columbus Laboratories to Naval Air Development Center, Contract No. N00156-68-C-1344 (March 15, 1970).
- (2) Lindh, D. V., and Eichenberger, T. W., "The Behavior of Several Materials With and Without Notches Under the Influence of Biaxial Stresses of Various Ratios", Boeing Company (March, 1963).
- (3) Anon., "Fracture Toughness and Tear Tests", ML-TDR-64-238, Boeing - North American, A Joint Venture, (October, 1964).
- (4) Feddersen, C. E., "Evaluation and Prediction of the Residual Strength of Center-Cracked Tension Panels", Damage Tolerance in Aircraft Structures, ASTM STP 486 (1971), pp 50-78.
- (5) Forman, R. G., Kearney, V. E., and Engle, R. M., "Numerical Analysis of Crack Propagation in Cyclic-Load Structures", Journal of Structural Engineering, (September, 1967), pp 459-464
- (6) Engle, R. M., Jr., "CRACKS, A Fortran IV Digital Computer Program for Crack Propagation Analysis", AFFDL-TR-70-107, Air Force Flight Dynamics Laboratory, Wright-Patterson Air Force Base, Ohio (October, 1970).
- (7) Paris, P. C., Gomez, M. P., and Anderson, W. E., "A Rational Analytic Theory of Fatigue", Trends in Engineering (University of Washington), Vol 13, No. 1 (1961).
- (8) Paris, P. C., "The Growth of Cracks Due to Variations in Loads", PhD Thesis, Lehigh University (1962).

APPENDIX A

BASIC FATIGUE-CRACK PROPAGATION DATA

## APPENDIX A

BASIC FATIGUE-CRACK PROPAGATION DATA

The actual cycle counts and associated surface crack length measurements made in the fatigue crack propagation studies of this program are recorded in this appendix. These are the basic data on which the crack-growth curves (i.e., crack length versus cycles) and the fatigue crack propagation rate analyses are based. The data are categorized first by panel width and then by maximum cyclic stress. Within this grouping, individual data listings are ordered by stress ratio.

As cited in the main body of this report, it is not usually possible to "catch" the final crack length measurement immediately prior to the cycle of failure. Frequently, however, macrostriations were visible on the fatigue surface, such that an estimate of the final crack length could be made. When available these measurements are listed at the bottom of each data column along with the final cycle count.

A-2

TABLE A-1. CYCLE LIMITS AND CRACK LENGTH MEASUREMENTS FOR  
9.6-INCH-WIDE PANELS AT LOW STRESS LEVELS

S <sub>max</sub> = 5 ksi				S <sub>max</sub> = 10 ksi					
R = 0.1 Specimen 9CC13		R = 0.4 Specimen 9CC14		R = 0.1 Specimen 9CC12		R = 0.4 Specimen 9CC07		R = 0.7 Specimen 9CC11	
N, kc	2c, in.	N, kc	2c, in.	N, kc	2c, in.	N, kc	2c, in.	N, kc	2c, in.
986.3	0.94	517.0	1.13	61.0	0.83	621.5	0.65	310.0	0.84
1178.0	0.98	746.0	1.17	70.0	0.88	672.0	0.66	378.0	0.85
1344.7	1.02	976.0	1.22	85.6	0.94	700.0	0.68	567.0	0.86
1865.0	1.15	1200.0	1.24	95.0	0.98	730.0	0.70	723.3	0.88
2193.5	1.23	1339.0	1.25	105.0	1.04	780.0	0.73	855.0	0.89
2569.5	1.33	2345.0	1.47	121.0	1.14	820.0	0.75	991.0	0.90
2801.0	1.43	3052.0	1.66	135.0	1.24	880.0	0.79	1100.0	0.91
3000.0	1.52	5301.0	2.29	145.3	1.33	900.0	0.81	1260.0	0.93
3200.0	1.59	5587.0	2.40	151.0	1.37	990.0	0.87	1406.0	0.95
3425.0	1.69	5993.0	2.59	155.0	1.40	1050.0	0.92	1619.1	0.97
3866.2	1.92	6390.0	2.79	160.2	1.45	1130.0	1.02	1790.2	1.00
4085.0	2.11	6807.0	3.09	165.0	1.50	1206.0	1.20	2017.1	1.03
4285.0	2.29	7141.5	3.49	176.1	1.60	1282.0	1.45	2136.0	1.05
4485.9	2.53	7400.0	3.99	190.5	1.76	1350.5	1.74	2230.0	1.06
4686.0	2.94	7500.0	4.19	200.0	1.89	1387.0	1.93	2320.0	1.07
4786.0	3.22	7570.0	4.47	210.0	2.05	1423.0	2.18	2424.0	1.09
4886.0	3.66	7620.0	4.62	215.3	2.13	1440.0	2.31	255.0	1.11
4986.0	4.26	7670.0	4.83	222.0	2.25	1452.0	2.42	2655.0	1.14
5005.9	4.44	7720.0	5.07	230.0	2.43	146.0	2.50	2860.0	1.18
5026.0	4.57	7740.0	5.18	235.0	2.54	1473.0	2.93	3022.0	1.22
5046.0	4.75	7760.0	5.27	241.0	2.69	1488.0	2.81	3210.0	1.27
5066.0	4.97	7780.0	5.45	246.0	2.83	1503.0	3.00	3337.0	1.31
5086.1	5.21	7800.0	5.58	250.0	2.96	1513.0	3.16	3500.3	1.36
5096.1	5.34	7820.0	5.73	253.0	3.05	1526.0	3.36	3654.0	1.40
5106.1	5.46	7840.0	5.86	256.0	3.16	1538.0	3.60	3855.0	1.47
5116.1	5.6	7880.0	6.26	259.0	3.27	1550.0	3.86	4051.0	1.53
5126.1	5.80	7900.0	6.50	262.0	3.38	1557.0	4.03	4235.0	1.60
5136.1	5.98	7920.0	6.79	265.0	3.15	1565.0	4.26	4536.0	1.73
5146.1	6.19	7930.0	6.97	268.0	3.64	1573.0	4.54	4838.1	1.87
5156.1	6.46	7940.0	7.17	271.0	3.79	1581.0	4.89	5040.0	1.99
5161.1	6.59	7950.0	7.48	274.0	3.92	1589.0	5.36	5186.0	2.10
5166.1	6.76	7955.0	7.67	277.0	4.13	1594.0	5.75	5310.5	2.18
5171.1	6.93	7960.0	7.91	279.0	4.27	1596.0	5.96	5524.6	2.38
5176.1	7.18	7962.0	8.04	281.0	4.42	1598.0	6.20	5680.0	2.58
5181.1	7.49	7965.0	8.39	283.0	4.60	1601.0	6.65	5730.0	2.65
5186.1	7.96			285.0	4.77	1603.0	7.19	5800.0	2.76
5187.1	8.22			287.0	5.02	1604.0	7.62	5890.0	2.91
		288.0	5.14					6000.0	3.12
		289.0	5.27					6110.0	3.38
		290.0	5.41					6200.0	3.64
		291.0	5.57					6250.0	3.81
		292.0	5.76					6300.0	3.98
		293.0	5.95					6361.0	4.28
		294.0	6.21					6391.0	4.47
		294.5	6.35					6430.0	4.73
		295.0	6.52					6450.0	4.91
		295.5	6.72					6475.0	5.16
		296.0	6.93					6501.0	5.46
		296.5	7.17					6515.0	5.71
		297.0	7.49					6525.0	5.87
		297.6	7.95					6535.0	6.10
								6544.0	6.32
								6550.0	6.51
								6555.0	6.70
								6560.0	6.91
								6565.0	7.15
								6567.5	7.31
								6570.0	7.49
								6572.0	7.65
								6573.0	7.73
								6574.0	7.84
								6575.0	7.96
								6576.0	8.05
								6577.0	8.19
								6578.0	8.37

TABLE A-2. CYCLE LIMITS AND CRACK LENGTH MEASUREMENTS FOR  
9.6-INCH-WIDE PANELS AT HIGH STRESS LEVELS

$S_{max} = 30 \text{ ksi}$				$S_{max} = 50 \text{ ksi}$			
$R = 0.1$		$R = 0.4$		$R = 0.7$		$R = 0.4$	
Specimen 9CC04	Specimen 9CC05	Specimen 9CC06	Specimen 9CC10	Specimen 9CC09			
N, kc	2c, in.	N, kc	2c, in.	N, kc	2c, in.	N, kc	2c, in.
3.1	0.56	8.7	0.55	34.0	0.54	2.0	0.87
4.5	0.73	12.1	0.78	42.0	0.57	2.3	1.06
6.0	0.93	14.0	0.96	53.0	0.67	2.5	1.20
7.5	1.30	15.0	1.09	60.6	0.74	2.7	1.37
8.0	1.45	16.0	1.28	68.0	0.82	2.9	1.52
8.5	1.65	17.0	1.49	76.0	0.92	3.0	1.65
8.8	1.77	18.0	1.77	84.8	1.07	3.1	1.75
9.0	1.90	18.5	1.93	94.0	1.30	3.2	1.91
9.3	2.05	19.1	2.16	102.5	1.63	3.3	2.04
9.5	2.17	19.5	2.35	107.0	1.87	3.4	2.17
9.7	2.33	19.8	2.48	110.0	2.05	3.5	2.33
9.9	2.44	20.0	2.62	113.0	2.31	3.6	2.55
10.1	2.59	20.3	2.72	115.0	2.50	3.7	2.71
10.3	2.81	20.5	2.83	116.0	2.61	3.8	2.86
10.5	2.95	20.8	2.98	117.0	2.72	3.8	3.00
10.7	3.28	21.0	3.17	118.0	2.87	3.9	3.17
10.9	3.51	21.3	3.36	119.0	3.00	3.9	3.37
11.1	3.99	21.5	3.55	120.0	3.15	4.0	3.63
11.3	4.44	21.8	3.83	121.0	3.32	4.0	3.95
11.5	5.24	22.0	4.12	122.0	3.49	4.1	4.62
		22.1	4.21	123.0	3.68		16.0
		22.2	4.35	124.0	3.85		16.5
		22.3	4.48	125.0	4.07		17.0
		22.4	4.63	126.0	4.32		17.5
		22.5	4.81	127.0	4.68		18.0
		22.6	5.02	127.5	4.85		18.5
		22.7	5.21	128.1	5.09		18.8
		22.8	5.41	128.5	5.22		19.0
		22.9	5.73	129.0	5.46		19.3
		23.0	6.01	129.5	5.72		19.5
		23.1	6.44	130.0	6.00		19.8
				130.3	6.17		2.26
				130.5	6.35		2.45
				130.8	6.55		2.70
				131.0	6.76		2.93
$N_f = 11,690$		$N_f = 23,190$		$N_f = 131,300$		$N_f = 4,080$	
$2c_{fm} = 7.40$		$2c_{fm} = 7.60$		$2c_{fm} = --$		$2c_{fm} = 5.92$	
$2c_{fe} = 6.37$		$2c_{fe} = 6.90$		$2c_{fe} = 7.03$		$2c_{fe} = 5.19$	
Freq. = 5 Hz		Freq. = 5 Hz		Freq. = 25 Hz		Freq. = 5 Hz	
						Freq. = 10 Hz	

TABLE A-3. CYCLE LIMITS AND CRACK LENGTH MEASUREMENTS FOR 16-INCH-WIDE PANELS

$\sigma_{max} = 10 \text{ ksi}$	$\sigma_{min} = 13 \text{ ksi}$		$\sigma_{min} = 16 \text{ ksi}$		$\sigma_{min} = 19 \text{ ksi}$		$\sigma_{min} = 20 \text{ ksi}$		$\sigma_{min} = 24 \text{ ksi}$		$\sigma_{min} = 26 \text{ ksi}$		$\sigma_{min} = 30 \text{ ksi}$		
	$\alpha = 0.1$		$\alpha = 0.4$		$\alpha = 0.7$		$\alpha = 1.0$		$\alpha = 1.1$		$\alpha = 1.4$		$\alpha = 1.7$		
	Specimen No.	Specimen Length	Specimen No.												
116.0	0.19	313.7	0.34	1690.1	0.19	4.4	0.63	4.6	0.63	91.3	0.63	0.63	0.38	103.3	0.38
116.0	0.47	267.5	0.55	202.6	0.45	4.0	0.54	4.0	0.54	169.3	0.54	0.54	0.34	103.3	0.34
117.0	1.13	277.0	0.44	239.5	1.00	4.0	1.52	4.0	1.52	121.0	0.53	0.53	0.42	104.3	0.42
117.0	1.39	291.6	0.54	284.0	0.50	16.0	1.92	16.0	1.92	132.3	0.53	0.53	0.42	104.3	0.42
117.0	1.54	301.0	1.01	324.0	1.01	11.0	2.41	16.0	1.92	132.3	0.53	0.53	0.42	104.3	0.42
117.0	1.79	316.0	1.12	319.1	1.01	11.5	2.72	17.0	1.92	132.3	0.53	0.53	0.42	104.3	0.42
117.0	2.03	339.1	1.74	439.7	1.74	12.0	3.04	18.0	1.92	151.4	1.92	1.92	1.28	112.3	1.28
117.0	2.20	348.1	1.44	499.7	1.39	11.5	3.50	18.5	1.92	150.3	1.92	1.92	1.28	112.3	1.28
117.0	2.45	364.3	1.64	520.0	1.32	15.0	4.01	19.0	1.92	197.3	1.92	1.92	1.28	112.3	1.28
117.0	2.60	381.1	1.90	510.7	1.36	12.0	4.63	19.5	1.92	194.3	1.92	1.92	1.28	112.3	1.28
117.0	2.90	396.0	1.60	441.0	1.36	16.0	5.25	20.0	1.92	212.6	1.92	1.92	1.28	112.3	1.28
117.0	3.15	407.2	1.70	466.0	1.36	14.0	5.83	20.5	1.92	218.8	1.92	1.92	1.28	112.3	1.28
117.0	3.40	422.0	1.69	481.9	1.36	14.0	6.41	21.0	1.92	220.0	1.92	1.92	1.28	112.3	1.28
117.0	3.65	432.0	1.60	481.0	1.36	14.0	6.99	21.5	1.92	218.0	1.92	1.92	1.28	112.3	1.28
117.0	3.90	447.1	1.44	482.0	1.36	14.0	7.57	22.0	1.92	217.0	1.92	1.92	1.28	112.3	1.28
117.0	4.15	457.1	1.60	482.0	1.36	14.0	8.15	22.5	1.92	216.0	1.92	1.92	1.28	112.3	1.28
117.0	4.40	472.1	1.60	482.0	1.36	14.0	8.73	23.0	1.92	215.0	1.92	1.92	1.28	112.3	1.28
117.0	4.65	487.1	1.60	482.0	1.36	14.0	9.31	23.5	1.92	214.0	1.92	1.92	1.28	112.3	1.28
117.0	5.00	502.1	1.60	482.0	1.36	14.0	9.89	24.0	1.92	213.0	1.92	1.92	1.28	112.3	1.28
117.0	5.25	518.1	1.60	482.0	1.36	14.0	10.47	24.5	1.92	212.0	1.92	1.92	1.28	112.3	1.28
117.0	5.50	533.1	1.60	482.0	1.36	14.0	11.05	25.0	1.92	211.0	1.92	1.92	1.28	112.3	1.28
117.0	5.75	548.1	1.60	482.0	1.36	14.0	11.63	25.5	1.92	210.0	1.92	1.92	1.28	112.3	1.28
117.0	6.00	563.1	1.60	482.0	1.36	14.0	12.21	26.0	1.92	209.0	1.92	1.92	1.28	112.3	1.28
117.0	6.25	578.1	1.60	482.0	1.36	14.0	12.79	26.5	1.92	208.0	1.92	1.92	1.28	112.3	1.28
117.0	6.50	593.1	1.60	482.0	1.36	14.0	13.37	27.0	1.92	207.0	1.92	1.92	1.28	112.3	1.28
117.0	6.75	608.1	1.60	482.0	1.36	14.0	13.95	27.5	1.92	206.0	1.92	1.92	1.28	112.3	1.28
117.0	7.00	623.1	1.60	482.0	1.36	14.0	14.53	28.0	1.92	205.0	1.92	1.92	1.28	112.3	1.28
117.0	7.25	638.1	1.60	482.0	1.36	14.0	15.11	28.5	1.92	204.0	1.92	1.92	1.28	112.3	1.28
117.0	7.50	653.1	1.60	482.0	1.36	14.0	15.69	29.0	1.92	203.0	1.92	1.92	1.28	112.3	1.28
117.0	7.75	668.1	1.60	482.0	1.36	14.0	16.27	29.5	1.92	202.0	1.92	1.92	1.28	112.3	1.28
117.0	8.00	683.1	1.60	482.0	1.36	14.0	16.85	30.0	1.92	201.0	1.92	1.92	1.28	112.3	1.28
117.0	8.25	698.1	1.60	482.0	1.36	14.0	17.43	30.5	1.92	200.0	1.92	1.92	1.28	112.3	1.28
117.0	8.50	713.1	1.60	482.0	1.36	14.0	18.01	31.0	1.92	199.0	1.92	1.92	1.28	112.3	1.28
117.0	8.75	728.1	1.60	482.0	1.36	14.0	18.59	31.5	1.92	198.0	1.92	1.92	1.28	112.3	1.28
117.0	9.00	743.1	1.60	482.0	1.36	14.0	19.17	32.0	1.92	197.0	1.92	1.92	1.28	112.3	1.28
117.0	9.25	758.1	1.60	482.0	1.36	14.0	19.75	32.5	1.92	196.0	1.92	1.92	1.28	112.3	1.28
117.0	9.50	773.1	1.60	482.0	1.36	14.0	20.33	33.0	1.92	195.0	1.92	1.92	1.28	112.3	1.28
117.0	9.75	788.1	1.60	482.0	1.36	14.0	20.91	33.5	1.92	194.0	1.92	1.92	1.28	112.3	1.28
117.0	10.00	803.1	1.60	482.0	1.36	14.0	21.49	34.0	1.92	193.0	1.92	1.92	1.28	112.3	1.28
117.0	10.25	818.1	1.60	482.0	1.36	14.0	22.07	34.5	1.92	192.0	1.92	1.92	1.28	112.3	1.28
117.0	10.50	833.1	1.60	482.0	1.36	14.0	22.65	35.0	1.92	191.0	1.92	1.92	1.28	112.3	1.28
117.0	10.75	848.1	1.60	482.0	1.36	14.0	23.23	35.5	1.92	190.0	1.92	1.92	1.28	112.3	1.28
117.0	11.00	863.1	1.60	482.0	1.36	14.0	23.81	36.0	1.92	189.0	1.92	1.92	1.28	112.3	1.28
117.0	11.25	878.1	1.60	482.0	1.36	14.0	24.39	36.5	1.92	188.0	1.92	1.92	1.28	112.3	1.28
117.0	11.50	893.1	1.60	482.0	1.36	14.0	24.97	37.0	1.92	187.0	1.92	1.92	1.28	112.3	1.28
117.0	11.75	908.1	1.60	482.0	1.36	14.0	25.55	37.5	1.92	186.0	1.92	1.92	1.28	112.3	1.28
117.0	12.00	923.1	1.60	482.0	1.36	14.0	26.13	38.0	1.92	185.0	1.92	1.92	1.28	112.3	1.28
117.0	12.25	938.1	1.60	482.0	1.36	14.0	26.71	38.5	1.92	184.0	1.92	1.92	1.28	112.3	1.28
117.0	12.50	953.1	1.60	482.0	1.36	14.0	27.29	39.0	1.92	183.0	1.92	1.92	1.28	112.3	1.28
117.0	12.75	968.1	1.60	482.0	1.36	14.0	27.87	39.5	1.92	182.0	1.92	1.92	1.28	112.3	1.28
117.0	13.00	983.1	1.60	482.0	1.36	14.0	28.45	40.0	1.92	181.0	1.92	1.92	1.28	112.3	1.28
117.0	13.25	998.1	1.60	482.0	1.36	14.0	29.03	40.5	1.92	180.0	1.92	1.92	1.28	112.3	1.28
117.0	13.50	1013.1	1.60	482.0	1.36	14.0	29.61	41.0	1.92	179.0	1.92	1.92	1.28	112.3	1.28
117.0	13.75	1028.1	1.60	482.0	1.36	14.0	30.19	41.5	1.92	178.0	1.92	1.92	1.28	112.3	1.28
117.0	14.00	1043.1	1.60	482.0	1.36	14.0	30.77	42.0	1.92	177.0	1.92	1.92	1.28	112.3	1.28
117.0	14.25	1058.1	1.60	482.0	1.36	14.0	31.35	42.5	1.92	176.0	1.92	1.92	1.28	112.3	1.28
117.0	14.50	1073.1	1.60	482.0	1.36	14.0	31.93	43.0	1.92	175.0	1.92	1.92	1.28	112.3	1.28
117.0	14.75	1088.1	1.60	482.0	1.36	14.0	32.51	43.5	1.92	174.0	1.92	1.92	1.28	112.3	1.28
117.0	15.00	1103.1	1.60	482.0	1.36	14.0	33.09	44.0	1.92	173.0	1.92	1.92	1.28	112.3	1.28
117.0	15.25	1118.1	1.60	482.0	1.36	14.0	33.67	44.5	1.92	172.0	1.92	1.92	1.28	112.3	1.28
117.0	15.50	1133.1	1.60	482.0	1.36	14.0	34.25	45.0	1.92	171.0	1.92	1.92	1.28	112.3	1.28
117.0	15.75	1148.1	1.60	482.0	1.36	14.0	34.83	45.5	1.92	170.0	1.92	1.92	1.28		

TABLE A-3. CYCLE LIMITS AND CRACK LENGTH MEASUREMENTS FOR

$S_{max} = 10 \text{ ksi}$		$S_{max} = 15 \text{ ksi}$		$S_{max} = 10 \text{ ksi}$		$S_{max} = 30 \text{ ksi}$					
$R = 0.1$		$R = 0.4$		$R = 0.7$		$R = 0.1$		$R = 0.4$		$R = 0.7$	
Specimen 16CC10		Specimen 16CC05		Specimen 16CC12		Specimen 16CC02		Specimen 16CC11		Specimen 16CC01	
$N_c$	2c, in.	$N_c$	2c, in.	$N_c$	2c, in.						
92.2	0.75	212.7	0.56	1800.1	0.79	4.4	0.63	6.0	0.59	91.5	0.61
116.0	0.87	237.5	0.65	1952.0	0.81	6.1	0.84	10.0	0.78	109.5	0.67
140.0	0.99	267.5	0.75	2263.0	0.85	8.0	1.22	12.0	0.93	121.0	0.73
163.0	1.15	277.0	0.84	2595.0	0.90	9.0	1.52	14.0	1.12	133.2	0.85
191.0	1.39	291.6	0.94	2860.0	0.93	10.0	1.92	15.0	1.25	145.2	0.94
205.0	1.54	302.0	1.01	3424.0	1.02	11.0	2.41	16.0	1.42	159.5	1.12
225.0	1.79	316.0	1.13	3792.0	1.08	11.5	2.72	17.0	1.61	171.1	1.30
240.0	2.03	329.1	1.26	4292.2	1.18	12.0	3.06	18.0	1.82	180.1	1.43
250.0	2.20	348.1	1.44	4893.7	1.29	12.5	3.50	18.5	1.94	188.8	1.64
260.0	2.41	364.3	1.64	5370.0	1.42	13.0	4.01	19.0	2.09	197.5	1.94
270.0	2.64	381.7	1.90	5870.7	1.56	13.5	4.65	19.5	2.26	204.3	2.24
280.0	2.92	394.1	2.18	6410.0	1.75	14.0	5.75	20.0	2.36	212.6	2.64
290.0	3.30	407.4	2.50	6560.0	1.82	14.3	6.52	20.5	2.55	218.8	3.47
295.0	3.54	415.7	2.75	6859.9	1.95	14.4	6.91	21.0	2.77	228.0	4.94
300.0	3.78	422.0	2.99	7155.0	2.11	14.5	7.69	21.5	2.99	234.0	6.41
305.0	4.07	432.6	3.58	7375.0	2.25	14.6	8.97	22.0	3.25	236.3	7.11
310.0	4.44	441.6	4.35	7600.0	2.46			22.5	3.50	237.5	7.61
315.0	4.82	447.5	5.05	7791.0	2.65			23.0	3.78	238.3	8.61
317.5	5.05	451.3	5.53	7990.9	2.91			23.3	3.96	239.2	8.81
320.0	5.31	454.4	6.15	8190.9	3.21			23.5	4.11	240.5	9.21
322.5	5.58	456.7	5.59	8280.0	3.40			23.8	4.29	240.9	9.61
325.0	5.92	460.2	7.73	8330.0	3.51			24.0	4.44	241.7	10.34
327.5	6.29	460.9	8.02	8380.0	3.61			24.3	4.69		
330.0	6.70	461.6	8.23	8430.0	3.72			24.5	4.91		
331.0	6.89	462.2	8.45	8480.0	3.83			24.8	5.15		
332.0	7.10	462.7	8.68	8530.0	3.93			25.0	5.34		
333.0	7.31	463.4	9.02	8580.0	4.05			25.3	5.59		
334.0	7.54	463.9	9.20	8630.0	4.18			25.5	5.87		
335.0	7.79	464.4	9.51	8680.0	4.32			25.7	6.09		
336.0	8.06	465.0	9.92	8730.0	4.48			25.8	6.30		
337.0	8.38			8780.0	4.63			25.9	6.45		
338.0	8.72			8850.0	4.90			26.0	6.63		
339.0	9.14			8900.0	5.07			26.1	6.78		
340.0	9.56			8950.0	5.27			26.2	6.94		
340.5	9.82			9000.0	5.55			26.3	7.19		
341.0	10.05			9050.0	5.76			26.4	7.34		
341.5	10.33			9100.0	6.21			26.5	7.55		
342.0	10.64			9120.0	6.35			26.6	7.81		
342.5	11.00			9140.0	6.55			26.7	8.08		
343.0	11.40			9160.3	6.70			26.8	8.38		
343.5	11.89			9180.3	6.92			26.9	8.97		
344.0	12.50			9200.6	7.14			27.0	9.66		
				9220.7	7.38			27.1	11.10		
				9240.8	7.65						
				9260.9	8.00						
				9280.9	8.37						
				9300.9	8.87						
				9310.9	9.16						
				9321.0	9.53						
				9331.0	9.92						
				9341.0	10.43						
				9351.0	11.09						
				9356.0	11.58						
				9357.0	11.63						
				938.0	11.72						
				9359.0	11.84						
				9360.0	11.97						
				9361.0	12.10						
				9362.0	12.25						
				9363.0	12.43						
				9364.0	12.61						
				9365.0	12.77						
				9366.0	12.97						
				9367.0	13.22						
				9368.0	13.58						

$N_f = 344,500$   
 $2c_{fm} = 12.90$   
 $2c_{fe} = 13.27$   
 $\text{Freq.} = 10 \text{ Hz}$

$N_f = 467,000$   
 $2c_{fm} = --$   
 $2c_{fe} = 13.48$   
 $\text{Freq.} = 10 \text{ Hz}$

$N_f = 9,368,010$   
 $2c_{fm} = --$   
 $2c_{fe} = 13.61$   
 $\text{Freq.} = 25 \text{ Hz}$

$N_f = 14,690$   
 $2c_{fm} = 12.90$   
 $2c_{fe} = 10.64$   
 $\text{Freq.} = 5 \text{ Hz}$

$N_f = 27,130$   
 $2c_{fm} = 11.95$   
 $2c_{fe} = 11.68$   
 $\text{Freq.} = 5 \text{ Hz}$

$N_f = 242,550$   
 $2c_{fm} = --$   
 $2c_{fe} = 11.10$   
 $\text{Freq.} = 5 \text{ Hz}$

## A-4

## 3. CYCLE LIMITS AND CRACK LENGTH MEASUREMENTS FOR 16-INCH-WIDE PANELS

E12 2c, in.	$S_{max} = 30 \text{ ksi}$								$S_{max} = 50 \text{ ksi}$											
	R = 0.1				R = 0.4				R = 0.7				R = 0.1				R = 0.4			
	Specimen 16CC02		Specimen 16CC11		Specimen 16CC01		Specimen 16CC07		Specimen 16CC09		Specimen 16CC16									
N, kc	2c, in.	N, kc	2c, in.	N, kc	2c, in.	N, kc	2c, in.	N, kc	2c, in.	N, kc	2c, in.	N, kc	2c, in.	N, kc	2c, in.	N, kc	2c, in.	N, kc	2c, in.	
0.79	4.4	0.63	6.0	0.59	91.5	0.61	0.7	0.58	1.3	0.54	9.8	0.57								
0.81	6.1	0.84	10.0	0.78	109.5	0.67	0.8	0.64	1.5	0.58	10.3	0.60								
0.85	8.0	1.22	12.0	0.93	121.0	0.75	0.8	0.67	1.7	0.64	10.8	0.62								
0.90	9.0	1.52	14.0	1.12	133.2	0.85	0.9	0.71	1.9	0.71	11.8	0.69								
0.93	10.0	1.92	15.0	1.25	145.2	0.94	1.0	0.74	2.1	0.78	12.8	0.79								
1.02	11.0	2.41	16.0	1.42	159.5	1.12	1.0	0.71	2.3	0.87	13.8	0.89								
1.08	11.5	2.72	17.0	1.61	171.6	1.30	1.1	0.81	2.5	0.96	14.8	1.02								
1.18	12.0	3.06	18.0	1.82	180.5	1.43	1.1	0.85	2.7	1.08	15.8	1.20								
1.29	12.5	3.50	18.5	1.94	188.8	1.66	1.2	0.90	2.9	1.19	16.3	1.28								
1.42	13.0	4.01	19.0	2.09	197.5	1.96	1.2	0.92	3.1	1.30	16.8	1.40								
1.56	13.5	4.65	19.5	2.26	204.3	2.26	1.3	0.95	3.3	1.46	17.3	1.51								
1.75	14.0	5.75	20.0	2.36	212.6	2.84	1.3	0.98	3.5	1.62	17.8	1.64								
1.82	14.3	6.52	20.5	2.55	218.8	3.47	1.4	1.02	3.7	1.78	18.3	1.79								
1.95	14.4	6.91	21.0	2.77	228.0	4.90	1.4	1.07	3.9	1.99	18.8	1.92								
2.11	14.5	7.69	21.5	2.99	234.0	6.41	1.5	1.16	4.0	2.09	19.3	2.11								
2.25	14.6	8.97	22.0	3.25	236.3	7.17	1.5	1.17	4.1	2.18	19.8	2.31								
2.46		22.5	3.50	237.5	7.63	1.6	1.22	4.2	2.30	20.0	2.38									
2.65		23.0	3.78	238.3	8.03	1.6	1.28	4.3	2.43	20.2	2.47									
2.91		23.3	3.95	239.2	5.43	1.7	1.35	4.4	2.55	20.4	2.53									
3.21		23.5	4.11	240.5	9.27	1.7	1.42	4.5	2.69	20.6	2.63									
3.40		23.8	4.29	240.9	9.60	1.8	1.54	4.6	2.81	20.8	2.72									
3.51		24.0	4.44	241.7	10.30	1.8	1.60	4.7	2.97	21.0	2.83									
3.61		24.3	4.69			1.9	1.67	4.8	3.12	21.2	2.89									
3.72		24.5	4.91			1.9	1.81	4.9	3.33	21.4	3.03									
3.83		24.8	5.15			2.0	1.93	5.0	3.53	21.6	3.15									
3.93		25.0	5.34			2.0	2.05	5.1	3.75	21.8	3.24									
4.05		25.3	5.59			2.1	2.20	5.2	3.85	22.0	3.38									
4.18		25.5	5.87			2.1	2.35	5.2	4.00	22.2	3.54									
4.32		25.7	6.09			2.2	2.55	5.3	4.14	22.4	3.67									
4.48		25.8	6.30			2.2	2.90	5.3	4.29	22.6	4.04									
4.63		25.9	6.45			2.2	2.90	5.3	4.45	22.8	4.04									
4.90		26.0	6.63			2.3	3.62	5.4	4.66	23.0	4.31									
5.07		26.1	6.78			2.3	3.79	5.4	4.81	23.1	4.28									
5.27		26.2	6.94			2.3	3.94	5.4	4.97	23.2	4.39									
5.55		26.3	7.19			2.3	4.14	5.5	5.09	23.3	4.45									
5.76		26.4	7.34			2.3	4.42	5.5	5.24	23.4	4.56									
6.21		26.5	7.55			2.3	4.76	5.5	5.33	23.5	4.65									
6.35		26.6	7.81			2.3	5.27	5.5	5.54	23.6	4.79									
6.55		26.7	8.08			2.3	5.54	5.5	5.84	23.7	4.95									
7.0		26.8	8.38			2.3	7.15	5.6	6.09	23.8	5.05									
7.92		26.9	8.97					5.6	6.35	23.9	5.19									
7.14		27.0	9.66					5.6	6.61	24.0	5.34									
7.38		27.1	11.10					5.6	7.02	24.1	5.47									
7.65								5.6	7.38	24.2	5.66									
7.80								5.6	7.89	24.3	5.78									
7.87								5.6	8.83	24.3	5.88									
7.96										24.4	6.00									
8.16										24.4	6.11									
8.53										24.5	6.20									
8.92										24.5	6.31									
9.43										24.6	6.43									
9.99										24.6	6.58									
10.38										24.7	6.72									
10.61										24.7	6.87									
10.77										24.8	7.22									
10.97																				
11.22																				
11.58																				
$N_f = 14,690$		$N_f = 27,130$		$N_f = 242,550$		$N_f = 2,350$		$N_f = 5,630$		$N_f = 24,763$										
$2c_{fm} = 12.90$		$2c_{fm} = 11.95$		$2c_{fm} = --$		$2c_{fm} = 9.30$		$2c_{fm} = 9.70$		$2c_{fm} = --$										
$2c_{fe} = 10.64$		$2c_{fe} = 11.68$		$2c_{fe} = 11.10$		$2c_{fe} = 8.90$		$2c_{fe} = 9.46$		$2c_{fe} = 7.34$										
Freq. = 5 Hz		Freq. = 5 Hz		Freq. = 5 Hz		Freq. = 1 Hz		Freq. = 1 Hz		Freq. = 4 Hz										

A-4.2

A-4.3

TABLE A-4. CYCLE LIMITS AND CRACK LENGTH MEASUREMENTS FOR  
32-INCH-WIDE PANELS AT LOW STRESS LEVELS

$S_{max} = 10 \text{ ksi}$ $R = 0.1$	$S_{max} = 30 \text{ ksi}$ $R = 0.1$	$S_{max} = 50 \text{ ksi}$ $R = 0.1$			
Specimen 32CC06		Specimen 32CC05			
$N_c$ kc	2c, in.	$N_c$ kc	2c, in.	$N_c$ kc	2c, in.
0	0.51	3.0	0.56	0.6	0.58
212.0	0.63	3.8	0.67	0.6	0.60
254.0	0.68	4.3	0.74	0.7	0.68
317.0	0.87	5.3	0.90	0.8	0.75
350.0	1.06	5.8	0.99	0.9	0.82
381.0	1.28	6.3	1.10	1.0	0.88
400.0	1.44	6.8	1.22	1.1	0.97
410.0	1.55	7.3	1.37	1.3	1.14
420.0	1.67	7.8	1.54	1.4	1.24
430.0	1.81	8.3	1.75	1.5	1.33
440.0	1.94	8.8	1.97	1.6	1.48
450.0	2.12	9.0	2.07	1.7	1.60
460.0	2.31	9.2	2.18	1.8	1.73
465.0	2.39	9.4	2.31	1.9	1.91
470.0	2.52	9.6	2.45	2.0	2.08
475.0	2.61	9.8	2.59	2.1	2.29
480.0	2.73	10.0	2.72	2.2	2.52
485.0	2.86	10.2	2.88	2.3	2.91
490.0	2.98	10.4	3.07	2.4	3.18
495.0	3.11	10.6	3.27	2.4	3.61
500.0	3.27	10.8	3.46	2.4	3.92
505.0	3.43	11.0	3.69	2.5	4.50
510.0	3.61	11.2	3.96	2.5	4.90
515.0	3.79	11.3	4.10	2.5	5.72
520.0	3.97	11.4	4.25	2.5	6.18
525.0	4.17	11.5	4.44	2.5	6.99
530.0	4.40	11.6	4.63	2.5	7.89
535.0	4.61	11.7	4.74	2.5	8.76
540.0	4.89	11.7	4.86	2.6	10.00
545.0	5.16	11.8	4.95	2.6	13.41
550.0	5.46	11.8	5.08		
555.0	5.81	11.9	5.19		
560.0	6.17	11.9	5.32		
565.0	6.50	12.0	5.45		
570.0	7.05	12.0	5.58		
575.0	7.57	12.1	5.71		
580.0	8.09	12.1	5.90		
585.0	8.70	12.2	6.07		
590.0	9.40	12.2	6.25		
595.0	10.19	12.3	6.45		
600.0	11.10	12.3	6.69		
605.0	12.11	12.4	6.93		
606.0	12.30	12.4	7.20		
607.0	12.53	12.5	7.55		
608.0	12.75	12.5	8.00		
609.0	12.98	12.5	8.25		
610.0	13.22	12.6	8.51		
611.0	13.50	12.6	8.80		
612.0	13.74	12.6	9.15		
613.0	14.04	12.6	9.43		
614.0	14.34	12.7	9.90		
615.0	14.63	12.7	10.53		
616.0	14.96	12.7	10.92		
617.0	15.31	12.7	11.50		
618.0	15.66	12.8	12.24		
619.0	16.06	12.8	13.39		
620.0	16.44	12.8	13.98		
621.0	16.86	12.8	14.70		
622.0	17.32	12.9	15.35		
623.0	17.83	12.8	16.34		
624.0	18.41	12.9	18.03		
625.0	18.85				
626.0	19.40				
627.0	20.04				
627.5	20.41				
628.0	20.80				
628.5	21.22				
629.0	21.67				
629.5	22.20				
630.0	22.77				
630.5	23.42				
631.0	24.12				

 $N_f = 631,820$  $2c_{fe} = 28.80$  $2c_{fe} = 25.38$ 

Freq. = 10 Hz

 $N_f = 12,835$  $2c_{fe} = 21.20$  $2c_{fe} = 20.42$ 

Freq. = 2 Hz

 $N_f = 2,563$  $2c_{fe} = 15.30$  $2c_{fe} = 14.86$ 

Freq. = 1 Hz

APPENDIX B

ESTIMATION OF FATIGUE-CRACK LENGTH  
AT FINAL LOADING CYCLE

## APPENDIX B

ESTIMATION OF FATIGUE-CRACK LENGTH  
AT FINAL LOADING CYCLE

As discussed in the Terminal Crack Behavior section, the final fatigue crack length (i.e., length immediately prior to cycle of fracture) is an important experimental quantity to measure. Although it sometimes can be detected from striation markings after fracture, many times it is not at all discernible. As mentioned in the Fatigue-Crack-Propagation Procedures section, such measurements are elusive to obtain during the test. As a result, it frequently is desirable to obtain an estimate of the final crack from an extrapolation of the terminal data readings. The procedure adopted in this program is described in this appendix.

Consider the idealized crack-growth curve of Figure B-1. A simpler linear extrapolation of the last two data readings can provide an initial approximation to the final crack length as shown. However, since physical evidence indicates that both this curve and its slope (first derivative) are monotonically increasing with increasing cycle count, the techniques of divided differences can provide a higher degree, yet conservative approximation, of the final crack length. This is a purely mathematical approximation based on the observed monotonic behavior of crack growth.

The technique adopted herein is illustrated in Figure B-2, wherein the last three data readings are used to extrapolate a final crack length value. The first divided difference for the last two data points is expressed as

$$f[N_{\ell-1}, N_\ell] = \frac{(2c)_\ell - (2c)_{\ell-1}}{N_\ell - N_{\ell-1}}, \quad (B-1)$$

and for the next and second-to-last points, as

$$f[N_{\ell-2}, N_{\ell-1}] = \frac{(2c)_{\ell-1} - (2c)_{\ell-2}}{N_{\ell-1} - N_{\ell-2}}. \quad (B-2)$$

B-2

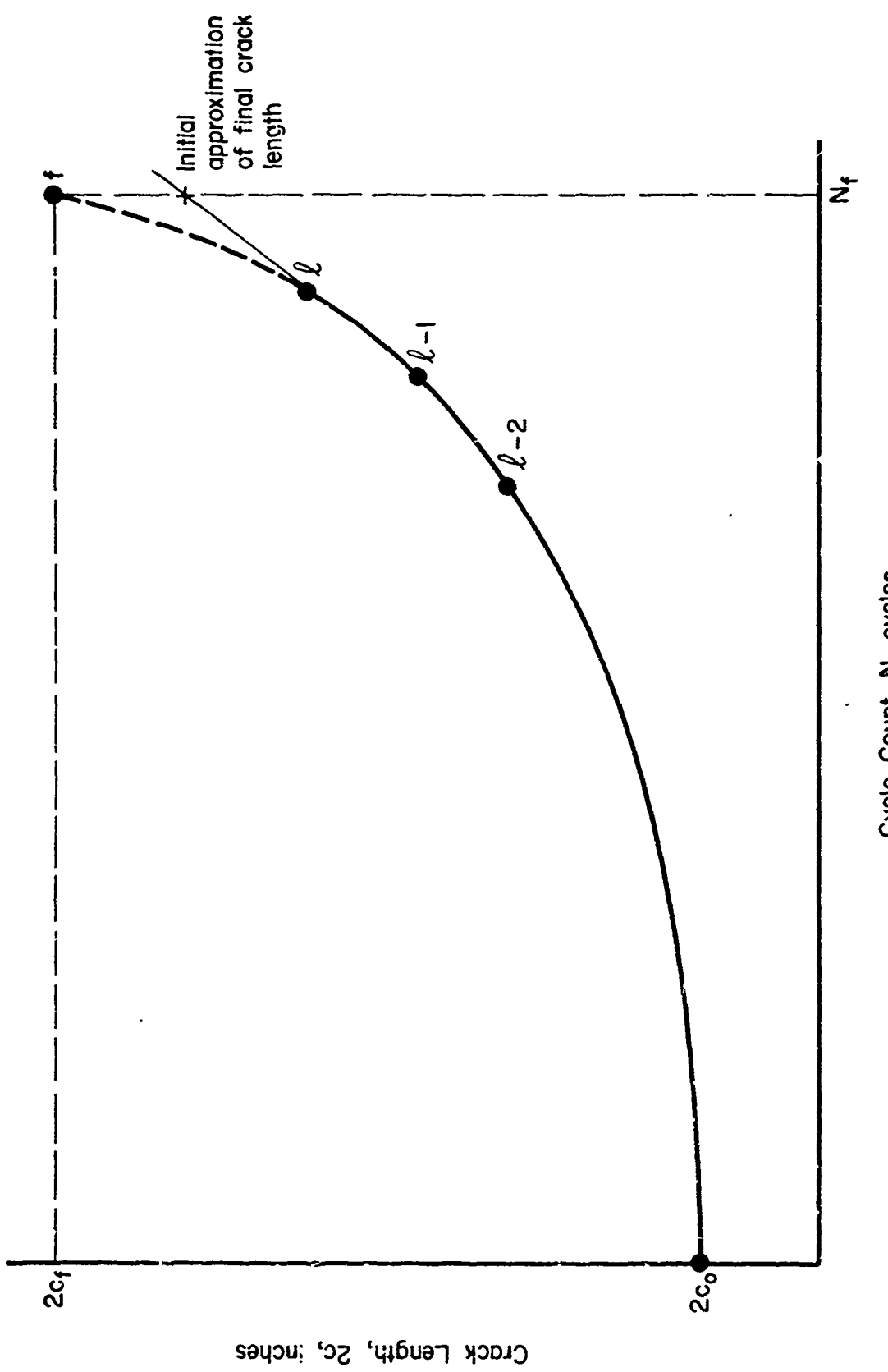


FIGURE B-1. IDEALIZED CRACK GROWTH CURVE WITH THREE TERMINAL DATA POINTS

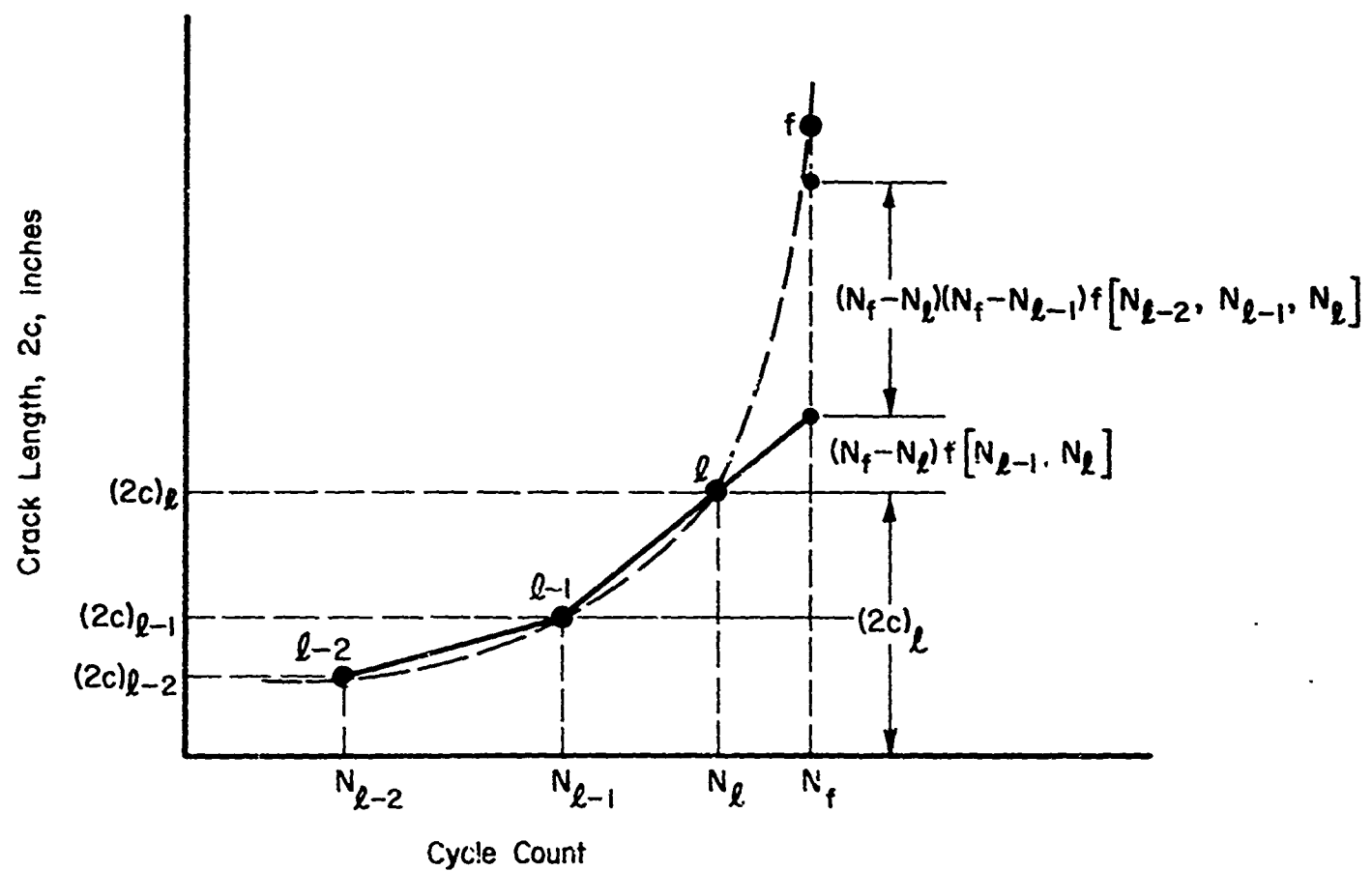


FIGURE B-2. FINITE DIFFERENCE EXTRAPOLATION OF TERMINAL CRACK GROWTH MEASUREMENTS

The second divided difference over the last three data points is expressed as

$$f[N_{\ell-2}, N_{\ell-1}, N_\ell] = \frac{f[N_{\ell-1}, N_\ell] - f[N_{\ell-2}, N_{\ell-1}]}{N_\ell - N_{\ell-2}} \quad (B-3)$$

Then, by using Newton's interpolation formula with divided differences in an extrapolation mode, the final crack length can be approximated as

$$(2c)_f = (2c)_\ell + (N_f - N_\ell) f[N_{\ell-1}, N_\ell] + (N_f - N_\ell)(N_f - N_{\ell-1}) f[N_{\ell-2}, N_{\ell-1}, N_\ell]. \quad (B-4)$$

It should be re-emphasized that this approximation is conservative because both the crack growth curve and its slope are monotonically increasing. Although higher order divided differences reflecting more data points could be proposed, higher order rate behavior is not adequately well understood to justify this step. Furthermore, the magnitude of this additional refinement would be expected to be small.

An estimated final crack length for each fatigue-crack propagation test of this program has been calculated from the terminal data of each test. These data and results are presented in Table B-1, along with the measured final crack lengths where the striations were detectable. The agreements between estimated and measured values appear to be good, or at least conservative. Although this technique is not a substitute for terminal crack length measurements, it can be a useful tool to anticipate failure conditions during the experiment.

TABLE B-1. CORRELATION OF ESTIMATED AND MEASURED FINAL CRACK LENGTHS

Specimen Number	Panel Width W inches	Max Stress S ksi	Stress Ratio R	Total Cycles N <sub>E</sub>	Last				Terminal Measurements				Final Crack Length, 2c <sub>f</sub> Estimated	Final Crack Length, 2c <sub>f</sub> Measured		
					Cycles 2c <sub>f</sub> , N <sub>E</sub>		Length 2c <sub>f</sub> , N <sub>E</sub> -1		Cycles 2c <sub>f</sub> , N <sub>E</sub> -1		Length 2c <sub>f</sub> , N <sub>E</sub> -2					
					Next	Last	Length	2c <sub>f</sub> , N <sub>E</sub> -1	Next	Last	Length	2c <sub>f</sub> , N <sub>E</sub> -2				
9CC13	9.6	5	{ 0.1 0.4	5,187,180 7,965,810	5,187,050 7,965,000	8.22 8.39	5,186,050 7,962,000	7.96 8.04	5,181,050 7,960,000	7.49 7.91	7.49 7.91	8.26 8.52	8.50	8.50		
9CC14			{ 0.7 0.1	No continuous propagation test stopped after 32 x 10 <sup>6</sup> cycles												
9CC16			{ 0.7 0.4	297,880 1,604,840	297,500 1,604,000	7.95 7.62	297,000 1,603,000	7.49 7.19	296,500 1,601,000	7.17 6.65	8.39 8.06	8.10	--	--		
9CC12	9.6	10	{ 0.7 0.1	6,578,560 11,690	6,578,000 11,500	8.37 5.24	6,577,000 11,300	8.19 4.44	6,576,000 11,000	8.05 3.99	8.49 6.37	8.10	--	--		
9CC07	9.6		{ 0.7 0.1	23,190 23,100	23,100 23,100	6.44 6.44	23,000 23,000	6.01 6.01	22,920 22,920	5.73 5.73	6.90 6.90	7.60	7.60	7.60		
9CC11			{ 0.7 0.4	131,300 4,080	131,000 4,050	6.76 4.62	130,750 4,000	6.55 3.95	130,500 3,950	6.35 3.63	7.03 5.19	7.03 5.92	--	--		
9CC04	9.6	30	{ 0.7 0.4	19,850 19,850	19,750 19,750	5.33 5.33	19,500 19,500	4.59 4.59	19,250 19,250	4.29 4.29	5.75 5.75	--	--	--		
9CC05	9.6		{ 0.7 0.4													
9CC06			{ 0.7 0.4													
9CC10	9.6	50	{ 0.7 0.4													
9CC09	9.6		{ 0.7 0.4													
16CC10	10	0.1	344,500	344,000	12.50	343,500	11.89	343,000	11.40	13.23	12.90					
16CC05	15	0.4	467,500	465,000	9.92	464,400	9.51	463,900	9.30	13.48	--					
16CC12	10	0.7	9,368,010	9,367,950	13.58	9,366,950	13.22	9,365,950	12.97	13.61	--					
16CC02			{ 0.1 0.4	14,690 27,130	14,600 27,100	8.97 11.10	14,500 27,000	7.69 9.66	14,350 26,900	6.91 8.97	12.90 11.68	12.90 11.95	--	--		
16CC11	16	30	{ 0.4 0.7	242,550 2,350	241,700 2,340	10.30 7.15	240,900 2,330	9.60 5.94	240,500 2,320	9.27 5.27	11.10 8.90	11.10 9.30	--	--		
16CC01			{ 0.7 0.1	5,625 5,625	5,620 5,620	8.83 5,610	5,610 7.89	5,600 7.89	5,600 7.38	5,600 7.38	9.70 9.46	9.70 9.30	--	--		
16CC07	16	50	{ 0.4 0.7	24,763 24,750	24,722 24,700	24,700 24,700	6.87 6.87	24,650 6.72	24,650 6.72	7.34 7.34	--	--	--	--		
32CC06	10		{ 0.1 0.1	631,320 12,835	631,000 12,825	24.12 18.03	630,500 12,815	23.42 16.34	630,000 12,805	22.77 15.35	25.38 20.42	28.8 21.2	--	--		
32CC05	32	30	{ 0.1 0.1	2,563 2,563	2,560 2,560	13.41 13.41	2,550 2,550	10.00 10.00	2,540 2,540	8.76 8.76	14.86 14.86	15.3 15.3	--	--		
32CC04			{ 0.1 0.1													